NATURAL RESOURCES

GEOLOGIC MAP OF THE PORT LUDLOW AND SOUTHERN HALF OF THE HANSVILLE 7.5-MINUTE QUADRANGLES, KITSAP AND JEFFERSON COUNTIES, WASHINGTON

by Michael Polenz, Jesse G. Favia, Ian J. Hubert,
Gabriel Legorreta Paulín, and Recep Cakir

WASHINGTON
DIVISION OF GEOLOGY
AND EARTH RESOURCES
Map Series 2015-02
October 2015

WASHINGTON STATE DEPARTMENT OF
Natural Resources
Peter Goldmark - Commissioner of Public Lands

GEOLOGIC MAP OF THE PORT LUDLOW AND SOUTHERN HALF OF THE HANSVILLE 7.5-MINUTE QUADRANGLES, KITSAP AND JEFFERSON COUNTIES, WASHINGTON

by Michael Polenz, Jesse G. Favia, Ian J. Hubert,
Gabriel Legorreta Paulín, and Recep Cakir

WASHINGTON
DIVISION OF GEOLOGY
AND EARTH RESOURCES
Map Series 2015-02
October 2015

This geologic map was funded in part by the USGS National Cooperative Geologic Mapping Program, award no. G14AC00212

WASHINGTON STATE DEPARTMENT OF
Natural Resources
Peter Goldmark - Commissioner of Public Lands

DISCLAIMER

Neither the State of Washington, nor any agency thereof, nor any of their employees, makes any warranty, express or implied, or assumes any legal liability or responsibility for the accuracy, completeness, or usefulness of any information, apparatus, product, or process disclosed, or represents that its use would not infringe privately owned rights. Reference herein to any specific commercial product, process, or service by trade name, trademark, manufacturer, or otherwise, does not necessarily constitute or imply its endorsement, recommendation, or favoring by the State of Washington or any agency thereof. The views and opinions of authors expressed herein do not necessarily state or reflect those of the State of Washington or any agency thereof.

This map product has been subjected to an iterative internal review process by agency geologists, cartographers, and editors and meets Map Series standards as defined by Washington Division of Geology and Earth Resources.

INDEMNIFICATION

Research supported by the U.S. Geological Survey, National Cooperative Geologic Mapping Program, under USGS award number G14AC00212. The views and conclusions contained in this document are those of the authors and should not be interpreted as necessarily representing the official policies, either expressed or implied, of the U.S. Government.

WASHINGTON STATE DEPARTMENT OF NATURAL RESOURCES

Peter Goldmark—*Commissioner of Public Lands*

DIVISION OF GEOLOGY AND EARTH RESOURCES

David K. Norman—*State Geologist*
John P. Bromley—*Assistant State Geologist*

Washington State Department of Natural Resources
Division of Geology and Earth Resources

Mailing Address:
MS 47007
Olympia, WA 98504-7007

Street Address:
Natural Resources Bldg, Rm 148
1111 Washington St SE
Olympia, WA 98501

Phone: 360-902-1450
Fax: 360-902-1785
Email: geology@dnr.wa.gov
Website: http://www.dnr.wa.gov/geology

Publications and Maps:
www.dnr.wa.gov/programs-and-services/geology/publications-and-data/publications-and-maps

Washington Geology Library Searchable Catalog:
www.dnr.wa.gov/programs-and-services/geology/washington-geology-library

Suggested Citation: Polenz, Michael; Favia, J. G.; Hubert, I. J.; Legorreta Paulín, Gabriel; Cakir, Recep, 2015, Geologic map of the Port Ludlow and southern half of the Hansville 7.5-minute quadrangles, Kitsap and Jefferson Counties, Washington: Washington Division of Geology and Earth Resources Map Series 2015-02, 1 sheet, scale 1:24,000, 40 p. text. [http://www.dnr.wa.gov/publications/ger_ms2015-02_geol_map_port_ludlow_hansville_24k.zip]

Contents

Introduction 1
Geologic Overview 1
- Bedrock Units 3
- Quaternary Deposits 3
  - Pre-Vashon Deposits 3
  - Vashon Drift 3
  - Post-glacial Deposits 4
- Regional Structural Setting 4

Methods 6
Description of Map Units 6
- Quaternary Unconsolidated Deposits 6
  - Holocene Nonglacial Deposits 6
  - Latest Pleistocene to Holocene Nonglacial Deposits 8
  - Pleistocene Glacial and Nonglacial Deposits 8
    - Vashon Drift of the Fraser Glaciation 9
    - Pre-Vashon Glacial Deposits 10
    - Pre-Vashon Nonglacial Deposits 11
    - Undivided Glacial and Nonglacial Deposits 12
- Tertiary Sedimentary and Volcanic Bedrock 13

Ages of Bedrock Units 15
Ages of Quaternary Units and Timing of Glacial Events 15
- Paleomagnetically Reversed Deposits 15
- Deposits of the Possession Glaciation 16
- Deposits of the Olympia Nonglacial Interval 16
- Deposits and Shorelines of the Fraser Glaciation 17
  - Glacial Advance 17
  - Glacial Recession 17
  - Deglaciation, Meltwater Channels, and Valley Incision 18
  - Glaciomarine Conditions and the Everson Interstade 19
  - Post-Glacial Conditions 19
- Glacial Lakes and Shorelines 19
  - Everson Interstade Glaciomarine Shorelines at ~140 ft Elevation 19
  - Lake Bretz Glaciolacustrine Shorelines at ~350 ft Elevation 20

Structural Interpretation of the Map Area 20
- Northwest-striking Faults 20
  - Portage Canal Fault 20
  - Unnamed Faults at Pilot Point 21
  - Faults Beneath Hood Canal 21
- Faults of Other Orientations 22
  - Lofall Fault 22
  - Faults Between Crescent Formation and Sedimentary Rocks 22
  - Unnamed Fault South of Beaver Valley 23
  - North-striking Fault Along Chimacum Valley 23
  - Unnamed Faults in Basalt Southwest of Port Ludlow 23
  - Faulting in Basalt Northwest of Mats Mats Bay 24
- Other Structures 24
  - Port Ludlow uplift 24

Evidence for Pleistocene to Recent Deformation 25
Seismicity 25
Deformation of Quaternary Units 25
Paleogeographic Considerations 25
Acknowledgments 26
References Cited 26
Appendix A. New Radiocarbon, Luminescence, and $^{40}Ar/^{39}Ar$ Age Estimates 33
Appendix B. Geochemical Data 39

FIGURES

Figure 1. Shaded relief map with regional structures and bedrock exposures 2
Figure 2. Comparison of geologic time scale, global magnetic polarity, Marine Oxygen Isotope Stages (MIS), and ages of climatic intervals in the Puget and Fraser Lowlands. 4
Figure 3. Timing of Vashon-age Puget lobe ice advance and recession 5
Figure 4. Basalt flows and clastic dike at Shine Quarry. 14
Figure 5. Fault at east end of Shine Quarry excavation. 24
Figure A1. $^{40}Ar/^{39}Ar$ step-heating age and K/Ca spectra for sample GD33/X166D 37

TABLES

Table 1. Summary of new age data from the Port Ludlow–Hansville quadrangles 7
Table 2. Columnar section names and locations 7
Table A1. Radiocarbon ages from the map area 33
Table A2. Infrared and optically stimulated luminescence age-control results 35
Table A3. $^{40}Ar/^{39}Ar$ age control data and summary of results for sample GD33/X166D 37
Table A4. $^{40}Ar/^{39}Ar$ step-heating results for sample GD33/X166D 38
Table B1. Major oxide geochemical analyses 39
Table B2. Trace-element geochemical analyses 40

MAP SHEET

Geologic Map of the Port Ludlow and Southern Half of the Hansville 7.5-minute Quadrangles, Kitsap and Jefferson Counties, Washington

Geologic Map of the Port Ludlow and Southern Half of the Hansville 7.5-minute Quadrangles, Kitsap and Jefferson Counties, Washington

by Michael Polenz[1], Jesse G. Favia[2], Ian J. Hubert[1], Gabriel Legorreta Paulín[3], Recep Cakir[1]

[1] Washington Division of Geology and Earth Resources
MS 47007
Olympia, WA 98504-7007

[2] Aspect Consulting, LLC
350 Madison Avenue North
Bainbridge Island, WA 98110

[3] Universidad Nacional Autónoma de México
Instituto de Geografía
Ciudad Universitaria, Del Coyoacán
cp 04510, México, D.F.

INTRODUCTION

The Hansville and Port Ludlow 7.5-minute quadrangles are located in Kitsap and Jefferson Counties along the northwestern edge of the Puget Lowland, near the base of the Olympic Mountains. These two quadrangles straddle the mouth of Hood Canal (Map Sheet and Fig. 1) and are the last quadrangles in a 7-year campaign to map the geology along Hood Canal at a scale of 1:24,000. This map excludes the Whidbey Island portion of the Hansville quadrangle, which was previously mapped by Polenz and others (2006).

The Hood Canal area is geologically active, ecologically sensitive, increasingly populated, and contains national defense infrastructure. Mapping along Hood Canal was undertaken to better understand the area's geological hazards, stratigraphy, and hydrologic resources. Water resources are becoming increasingly scarce, and improved geologic mapping is needed to inform resource management efforts by local government, property owners, and scientists.

Our map and cross sections revise and add detailed field observations and new geological analyses to previous mapping and studies of the area (Jillson, 1915; Allison, 1959; Thoms, 1959; Hanson, 1976, 1977; Gayer, 1976, 1977; Deeter, 1979; Carson, 1980; Grimstad and Carson, 1981; Rauch, 1985; Roberts, 1991; Yount and Gower, 1991; Yount and others, 1993; Simonds and others, 2004; Haugerud, 2009; unpub. field notes of Kathryn Hanson, AMEC, and Robert Carson, Whitman College, 2013). Like recent projects in nearby areas (Contreras and others, 2013, 2014; Polenz and others, 2013), our mapping documents previously unknown faults. Overall, we find that bedrock exposures are structurally controlled. Basalt geochemistry, flow character, texture, and a new high-quality $^{40}Ar/^{39}Ar$ age support assignment of basalt to the Eocene Crescent Formation. Sedimentary rocks of the overlying Quimper Sandstone are as young as the Oligocene. Surficial pre-Vashon sediments may be as old as 780 ka. A river sourced from the Olympic Mountains flowed through the Port Ludlow quadrangle during the Olympia nonglacial interval, indicating a topography markedly different than the modern. Deformed deposits of the Olympia nonglacial interval suggest that Quaternary faults may traverse the Hansville quadrangle, but further work is needed.

GEOLOGIC OVERVIEW

The Hansville and Port Ludlow 7.5-minute quadrangles are located on the eastern margin of the poorly understood Port Ludlow uplift (Fig. 1) and northwest of the Seattle basin and Kingston arch (Pratt and others, 1997; Brocher and others, 2001; ten Brink and others, 2002). The Lofall fault approximates the southern map edge (Brocher and others, 2001; Contreras and others, 2013), and the southern Whidbey Island fault zone (SWIF) lies to the northeast of the quadrangles (Gower, 1980; Johnson and others, 1996; Brocher and others, 2001, 2005; Kelsey and others, 2004; Sherrod, 2005; Sherrod and others, 2005, 2008). The SWIF separates the map area from pre-Eocene rocks exposed in the San Juan Islands to the north. To the west are the Olympic Mountains and late Paleocene to Eocene basalt and sedimentary rocks mostly mapped as Crescent Formation (Arnold, 1906; Brown and others, 1960; Cady and others, 1972a,b; Wolfe and McKee, 1972; Tabor and Cady, 1978a,b; Snavely, 1983; Einarsen, 1987; Whetten and others, 1988; Yount and Gower, 1991; Babcock and others, 1994). The oldest known rocks of the eastern Olympic Mountains and the Puget Lowland south of the SWIF are Paleocene to Eocene sedimentary rocks—most notably, the Blue Mountain unit (Tabor and Cady, 1978a; Einarsen, 1987).

Crescent Formation basalt appears to have been emplaced in the early to middle Eocene, either along the Kula-Farallon ridge before accretion to the North American continent (Duncan, 1982), or along the North American continental margin during rifting (Babcock and others, 1994). Either way the extrusive volcanics and associated sediments are related to the interaction of the Pacific–Kula–Farallon triple junction with the North American plate margin (Engebretson and others, 1985; Stock and Molnar, 1988; Babcock and others, 1994). Overlying the Crescent Formation are Eocene to Oligocene (?) shallow- to deep-marine sedimentary rocks (Jillson, 1915; Jacobson, 1927; Allison, 1959; Thoms, 1959; Rauch, 1985; Yount and Gower, 1991).

Marine sedimentation may have continued without interruption through the mid- to late-Miocene west of the map area, along the north side of the Olympic Peninsula (Brown and others, 1960; Snavely and others, 1978; Snavely, 1983; Schasse and Wegmann, 2000; Schasse and Polenz, 2002; Schasse and others, 2004; Polenz and others, 2004). Uplift of the Olympic Mountains

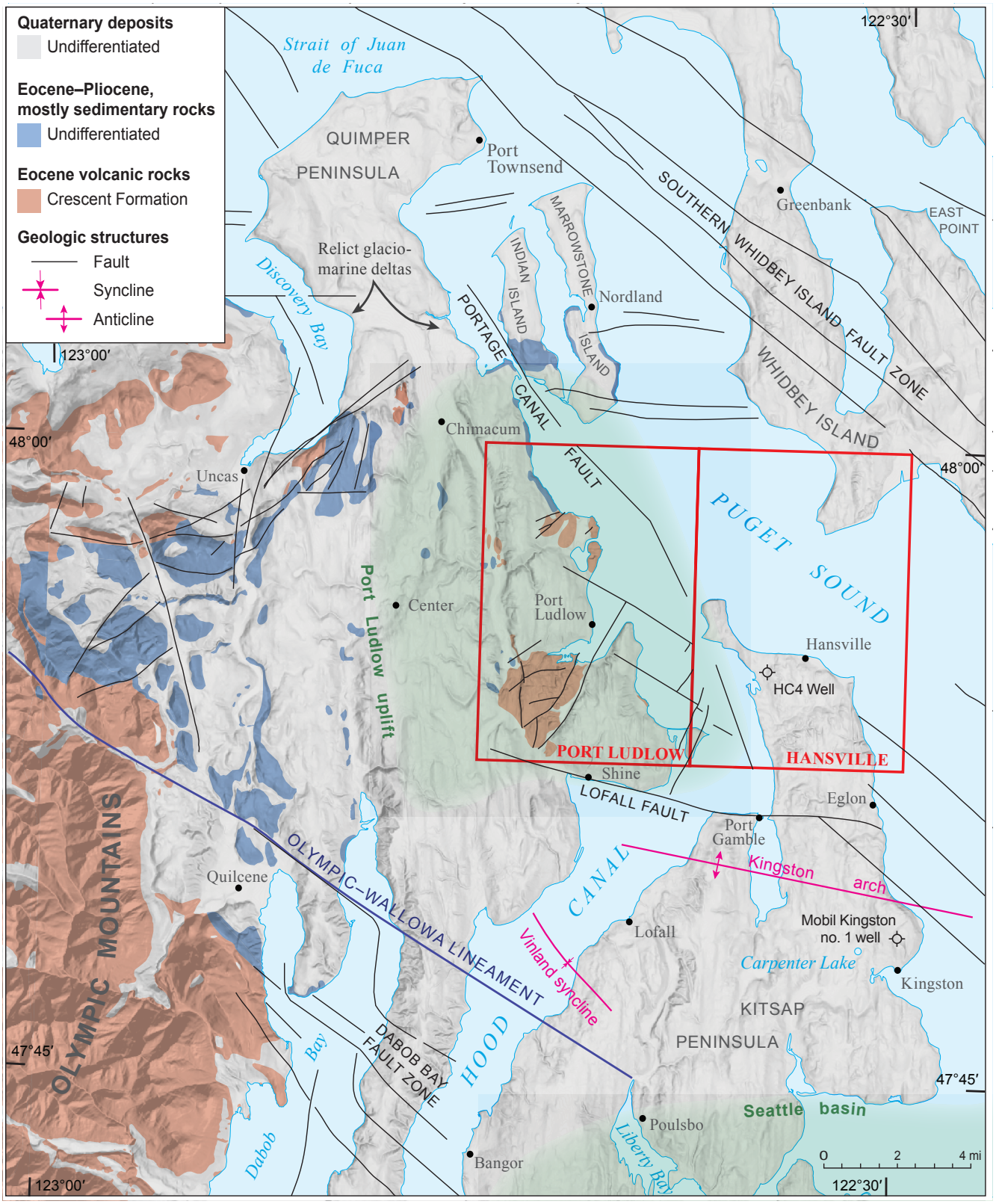

Figure 1. Shaded relief map with regional structures and bedrock exposures. Black lines indicate faults. Faults inside, south, and southwest of the Port Ludlow and Hansville quadrangles (red rectangles) are from current and recent field investigations (this study; Contreras and others 2013, 2014; Polenz and others, 2013). The northwest-striking faults southeast of Hansville are from Mace and Keranen (2012), the two southwest-striking faults at the south shore of Discovery Bay are adapted from Tabor and Cady (1978). The west-striking fault across Discovery Bay is from Whetten and others (1988). Faults west of the quadrangle are from Polenz and others (2014) and Tabor and others (2011; see also Haeussler and others, 1999). The Olympic–Wallowa lineament is from Raisz (1945). The Kingston arch, Vinland syncline, and Lofall fault are from Brocher and others (2001) as modified by Contreras and others (2013). All other faults are from Bowman and Czajkowski (2013). Green shading identifies the Port Ludlow uplift and the Seattle basin (Pratt and others, 1997). The southern boundary of the Port Ludlow uplift is now defined by the Lofall Fault and fits steep magnetic (Blakely, 1999) and gravity anomaly gradients.

concurrently (?) provided a source for the non-marine Montesano Formation (Bigelow, 1987) and possibly the non-marine Blakely Harbor Formation (Weaver, 1937; Fulmer, 1975) south and east of the Olympic Peninsula. This change suggests a regional shift to subaerial conditions, and may help explain an apparent hiatus in the map area where unlithified Quaternary sediments lie uncomformably on Oligocene to Eocene (?) marine sedimentary rocks.

Bedrock Units

Bedrock (pre-Quaternary) exposures in the Port Ludlow quadrangle coincide with the poorly understood Port Ludlow uplift (Fig. 1). No bedrock is exposed in the map area east of Hood Canal where structures and basins have been interpreted in the context of regional north–south shortening (Pratt and others, 1997; Wells and others, 1998; McCaffrey and others, 2007). Bedrock units include Eocene basalt (unit Evc) and Oligocene–Eocene (?) marine sedimentary rocks (units ΦEm, ΦEmq).

Name usage can be complicated in these bedrock units. Some prior studies did not assign formal bedrock unit names (Jillson, 1915; Gayer, 1976, 1977; Hanson, 1976, 1977; Grimstad and Carson, 1981; Clark, 1989; Simonds and others, 2004). Other studies mapped basalt as early to middle Eocene Crescent Formation (unit Evc)(Weaver, 1937; Allison, 1959; Tabor and Cady, 1978a; Spencer, 1984; Yount and Gower, 1991; Dragovich and others, 2002). Allison (1959) divided the Crescent Formation into lower (Metchosin) and upper members, and identified only the Metchosin member in the map area. In contrast, Yount and Gower (1991) recognized only 'upper' Crescent Formation in the map area using criteria from Cady and others (1972a,b), Tabor and Cady (1978a), and Glassley (1974, 1976) for separation into upper and lower members. Glassley (1974) suggested that the members are tectonically separated, whereas Hirsch and Babcock (2009) advocated a difference in metamorphic grade. Some have also divided the Crescent Formation into a volcanic facies and a sedimentary facies (Tabor and Cady, 1978a; Gower, 1980; Spencer, 1984; Yount and Gower, 1991; Babcock and others, 1994). Crescent Formation sedimentary rocks in the map area have been documented near Olele Point and Mats Mats Bay (Allison, 1959; Thoms, 1959; Yount and Gower, 1991). Clark (1989) noted that basalt geochemistry from the Port Ludlow area is consistent with a back-arc basin, transitional from mid-ocean ridge basalt to island-arc tholeite, and that Port Ludlow samples resemble other Crescent Formation basalt from west of Hood Canal and basalt from west of Bremerton (Clark, 1989).

Rocks southwest through north of the map area have almost exclusively been mapped as Oligocene to Eocene in age. Rauch (1985) and Schweitzer-Hopkins (1996) mapped rocks north of the map area as Eocene. Durham (1942, 1944) reported Oligocene to Eocene ages at Discovery Bay (Fig. 1) and west of Indian Island (Fig. 1). Allison (1959) showed field stations and bedding orientation sites in support of his mapping of Oligocene through Eocene bedrock units; however, he reported constraining fossils only from Discovery Bay (Fig. 1). Spencer (1984) reported many additional fossil samples from the Uncas quadrangle 6 mi west of the Port Ludlow quadrangle and fewer from the Quilcene quadrangle to the southwest. Armentrout and Berta (1977) examined the foraminiferal record in Eocene and Oligocene rocks north of the map area, and Rau (2004) reported numerous Eocene and Oligocene samples from nearby 7.5-minute quadrangles.

Eocene to Oligocene shallow-marine sandstone and siltstone (unit ΦEmq) crop out along the western shore of Oak Bay (Jillson, 1915; Jacobson, 1927; Durham, 1942, 1944; Allison, 1959; Thoms, 1959; Armentrout and Berta, 1977; Gower, 1980; Rauch, 1985; Yount and Gower, 1991; Schweitzer-Hopkins, 1996). The sandstone appears to unconformably overlie Crescent Formation at the south end of Oak Bay (Jillson, 1915; Jacobson, 1927; Thoms, 1959; Yount and Gower, 1991), but the exact nature of the contact is unclear. Marine sedimentary rocks (unit ΦEm) in Chimacum Valley along the west edge of the Port Ludlow Quadrangle have been mapped as Tertiary by Hanson (1976) and Grimstad and Carson (1981). Yount and Gower (1991) assigned these sedimentary rocks to the middle and upper Eocene Twin River Group and noted a regional fining-upward trend. An arkosic clastic dike of uncertain age and source intruded Crescent Formation basalt at the Shine Quarry.

Quaternary Deposits

Surficial sediment is mostly composed of Quaternary glacial deposits of the late Wisconsinan Fraser glaciation (Fig. 2), which is associated with marine oxygen-isotope stage 2 (MIS 2) (Morrison, 1991; Booth and others, 2004; Troost and Booth, 2008; Polenz and others, 2013). These units include the Vashon Drift and Everson Glaciomarine Drift (Armstrong and others, 1965; Easterbrook, 1968; Domack, 1982, 1983, 1984), and work within our map area suggests that the two units may be partly coeval. Older Pleistocene sediment is commonly exposed in slopes and cliffs, and post-glacial sediment locally covers drainages and fills closed depressions.

PRE-VASHON DEPOSITS

Pre-Vashon sedimentary units have been identified within the Port Ludlow and Hansville quadrangles (Garling and others, 1965; Gayer, 1976, 1977; Hanson, 1976, 1977; Deeter, 1979; Carson, 1980; Grimstad and Carson, 1981; Yount and others, 1993) and in adjacent areas (Schasse and Slaughter, 2005; Schasse and others, 2009; Polenz and others, 2006; Contreras and others, 2013, 2014). In the Port Ludlow quadrangle, Hanson (1976, 1977) and Gayer (1976, 1977) used stratigraphic relations and weathering to interpret some undated pre-Vashon deposits in Chimacum Valley and along segments of the Hood Canal shore as Possession Drift and Whidbey Formation (Fig. 2); other deposits in the same areas were mapped simply as unspecified pre-Vashon deposits (Hanson, 1976; Grimstad and Carson, 1981). In the Hansville quadrangle, Deeter (1979) used radiocarbon data to help inform his interpretations of: (1) Olympia nonglacial deposits along the shore of the Kitsap Peninsula, (2) Possession Drift and Whidbey Formation near Norwegian Point, and (3) Double Bluff Drift at Foulweather Bluff and along the western shore near the southern quadrangle boundary. Directly west of the map area, Polenz and others (2014) found that nearly all sediment exposures older than Vashon till appear to be Vashon advance outwash.

VASHON DRIFT

Linear ridges (fluted uplands) and intervening troughs in the map area were largely formed during the Fraser Glaciation. Booth

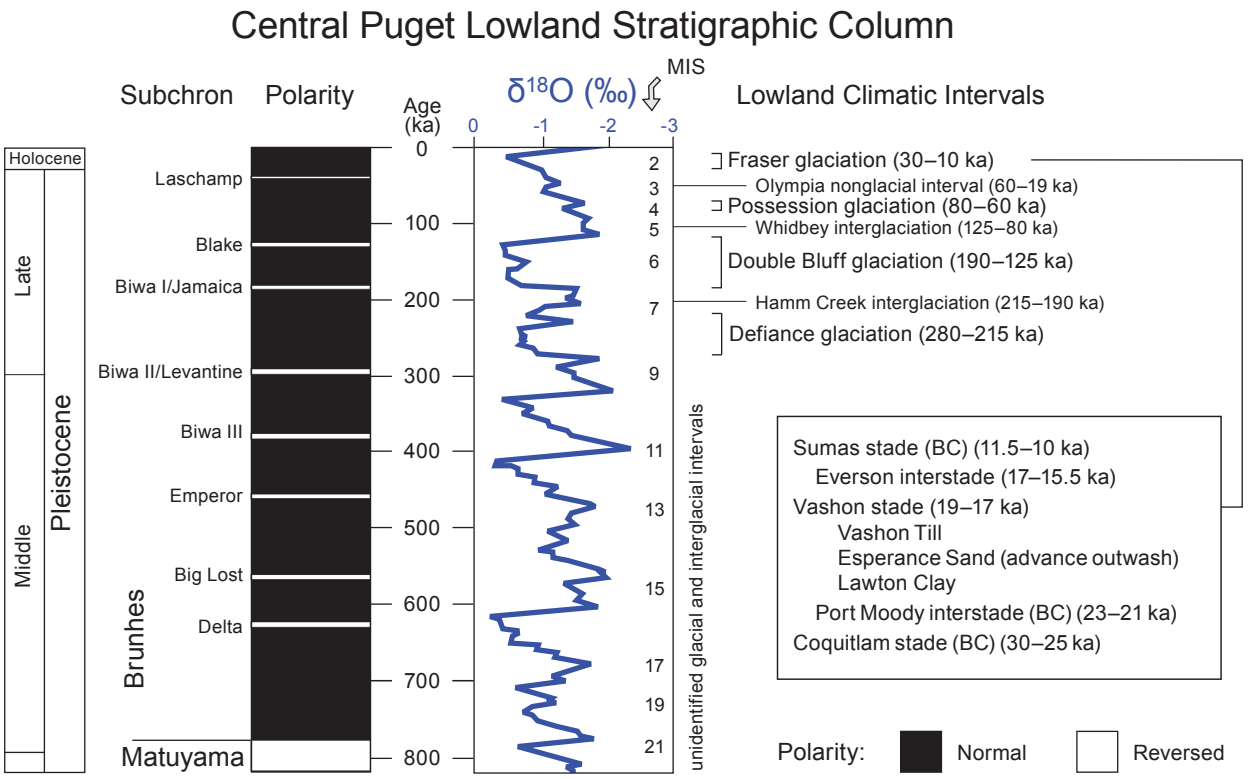

Figure 2. Comparison of geologic time scale, global magnetic polarity, Marine Oxygen Isotope Stages (MIS), and ages of climatic intervals in the Puget and Fraser Lowlands. Age ranges for the Olympia nonglacial interval, Vashon Stade, and Everson Interstade were modified by Polenz and others (2012b, 2013). We note that the time boundaries in the Puget Lowland are time transgressive, and that the Everson and Vashon Stades appear to overlap within the map area. Local age control data at GD11 and GD12 (sec. 22, T28N R2E) suggest that Vashon-age ice did not reach that part of the map area until after 18.4 ka. These dates, and comparison of GD9 and GD10 to dates presented by Anundsen and others (1994), appear to suggest that the Olympia to Vashon transition occurred in the map area several hundred years later than indicated on this figure (see Figure 3, and *Glacial Recession*). Data sources are explained in Troost and Booth (2008) and figure is modified from their fig. 6. BC, British Columbia

(1994) noted that deposition of proglacial advance outwash in the "great lowland fill" was followed by subglacial erosion and deposition of till. The resulting subglacial landforms and deposits of Vashon Stade outwash and till are the dominant surficial features within the map area and elsewhere in the Puget Lowland. At the end of the Fraser glacial advance, ice-dammed lakes and marine water of the Everson Interstade filled the topographic troughs (Bretz, 1910, 1913; Thorson, 1981, 1989; Dethier and others, 1995; Booth and others, 2004). As the ice dam(s) in the northern Puget Lowland disintegrated, lake levels dropped in stages, leaving behind a series of progressively lower and younger shorelines at discrete elevations (Haugerud, 2009; Ralph Haugerud, USGS, oral commun., 2013; Polenz and others, 2012c, 2013).

POST-GLACIAL DEPOSITS

Post-glacial deposits are separated into Holocene units and Pleistocene to Holocene units because the onset of the Holocene—11.7 ka (USGS Geologic Names Committee, 2010)—does not coincide with the end of the Fraser Glaciation in the Puget Lowland, which was likely between 15 and 16 ka (Fig. 3; *Deposits and Shorelines of the Fraser Glaciation*). As previously noted by Hanson (1977), the majority of post-glacial deposition occurred soon after glacial recession, when residual ice was still melting adjacent to ice-free areas of sediment deposition. Hillslope erosion, and fluvial transport and deposition, clearly continue in the modern environment.

Regional Structural Setting

The Hansville and Port Ludlow quadrangles are within the Cascadia subduction zone forearc. Oblique convergence causes active structures to accommodate crustal shortening (Pratt and others, 1997; Wells and others, 1998; Johnson and others, 2004; McCaffrey and others, 2007). Farallon and Juan de Fuca Plate convergence with North America and clockwise rotation of western Oregon into western Washington have created east-striking compressional faulting and northwest-striking transpressional faulting within the Puget Lowland. The Olympic subduction complex lies west of the Puget Lowland and south of the Canadian Coast Mountains (Blakely and others, 2002). The Olympic subduction complex and Leech River fault (on the north) partially accommodate Juan de Fuca Plate convergence with North America (Babcock, and others, 1994; Dickinson, 2006). The active and right-lateral-transpressional southern Whidbey Island fault zone (SWIF) accommodates movement of southwestern Washington relative to North America (Fig. 1) (Johnson and others, 1996; Kelsey and others, 2004; Brocher and others, 2005; Sherrod and others, 2005, 2008; Liberty and Pape, 2006; Blakely and others, 2011).

Northwest-striking structural elements are probably the most common orientation within 20 mi of the map area and include the regionally prominent Olympic–Wallowa lineament (Raisz, 1945; Blakely and others, 2011) and numerous mapped faults (Fig. 1). South of the map area, and sub-parallel to the

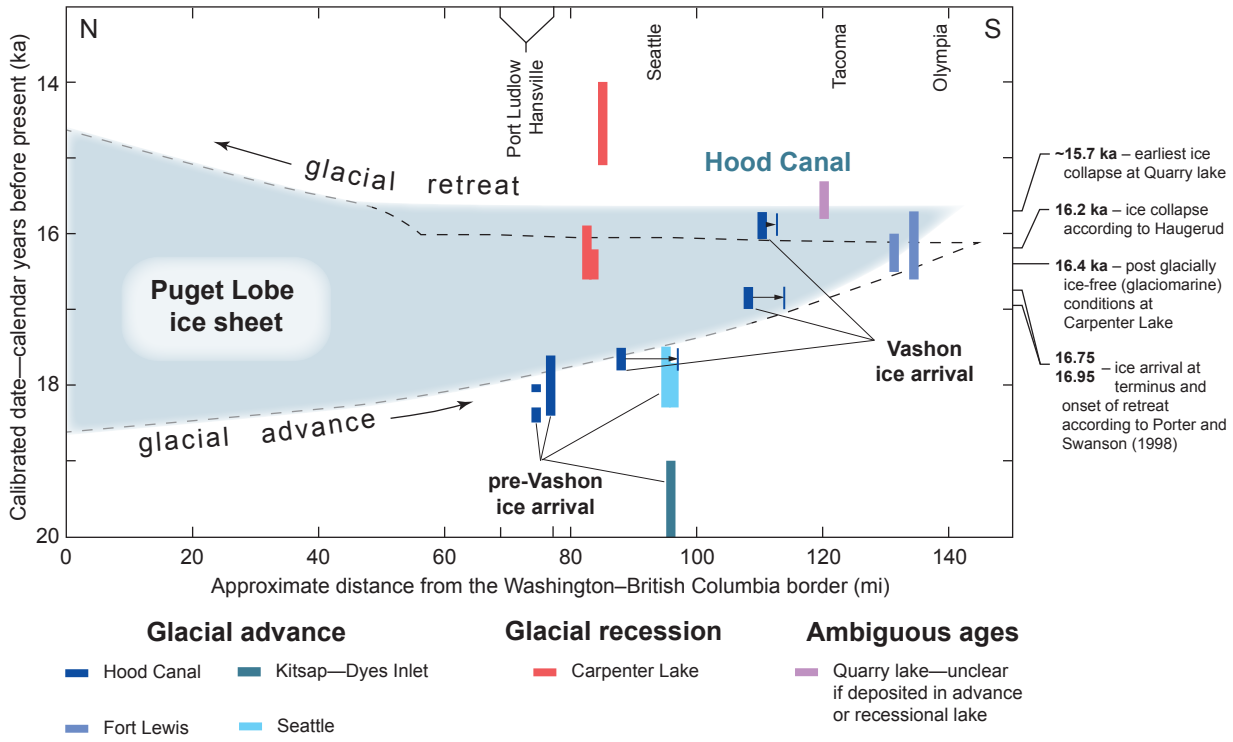

Figure 3. Timing of Vashon-age Puget lobe ice advance and recession in the Puget Lowland. Blue shaded area represents the interval when ice occupied the Puget Lowland at varied latitudes and is modified from Ralph Haugerud (dashed line; written commun., 2012; oral commun., 2015), who concluded that ice invaded the Puget Lowland at least 500 years later than estimated by Porter and Swanson (1998). We show only selected dates that we deem to be especially noteworthy. Dates with arrows extending to right (south) tightly constrain ice arrival at elevated sites by recording the presence of local lakes confined between ice and hillslopes. The southward arrows indicate how much farther south the ice front should have been assuming the "West Margin" ice slope line in figure 5 of Thorson (1981). We show ice arrival at the southern terminus and ice collapse at ~15.7 ka, about 500 years later than Haugerud, to honor the need to associate the "Quarry lake log" (Polenz and others, 2010, 2011) with Vashon drift but note that this record is incompatible with that from Carpenter Lake (Anundsen and others, 1994; Porter and Swanson, 1998).

SWIF, the potentially active transpressional Dabob Bay fault zone was suggested by Blakely and others (2009) and Polenz and others (2013). Contreras and others (2014) tentatively mapped this fault based on geomagnetic lineaments, disturbances in seismic sections beneath Hood Canal and Dyes Inlet, and disrupted Pleistocene sediments on the Toandos and Kitsap Peninsulas. The northwest-striking Portage Canal fault (Gower, 1978, 1980; Dragovich and others, 2002) has been mapped in the study area (Dragovich and others, 2002)—all three original authors agree that this fault was mapped on the basis of seismic section data. Mace and Keranen (2012) interpreted northwest-striking faults east of and on the Kitsap Peninsula as a high-angle flower structure that trends into the map area, where it would align with the Portage Canal fault.

Faults of other orientations have also been mapped in and near the Hansville and Port Ludlow quadrangles, including north-striking faults in and west of the map area (Gower, 1978; Gower and others, 1985; Yount and Gower, 1991; Haeussler and others, 1999; Dragovich and others, 2002; Tabor and others, 2011; Polenz and others, 2014). South of the map area, the west-striking Lofall fault appears to truncate the Oligocene and Eocene volcanic and sedimentary rocks brought to the surface by the Port Ludlow uplift. Klas Rock and Colvos Rocks, east of Basalt Point, are the most northeastern exposures of Crescent Formation basalt in the Puget Lowland and help define the extent of the uplifted area. The origin of the Port Ludlow uplift is unknown, but the margins are all defined by sharp crustal velocity, gravity, and aeromagnetic gradients (Macleod and others, 1977; Gower, 1978; Blakely and others, 1999; Brocher and others, 2001; Van Wagoner and others, 2002) and bedrock exposures in the Port Ludlow quadrangle are confined to its extent. The Lofall fault may also truncate the Kingston arch, an east-plunging anticline that has uplifted Oligocene and Eocene volcanic and sedimentary rocks south and southeast of the map area (Fig. 1)(Gower and others, 1985; Yount and Gower, 1991; Johnson and others, 1994; Pratt and others, 1997; Brocher and others, 2001; ten Brink and others, 2002). This structure was interpreted by Pratt and others (1997) as either a ramp anticline or a fault propagation fold.

In the map area east of Hood Canal, no bedrock has been documented shallower than 1,200 ft below the surface, suggesting a major structural change. Some investigators have inferred north-striking fault(s) at the western boundaries of structural basins in the Puget Lowland east of Hood Canal (Daneš and others, 1965; Gower and others, 1985; Johnson and others, 1994; Brocher and others, 2001; Dragovich and others, 2002). Southeast of the map area, the Seattle basin holds up to 10 km (6.25 mi) of folded Eocene and younger sedimentary rocks, including Quaternary sediment (Johnson, 1993). This basin appears to be related to regional north–south shortening since at least 16 Ma (Pratt and others, 1997; Wells and others, 1998; Wells and McCaffrey, 2013).

METHODS

We identified units from field observations between July 1st and November 7th, 2014. We used thin section analyses, 552 well and boring records, geotechnical reports, geophysical data, prior geologic mapping, geomorphic features identified from lidar-derived digital elevation models, 'T-sheet' historical topographic surveys along coastlines by the U.S. Coast & Geodetic Survey (USCGS, 1870), soils maps by the U.S. Department of Agriculture (USDA, 2013), and aerial orthophotos[1] to refine the mapping. In our analysis of lidar data, we used hillshade images with simulated sun angles at 90 degrees and multiple directions at 45 degrees; some renderings blended multiple sun angles and (or) contours. We adapted methods outlined by Singhroy and others (1992a,b) using LANDSAT satellite image analysis, calibrated by our field observations, to identify surface sediment particle sizes and bedrock character to refine our unit boundaries. Edge mismatches with adjacent quadrangles are intentional, and based on differences in unit classifications or interpretation.

We used USGS Fact Sheet 2010-3059 for the geologic time scale (USGS Geologic Names Committee, 2010) and the Udden-Wentworth scale (table 5 in Pettijohn, 1957) to classify unconsolidated sediment. We compiled 21 pre-processed marine seismic profiles within the map area (Harding and others, 1988; Dadisman and others, 1997; Brocher and others, 1999; USGS Pacific Coastal & Marine Science Center, 2015). With help from Bill Lingley (Leslie Geological Services), we interpreted seismic stratigraphic packages and tectonic structures from six of the profiles beneath Puget Sound and Hood Canal. We display on the map only those seismic lines that we found helpful for our interpretations.

We used clast counts, petrographic review of sand content, sedimentary attributes (such as bedding style, grain size, and textural changes), and field relations to infer sediment sources and glacial or nonglacial unit characteristics. We assumed that sediment in which the major constituent clasts are sedimentary, low-grade metasedimentary, and mafic volcanic (basalt) are derived from the Olympic Mountains and Eocene to Oligocene volcanic and sedimentary rocks exposed in and near the map area. We identified deposits sourced (distinctly and near-exclusively) from the Olympic Mountains only among Olympia-age nonglacial deposits. We inferred that sediment containing a majority of high-grade metamorphic and plutonic clasts (quartzite, gabbro, granite, gneiss and other high-grade metamorphic rocks) were transported into the map area as the Puget lobe of the Cordilleran ice sheet advanced from the Coast Mountains of British Columbia. Sediment with relatively high content of potassium feldspar and monocrystalline quartz from granitic sources may be at least partly derived from Cascade Range sources, such as the Snoqualmie batholith, as suggested south and southeast of our map area by Contreras and others (2013, 2014). However, we found that the lithology and mineralogy in this map area are too varied to specifically attribute deposits to the Cascade Range. Where age control was absent or inconclusive, we attributed the stratigraphically highest deposit of glacial drift to the Cordilleran ice sheet during the Vashon Stade of the Fraser Glaciation (MIS 2).

Analytical results and locations for one new $^{40}Ar/^{39}Ar$, eight new radiocarbon, and six new luminescence analyses are summarized in Table 1; detailed results are presented in Appendix A. Trace-element and major-oxide geochemistry was performed on nine new basalt samples from the map area, and are presented in Appendix B with four samples previously analyzed by Clark (1989). Paleomagnetic analysis on six samples from Quaternary sediment throughout the quadrangles was undertaken to constrain the age of the oldest Quaternary deposits. Geochemical samples were analyzed by ALS, radiocarbon samples by Beta Analytic, Inc., and paleomagnetic samples by Bernard Housen (Western Washington University). Luminescence samples were prepared and analyzed by Shannon Mahan (USGS). $^{40}Ar/^{39}Ar$ sample analysis was performed by Daniel Miggins and staff at the Argon Geochronology Lab at Oregon State University. Microfossil samples at 11 bedrock sites (age sites GD15, 17–21, 23–26, and 32) were prepared by Ellington and Associates, Inc., and analyzed by E. Nesbitt (Burke Museum at the University of Washington). None of the samples yielded biostratigraphic constraints, although a single sample contained four unidentifiable foraminifera (GD15).

Deeter (1979) presented continuous and informative stratigraphic section interpretations along all coastal bluffs within the Hansville quadrangle. We prepared three additional columnar sections (1, 2, and 3) in order to present notable stratigraphic details from our new mapping. Throughout this report, we refer to the coastal bluff section diagrams prepared by Deeter as part of his thesis (Deeter, 1979) and to other sections from his unpublished notes (Gerstel and others, 2012a,b). Gerstel and others (2012a) digitally located the unpublished section diagrams, and Kitsap County posted them as a downloadable file (Gerstel and others, 2012b). Our map and text identify these and additional detailed section locations from Deeter (1979) as "CS#" sites in Table 2. We have posted the original thesis online (link listed with reference) to make the remaining sections readily accessible.

DESCRIPTION OF MAP UNITS

Quaternary Unconsolidated Deposits

HOLOCENE NONGLACIAL DEPOSITS

af **Artificial fill**—Boulders, cobbles, pebbles, sand, silt, clay, diamicton, organic matter, rip-rap, and concrete, in varied amounts, placed to elevate the land, or, west of Basalt Point, to dispose of material excavated elsewhere; fill may be engineered. We show unit af where readily verifiable, fairly extensive, and thick enough (>5 ft) to be geotechnically significant. The unit excludes minor road fills and areas where underlying geology was deemed more informative. Unit af is manmade, historic in age, and mapped in scattered locations throughout the Port Ludlow quadrangle and at Coon Bay on the west shore of the Kitsap Peninsula; unit af is up to 100 ft thick along Paradise Bay Road.

[1] Photo series, in order of frequency of use: 2009 30-cm color; 2013 3-ft color (National Agriculture Imagery Program 4-band, includes infrared); 1990–2000 3-ft black and white; 2003–2005 18-in. color.

Table 1. Summary of new age data from the Port Ludlow and Hansville quadrangles. See Appendix A for detailed analytical results, sample descriptions, and ages compiled from previous studies. Radiocarbon ages are given as a calibrated 2σ range; luminescence and argon ages have a 2σ uncertainty. Paleomagnetic data were processed by Bernard Housen, Western Washington University.

Sample	Unit symbol	Location	Method	Result
GD1	Qa	sec. 32, T29N R1E	^{14}C (AMS)	0.29–0.24, 0.23–0.06, or 0.04–0 ka
GD2	Qco	sec. 13, T28N R1E	^{14}C (AMS)	26.59–26.19 ka
GD3	Qco	sec. 21, T28N R1W	^{14}C (AMS)	27.75–27.53 ka
GD4	Qco	sec. 12, T28N R1W	^{14}C (AMS)	41.81–40.68 ka
GD5	Qgas	sec. 25, T29N R1W	^{14}C (AMS)	47.68–45.21 ka
GD6	Qco	sec. 22, T28N R2E	^{14}C (AMS)	> 43,500 ^{14}C yr BP
GD7	Qc	sec. 17, T28N R2E	^{14}C (AMS)	> 43,500 ^{14}C yr BP
GD8	Qc in Qls block	sec. 12, T28N R1E	^{14}C (AMS)	> 43,500 ^{14}C yr BP
GD27	Qco	sec. 22, T28N R2E	OSL IRSL	>65 ka 71.07 ±12.08 ka
GD28	Qgdp	sec. 22, T28N R1E	OSL	56.36 ±10.16 ka
GD29	Qco	sec. 12, T28N R1W	OSL	30.68 ±4.90 ka
GD30	Qco	sec. 6, T28N R1E	OSL	46.57 ±7.98 ka
GD31	Qco	sec. 12, T28N R1E	OSL	34.77 ±3.82 ka
GD33	Evc	sec. 33, T29N R1E	^{40}Ar/^{39}Ar age plateau	50.51 ±0.16 Ma
M1	Qpdp	sec. 12, T28N R1W	paleomagnetic	normal
M2	Qpf	sec. 12, T28N R1W	paleomagnetic	reverse
M3	Qpf	sec. 7, T28N R1E	paleomagnetic	transitional (?)
M4	Qps	sec. 17, T28N R1E	paleomagnetic	normal
M5	Qpf	sec. 5, T28N R1E	paleomagnetic	reverse
M6	Qco	sec. 6, T28N R1E	paleomagnetic	normal

Table 2. Columnar section names and locations. Sections listed only by number are from this study. Sections listed as "CS#" identify locations and original page numbers from Deeter (1979). CS numbers are newly assigned by this study. Light gray shading indicates columns archived at DGER and published in appendix B-f of Gerstel and others (2012b); dark gray shading indicates columns published in appendix B-g of Gerstel and others (2012b). – – – indicates no data.

Section name	Location	Original figure number	Original page number
1	sec. 12, T28N R1W	– – –	– – –
2	sec. 22, T28N R2E	– – –	– – –
3	sec. 12, T28N R1E	– – –	– – –
CS1	sec. 29, T28N R2E	– – –	130
CS2	sec. 29, T28N R2E	– – –	129, south
CS3	sec. 29, T28N R2E	– – –	129, center
CS4	sec. 19, T28N R2E	– – –	129
CS5	sec. 18, T28N R2E	– – –	128
CS6	sec. 18, T28N R2E	– – –	126, east
CS7	sec. 13, T28N R1E	– – –	126
CS8	sec. 12, T28N R1E	– – –	125
CS9	sec. 12, T28N R1E	– – –	124
CS10	sec. 7, T28N R2E	– – –	124
CS11	sec. 7, T28N R2E	– – –	123, north
CS12	sec. 7, T28N R2E	– – –	123, center
CS13	sec. 7, T28N R2E	– – –	123, center
CS14	sec. 18, T28N R2E	– – –	122
CS15	sec. 18, T28N R2E	– – –	122, east
CS16	sec. 17, T28N R2E	– – –	121, east
CS17a	sec. 17, T28N R2E	– – –	120
CS18	sec. 17, T28N R2E	– – –	119, west
CS19b	sec. 22, T28N R2E	38C	66, 117
CS20	sec. 22, T28N R2E	38B	66, 118
CS21	sec. 22, T28N R2E	38A	66, 119
CS22	sec. 26, T28N R2E	6C	19

[a] Location here is 500 ft west of location shown by Gerstel and others (2012b).
[b] Radiocarbon site GD12 (samples UW-448 and I-10,374)

ml **Modified land**—Boulders, cobbles, pebbles, sand, silt, clay, diamicton, and organic matter, in varied amounts; locally derived but redistributed to modify topography; underlying units exposed in some cuts; we show unit ml where fairly extensive and thick enough (>5 ft) to be geotechnically significant, but exclude roads and pits where underlying units can be readily identified or were deemed more significant. It is mapped north and south of Port Ludlow.

Qb **Beach deposits**—Sand, pebbly sand, pebbles; less commonly cobbles, silt, clay, shells, wood, peat, and isolated boulders; loose; clasts typically moderately to well rounded and oblate; locally well sorted; derived from shore bluffs, streams, and underlying deposits. Unit Qb is transient in the modern environment and underlying units are intermittently exposed by episodic or periodic erosion. The age of unit Qb is constrained to less than about 6,000 yr BP; prior to this period, sea level was too low to deposit beach sediment at or above present-day

sea level (Eronen and others, 1987; Dragovich and others, 1994; Mosher and Hewitt, 2004).

Qm **Salt marsh deposits**—Organic sediment and (or) loose clay, silt, and sand in a saltwater to brackish coastal wetland; in most areas mapping of unit Qm is supported in part by wetlands and (or) ponding shown in 'T-sheet' historic coastal surveys. The age of unit Qm is constrained to less than about 6,000 yr BP for the same reason as unit Qb.

LATEST PLEISTOCENE TO HOLOCENE NONGLACIAL DEPOSITS

Qp **Peat**—Organic and organic-rich sediment; includes peat, gyttja, muck, silt, and clay; typically in closed depressions; up to 33 ft thick along peat survey line Rigg B (secs. 1 and 12, T28N R1W) from Rigg (1958, p. 66); unit thickness unconstrained elsewhere; mapped in wetland areas and distinctly flat-bottomed depressions, and (or) where identified based on prior mapping (Rigg, 1958; USDA, 2009), and (or) where color and vegetation patterns in infrared and color aerial photos suggest its presence.

Qls **Landslide deposits**—Cobbles, pebbles, sand, silt, clay, boulders, diamicton, siltstone, and sandstone in varied amounts within areas of mass-wasting; clasts angular to rounded; unsorted; generally loose, jumbled, and unstratified, but locally retaining primary bedding and compaction. Unit Qls deposits appear thickest in the southwest part of Chimacum Valley where the unit has 150 ft of relief, and at Foulweather Bluff, where it has 140 ft of relief. Absence of a mapped slide does not imply absence of sliding or hazard. Many slide areas are unmapped where too small to show at map scale, or because steep slopes, beach waves, or streams have dispersed their deposits. Mass-wasting features that are not confidently recognized as landslides are shown as unit Qmw. Some slide areas include exposures of underlying units.

Qmw **Mass-wasting deposits**—Cobbles, pebbles, sand, silt, clay, boulders, or diamicton, in varied amounts; typically loose; generally unsorted; locally stratified; mapped mostly along colluvium-covered or densely vegetated slopes that are potentially or demonstrably unstable; locally includes alluvial fans, debris fans, landslides too small to show separately or those that could not be confidently mapped, and exposures of underlying units. The maximum thickness of unit Qmw is indeterminate, but the unit spans up to 140 ft of relief northwest of Swansonville. Unit Qmw includes at least one possible landslide deposit (sec. 20, T28N R2E) that appears truncated at its base by a relict glaciomarine shoreline, suggesting that slide movement last occurred during or shortly after deglaciation. Absence of a mapped mass-wasting deposit does not imply absence of slope instability or hazard.

Qa, Qoa **Alluvium**—Sand, silt, clay, peat, pebbles, and cobbles along active or abandoned stream channels; clasts and matrix generally gray and fresh, but in some exposures weathered to orange brown and iron-stained red; loose; clasts typically well rounded and moderately to well sorted; stratified to massively bedded; derived from local sources and deposited in streams and on flood plains. Unit Qa resembles, and likely includes, relict alluvium (units Qoa and Qgo) and was mapped where modern geomorphic activity was inferred. Radiocarbon date GD1 (160 ±30 ^{14}C yr BP) documents that valley floor sediment at that site was recently deposited due to transient damming by a down-valley landslide. The date therefore implies significant on-going sediment flux in this drainage—whereas some drainages elsewhere in the map area are clearly inactive (units Qoa and Qgo). Unit Qa includes a marine-deltaic mudflat along the south shore of Port Ludlow.

Qaf **Alluvial fan deposits**—Pebbles, sand, cobbles, boulders, and silt, in varied amounts; gray to brown; loose; moderately to poorly sorted; stratified to poorly stratified; derived from local sources and deposited in concentric lobes where streams emerge from confining valleys. Deposition is commonly sudden, hazardous, and associated with significant storm events. Unit Qaf may be up to 80 ft thick in Chimacum Valley. We agree with Hanson (1977) who suggests that most fan material is Vashon recessional outwash; we therefore mapped unit Qgoaf where fans are sourced from valleys that lack active channels or streams are too incised to add sediment to the fan surface. We note that in many areas mapped as unit Qaf, much or most of the fan volume is likely also Vashon age.

PLEISTOCENE GLACIAL AND NONGLACIAL DEPOSITS

Qgdm$_e$ **Everson Glaciomarine Drift**—Silt and clay with sand, trace pebbles, cobbles, and boulders; locally grades to or contains lenses of diamicton, some of which resembles unit Qgt but tends to be less compact; pale gray to buff, weathers orange-tan; soft to medium soft; poorly sorted; prone to columnar jointing, and consequently, to block failure along cliffs. We did not observe marine shells in the unit, although Swanson (1994) did at sites GD9 and 10 (sec. 33, T29N R1E). Maximum apparent unit thickness is 25 ft in the Hansville quadrangle (sec. 21, T28N R2E). The unit resembles Vashon glaciomarine drift to the north of the map area (Domack, 1982, 1983, 1984; Dragovich and others, 2005; Schasse and Slaughter, 2005; Polenz and others, 2005, 2006). At least 20 ft of glaciomarine drift is exposed above Vashon till in bluffs in the Hansville quadrangle (sec. 18, T28N R2E). Unit Qgdm$_e$ most commonly overlies unit Qgt, but also onlaps units Qgos, Qgo, and older units across the northern portions of the Hansville quadrangle. Unit Qgdm$_e$ was recognized at a maximum elevation of ~135 ft above modern sea level, consistent with findings

from nearby areas at similar latitude (Polenz and others, 2006, 2014; Schasse and Slaughter, 2005). It is only covered by post-Vashon deposits (units Qm, Qp, Qa, and Qoa).

Vashon Drift of the Fraser Glaciation

Qgo **Vashon recessional outwash**—Sand with pebble and cobble gravel and occasional silt and clay; mostly quartzo-feldspathic, with high-grade metamorphic, metasedimentary, plutonic, and basalt clasts, supplemented in the Port Ludlow quadrangle by locally derived basalt clasts; mostly brown-gray where fresh, brown, red, and yellow where iron-stained from weathering; mostly thin in the map area—maximum observed thickness is 30 ft in sec. 28, T28N R2E. Unit Qgo is distinguished from similar, more recent alluvium (units Qa, Qoa) by better sorting and its geomorphic distribution. Unit Qgo was deposited by glacial meltwater, usually with a high rate of sedimentation. Subdivided into:

Qgog **Vashon recessional outwash gravel**—Pebble gravel with rare cobbles and coarse-sand matrix; brown and (or) gray where fresh, commonly weathered to orange-brown or red; well sorted, subrounded to rounded clasts; medium dense. Unit displays crossbedding and cut-and-fill structures and was deposited in large outwash channels in the southern Port Ludlow quadrangle where it is between 5 and 25 feet thick. Vashon recessional outwash lies stratigraphically above units Qgt, Qgic and Qgas, and it forms roughly flat terraces up to 20 ft thick in the southwest of the Port Ludlow quadrangle. Unit Qgog may be present in the subsurface beneath Chimacum Valley near the northwest map corner, although our review of well records there provided only limited and ambiguous evidence for it. Elsewhere in the map area, unit Qgog is not capped by any deposits, nor incised.

Qgos **Vashon recessional outwash sand**—Sand and some beds and lenses of pebbles, silt, and clay; gray to pale brown; clasts moderately to well rounded; moderately to well sorted and stratified; loose and generally less compact than glacially overridden advance outwash sand (units Qgas and Qpo). Well records suggest a maximum thickness of less than 30 ft southeast of Hansville. Unit Qgos was deposited by overland flow, or as slackwater deposits into a lake or marine water. Along the southern edge of the Port Ludlow quadrangle, unit Qgos is shown where exposures are sand-dominated and we interpret these deposits as a mostly fluvial part of the same fluvio-deltaic system mapped as unit Qgod just to the west. However, Contreras and others (2013) included equivalent deltaic downslope deposits as unit Qgos south of the Port Ludlow quadrangle.

Just south of Port Ludlow (sec. 21, T28N R1E), small excavations consistently exposed silt to very fine sand, suggesting low-energy deposition and a finer texture than is typical of unit Qgos elsewhere. In the Hansville quadrangle, south of Point No Point and west of Norwegian Point, thick sand to silty sand between ~135 and 290 ft elevation is included with unit Qgos because here sedimentary structures suggest a subaqueous setting, the deposits are above the apparent glaciomarine maximum inundation level, shells (which are more likely in marine waters than in proglacial lakes) were not observed, and the deposits were loose. The uppermost of these deposits approximate the 285 ft elevation estimate of Haugerud (2009) for the northernmost part of Lake Bretz. However, Haugerud (2009, fig. 1) also showed glaciomarine features at similar elevations, and we have not excluded a glaciomarine origin, especially in light of possible land level changes due to Quaternary deformation (see *Evidence for Pleistocene to Recent Deformation*).

Qgoaf **Vashon recessional alluvial and delta fan deposits**—Sand, pebbles, cobbles, boulders, and silt, in varied amounts; gray to brown; loose to moderately compact or slightly indurated; moderately to poorly sorted; stratified to poorly stratified; derived from local sources and deposited in concentric lobes where streams emerge from confining valleys. We map unit Qgoaf where fans are truncated by Vashon meltwater incision (for example, sec. 25, T29N R1W).

Qgod **Vashon recessional glacial delta deposits**—Sand and silt, locally with pebble gravel; gray to pale brown; soft and loose to slightly stiff and cohesive; moderately sorted; contains sandy to pebbly topsets and foresets with mostly silty bottomsets of relict glacial lake or marine deltas. Maximum unit thickness of less than 55 ft is inferred above the shore of Port Ludlow (sec. 17, T28N R1E) and south of Tala Point (sec. 22, T28N R1E). Deposits of unit Qgod straddle (and in places disrupt) relict shorelines, which we would expect to approximate delta front slope breaks. For simplicity of display, shorelines are shown along the upper edge of unit Qgod in many areas (such as near the southern edge of the Port Ludlow quadrangle). This choice locally exaggerates the elevation of some shoreline segments and could misleadingly suggest that all of unit Qgod was deposited subaqueously. Where unit Qgod

extends especially far upslope, some shoreline segments are omitted.

Qgic **Vashon ice-contact deposits**—Diamicton (ablation till, flow till, and poorly compacted or isolated exposures of lodgment till), pebble and cobble gravel, sand, lacustrine mud, and isolated boulders; pale- to ash-gray, tan, or brown; can be slightly weathered; loose to compact; poorly to well sorted; massive to well stratified; sand and clasts typically northern-sourced. Unit thickness ranges from a few feet to more than 80 ft as inferred from well records beneath Chimacum Valley (sec. 7, T28N R1W). Unit Qgic was deposited by meltwater and ice, mostly late in the Fraser Glaciation. The unit commonly coincides with landforms associated with stagnant ice near the end of glaciation, such as kettles, hummocky topography, topographic ripples and disrupted surfaces on or between flutes, and subglacial or subaerial outwash channels. Where such landforms are present, lodgment till is commonly absent or only a few feet thick. Unit Qgic also includes other ice-contact deposits (such as eskers). Unit Qgic locally contains over-steepened beds and isoclinal folds that developed due to sub-ice flow dynamics, and collapse features that formed after melting of nearby ice or by glaciotectonic deformation. Till facies in most exposures are more porous and more friable than unit Qgt. Because of this, much of the unit does not form an aquitard or may form a 'leaky' aquitard (Polenz and others, 2010) unlike the less permeable unit Qgt. Unit Qgic is mapped where till contains less mud than is commonly found in the matrix of well-developed lodgment till (unit Qgt). The unit locally grades to "sub-glacially reworked till" (Laprade, 2003). For additional discussion of the Fraser Glaciation, leaky aquitards, landforms associated with till, and similarities among units of Vashon Drift east and south of the map area, see also Haugerud (2009), Polenz and others (2009a,b, 2010, 2011), and Contreras and others (2012a,b,c).

Qgt **Vashon lodgment till**—Matrix supported diamicton consisting of silt and sand matrix with clay, pebbles, and cobbles, in varied amounts with isolated boulders; plutonic, basaltic, and metamorphic erratic boulders are common in the till and on fluted surfaces; sand and pebbles to cobbles are northern-sourced; gray to brown or tan; usually lightly weathered or unweathered; compact and resembles concrete where well-developed (commonly referred to as 'hardpan'); commonly hackly or looser near the surface, with loose diamicton (ablation till) comprising the upper 1 to 10 ft; less porous than unit Qgic in most exposures; clasts occasionally striated and faceted with subangular or rounded edges; unsorted; unstratified (but locally banded); forms a patchy cover, with typical exposures 3 to 15 ft thick, but up to 90 ft thick along the southeast shore of the Hansville quadrangle (sec. 35, T28N R2E). Except for surficial late-glacial ablation till, unit Qgt was deposited directly by the advancing Cordilleran ice sheet. Some exposures include locally sheared and jointed lenses or layers of sand, pebbles, and cobbles. Unit Qgt caps many fluted surfaces but is commonly discontinuous. Lodgment till locally forms an effective aquiclude, but varied till thickness and stratigraphic relationships (in some instances gradational) with more permeable ice-contact deposits and outwash channels suggest that the aquiclude is leaky at map scale (Haugerud, 2009; Polenz and others, 2009a,b, 2010; Contreras and others, 2012a,b,c). We mapped unit Qgt where we observed stronger lodgment till development—and typically better development of fluting—than where we mapped unit Qgic. Unit Qgt is typically in sharp, unconformable contact with underlying units. Unit Qgt lies stratigraphically below unit Qgo and above unit Qgas.

Qgas **Vashon advance outwash sand**—Sand with pebble gravel and trace silty layers; interbedded sand and silt overlie silt at columnar section 1 (Table 2; Map Sheet); pale brown, gray, or salt-and-pepper gray; compact in most exposures, but can be loose where well sorted; some compact exposures become cohesionless and lose all strength when either dry or saturated (but not when moist) and therefore may seem loose; clasts typically subrounded to well rounded and moderately to well sorted; massive, with graded (mostly fluvial) beds, cut-and-fill structures, trough-and-ripple crossbeds, or foreset deltaic beds; mostly quartzo-feldspathic with less than 4 percent potassium feldspar and more than 30 percent polycrystalline quartz; includes some granite, basalt, gabbro, and metamorphic lithics; also contains trace detrital wood, peat, and charcoal, such as at site GD5. Unit Qgas forms greater than 150-ft-thick packages across parts of both quadrangles, and is up to 240 ft of massive sand above Qc_o in the southeast Port Ludlow quadrangle (secs. 22 and 27, T28N R1E). Unit Qgas is stratigraphically below unit Qgt, but where unit Qgt was not deposited or was removed by erosion, unit Qgas is exposed at the surface or directly underlies recessional outwash. Qgas is faulted and jointed at site GD5, where the sand contains trace amounts of remobilized detrital wood and charcoal fragments dated at 47.7–45.2 ka (Table 2; Appendix A). The unit may include some unrecognized older deposits (see also units Qc_o and Qps).

Pre-Vashon Glacial Deposits

Qpo **Pre-Vashon outwash, undivided**—Sand, pebble gravel, and laminated silt, locally contains dropstones and diamicton (flow till); light gray, light brown, or tan; compact; moderately to well sorted; rounded to subangular clasts; silty facies are massive to laminated, sandy facies are crossbedded or massive, and both are locally interbedded. Patchy cliff exposures of interbedded sand and pebble gravel suggest that unit thickness may exceed 170 ft near Tala Point, where we mapped deposits directly beneath Vashon till as pre-Vashon outwash (unit Qpo) because well-exposed pre-Vashon drift (unit Qpd)

in the lower 100 ft at Tala Point appears laterally continuous. Furthermore, we identified no stratigraphic breaks downsection of Vashon till, documented Olympia-age nonglacial sediment at slightly higher elevation (180 ft) 1.5 mi farther west at age site GD3, and Contreras and others (2013) mapped sediments as Olympia age at up to 200 ft elevation 3.6 mi farther south. At Hood Head we mapped sediment directly beneath Vashon till as unit Qpo for the same reasons, and because Carson (1980) identified Double Bluff Drift, citing stratigraphic continuity (that we could not verify) with sediment southwest of the Hood Canal Bridge (1 mi south of Hood Head, sec. 2, T27N R1E); however, from our observations, the outwash at Hood Head could be Vashon age, not least because at least some of it appears to be subglacial.

Qpd **Pre-Vashon drift, undivided**—Sand, silt, and diamicton; tan, brown, and light to dark gray; compact; silty facies very stiff and hard; clasts subrounded and rarely angular; sand subrounded to subangular; well sorted where mostly sand, poorly sorted where diamicton; sand is quartzo-feldspathic, coarse sand and larger clasts are high-grade metamorphic, and less commonly basalt or metasediment; approximately 100 ft thick at Tala Point and the north side of Hood Head. At Tala Point, the south shore of Port Ludlow west of Tala Point, and within and east of Chimacum Valley (sec. 6, T28N R1E), the unit includes till that overlies up to 2 ft of pebble gravel above sand and fine-grained deposits. Unit is stratigraphically below unit Qgas at Tala Point, and below unit Qc_o east of Chimacum Valley. For the same reasons that unit Qpo was mapped southeast of Tala Point and at Hood Head, unit Qpd includes lacustrine (or marine?) drift directly beneath Vashon recessional deposits (unit Qgod) at White Rock, and beneath Vashon till along the north side of Hood Head. Locally subdivided into:

Qgd_p **Possession Drift**—Diamicton, sand and pebble gravel, and massive to crossbedded sand; diamicton matrix at Foulweather Bluff is mostly silt to clay, diamicton matrix 0.7 mi farther south at columnar section 3 (sec. 12, T28N R1E) is mostly sand to silt; diamicton is dark blue-gray, sand is light orange-brown or tan; compact and hard; diamicton at Foulweather Bluff and columnar section 3 includes granitic and high-grade metamorphic clasts (GD 13 and GD14) and shells that Elizabeth Nesbitt (Burke Museum of Natural History, oral and written commun., 2015) identified as marine, in agreement with previous assessments by W. Dall (cited by Bretz, 1913; see also CS9). Deposits below units $Qgdm_e$, Qgic, and Qps along the Skunk Bay shore (CS14) are included with unit Qgd_p because Deeter (1979) observed shell-bearing diamicton at beach-level, which matches the elevation of unit Qgd_p at Foulweather Bluff and columnar section 3. The most complete exposure of Possession Drift is at columnar section 3, where 65 feet of Vashon Drift (units $Qgdm_e$, Qgt) and Olympia nonglacial sediment (unit Qc_o) overlie at least 15 feet of glaciomarine drift directly above northern-sourced fluvial sand. This fluvial sand was dated using OSL at 56.37 ±5.08 ka (GD28) and provides our main rationale for mapping unit Qgd_p at and near Foulweather Bluff. The diamicton is paleomagnetically normal at Foulweather Bluff (site M1), where Bretz (1913) and Deeter (1979) reported underlying till (CS9). A detrital wood fragment from silt above the diamicton at Foulweather Bluff yielded a radiocarbon-infinite ^{14}C date (GD8). The silt appears to be part of a landslide block and therefore likely represents unit Qc_o from higher up in the Foulweather Bluff section (see also *Ages of Quaternary Units*).

Pre-Vashon Nonglacial Deposits

Qc **Pre-Vashon alluvium**—Sand, interbedded with and grading into silt and clay, locally contains sandy gravel, rare wood, and rare peat; pale- to medium-gray (where sandy), dark gray (where silty), gray brown, light brown, or brown; compact and usually stiff. The presence of appreciable quantities of wood and peat were used as an indicator that pre-Vashon sediment is nonglacial, especially in well records, and where not refuted by other stratigraphic evidence. Other criteria for identifying nonglacial deposits include low-energy fluvial and floodplain sedimentary structures, mostly north-directed paleocurrent indicators, mineralogy that does not clearly point to northern provenance, and prior mappers' assessments. Unit Qc is 130 ft thick along the east shore of the Kitsap Peninsula. The age of unit Qc may span multiple nonglacial periods. Locally subdivided into unit Qc_o where age control or lateral relationships permit.

Qc_o **Pre-Vashon alluvium of the Olympia nonglacial interval**—Sand, less commonly silt, clay, pebble gravel, peat, and trace detrital wood; light brown, brown, gray, or dark gray; compact and locally stiff; moderately well sorted; horizontally planar bedded, crossbedded, or massive. Clast content and petrographic analysis of sand (and silt) indicate that much of unit Qc_o east of and in Chimacum Valley is Olympic Mountains-sourced. Samples upsection from age site GD29 at columnar section 1 are especially rich in basalt clasts and suggest an Olympic Mountains source that derives sediment mainly from upper Crescent Formation rocks, such as the modern Quilcene River drainage. Sediment is more quartzo-feldspathic downsection from GD29, at site GD31 on the east side of the valley, and at site GD30 between Chimacum Valley

and Swansonville. We suspect these locations contain sediment derived from a large Olympic Mountains drainage with a mix of Crescent Formation and sedimentary rocks from the core of the Olympic Mountains. Likely rivers are the Dosewallips and (or) Duckabush Rivers which were mineralogically characterized in figure B2 of Polenz and others, 2012c. Elsewhere, sediment sources in unit Qc_o are less well defined and may include sources in the Cascade Range, Olympic Mountains, and (or) older deposits within the Puget Lowland.

Outside of Chimacum Valley, we observed very little pebble gravel within the unit. In the Hansville quadrangle, unit Qc_o contains low-energy floodplain and channel deposits. A 65-ft-thick section exposed mid-cliff at columnar section 2 (Map Sheet) contains at least five upward-fining sequences that grade from crossbedded sand to clay. Unit thickness at that site exceeds 100 ft if the unit extends down to beach level, which it does 1,275 ft farther north at CS19. However, age control data suggest that the section between columnar section sites 2 and CS19 may not be laterally continuous (see Ages of Quaternary Units). Farther south along the same shore, unit Qc_o is about 100 ft thick beneath a similar thickness of Vashon advance outwash sand (CS22). Unit Qc_o is widespread in the subsurface.

Most of the pre-Vashon Quaternary dates in the map area (11 of 15) are from unit Qc_o. Three other radiocarbon-infinite dates would have permitted mapping of the unit but were less stratigraphically constrained and were therefore mapped instead as units Qc and Qgas. Along Chimacum Valley, unit Qc_o is exposed below Vashon outwash and till (units Qgas and Qgt) and above either bedrock or Quaternary silt. At least some of the Quaternary silt is paleomagnetically reversed (site M2, sec. 12, T28N R1W). A nearby site in similar lithology may be paleomagnetically transitional (site M3, sec. 7, T28N R1W). If derived from the brief Laschamp subchron (Fig. 2), these silts could also be of Olympia age (see *Ages of Quaternary Units* for further discussion). Along the road northeast of Swansonville (sec.6, T28N R1E), Olympia age deposits overlie undivided pre-Vashon drift (unit Qpd).

Undivided Glacial and Nonglacial Deposits

Qps **Pre-Vashon sediment, sand**—Sand with minor silt and pebble gravel; light brown, tan, or gray-brown; brown to orange-brown where oxidized; dense to very dense, locally cohesive. We infer that deposits within unit Qps are glacial where quartzo-feldspathic with ample polycrystalline quartz, occasional potassium feldspar, and metamorphic lithic fragments. We infer a nonglacial provenance where monocrystalline quartz is more common, there is 0–12 percent potassium feldspar, up to 30 percent white mica, and rare Olympic Mountains-sourced metasedimentary and basalt lithic fragments. Many exposures are mapped as unit Qps in part because their provenance appears to be mixed. We infer a thickness of more than 150 ft south of Port Ludlow (sec. 32, T28N R1E). Unit Qps is mapped downsection from unit Qc_o southwest of Tala Point, where radiocarbon date site GD3 constrains the age of some pre-Vashon deposits to Olympia nonglacial age. At Foulweather Bluff, date sites GD4 and GD29 similarly suggest that Qps lies beneath Olympia nonglacial deposits. Where upsection Olympia nonglacial deposits were not recognized, the unit may include Vashon advance outwash.

Qpf **Pre-Vashon sediment, fine-grained**—Silt, clay, and mixtures of both, includes fine sand in some exposures; light-green-gray to dark-gray, dense and hard; commonly fractured with oxidation on fractures; planar bedded or massive. Up to 110 feet of unit Qpf is exposed beneath unit Qgas in both the Hansville and Port Ludlow Quadrangles. Unit Qpf includes some undated silt and clay directly beneath unit Qgas—and may therefore include some Vashon advance outwash (Lawton Clay). Three of six paleomagnetic samples in the map area are from unit Qpf, and all three are either reversed or at least potentially transitional, suggesting that the unit may include sediment of pre-Matuyama age (see *Ages of Quaternary Units*).

Qpu **Pre-Vashon sediment, undivided**—Sand, pebble gravel, silt, clay, diamicton, organic sediment, and boulders, in varied amounts; color and weathering varied; compact; varied grain size, rounding, sorting, and bedding. Hydrocarbon exploration well site HC4 (sec. 17, T28N R2E) documents nearly 1,100 ft of the unit, and it may be even thicker elsewhere in the Hansville quadrangle. In the Port Ludlow quadrangle, the unit is 200 ft thick northeast of Swansonville (sec. 6, T28N R1E). Unit Qpu is mapped where sediment age, paleoenvironment, and provenance were poorly known or too diverse to separately show (see also *Ages of Quaternary Units*). Although generally mapped as pre-Vashon, the unit may include some Vashon advance outwash (unit Qgas).

Qu **Quaternary sediment, undivided (cross section only)**—Unit Qu was entirely inferred from seismic section interpretation and is shown only beneath marine water in the cross section. We speculate that the unit is mainly Vashon drift and post-glacial marine sediment.

Tertiary Sedimentary and Volcanic Bedrock

ΦEm_q **Quimper Sandstone (Eocene to Oligocene)**—Sandstone, typically with calcite cement, locally grades

to siltstone; contains spherical and elliptical calcareous concretions up to 9 in. across, and rare well-rounded chert pebbles; gray to olive-gray, weathers yellowish tan; fine to coarse grained, mostly subangular or angular; typically massive to faintly bedded, locally thin bedded to laminated or crossbedded; contains marine mollusk shells, fossilized wood fragments, and euhedral pyrite grains. The sandstone has been identified in the map area only along the shore of Oak Bay (Durham, 1942, 1944; Allison, 1959; Thoms, 1959; Rauch, 1985; Yount and Gower, 1991). Water well W71 (sec. 19, T29N R1E) suggests a thickness of 162 ft. The depositional environment was interpreted by Rauch (1985) and Armentrout and Berta (1977) as a shallow marine (neritic to upper bathyal) transgressive continental shelf, and Rauch (1985) classified the sandstone as lithic and feldspathic arenites and wackes.

The gently dipping beds of unit ΦEm$_q$ unconformably overlie basalt flows of unit Ev$_c$. An angular unconformity, and the possibility of a faulted contact, are discussed below (see *Faults Between Crescent Formation and Sedimentary Rocks*). We agree with Yount and Gower (1991) and Schasse and Slaughter (2005) in mapping the unit as Oligocene to Eocene (see *Bedrock Units*). Rauch (1985) inferred from petrographic characteristics that Quimper Sandstone is derived from granitic rocks, andesite, basalt, and chert, such as that which would have been available on Vancouver Island, the Coast Plutonic Complex, or the North Cascades. Rauch (1985) additionally mentioned the San Juan Islands and Crescent Formation as possible sources, although the basalt-dominated Crescent Formation would require mixing with another source because it offers little andesite and no granitic rocks.

ΦEm **Undifferentiated sedimentary rocks (late Eocene to early Oligocene)**—Phyllosilicate mudstone, siltstone, and sandstone; pale tan, medium to dark gray, most exposures weathered to shades of brown; moderately compact with embayed mineral grains and clast impingement; no obvious grain cementation. Sandstone is medium-grained and equigranular. Sandstone is poorly sorted and angular to subrounded. Siltstone is rhythmically laminated with occasional fine sand. Unit ΦEm in the map area may be best exposed in a 15 ft section of horizontally bedded, relatively unweathered siltstone at GD23 (sec. 6, T29N R1E). Unlike nearby exposures of Quaternary sediment, the deposits within unit ΦEm are more lithified. We assign these rocks an Oligocene to Eocene age based on lithologic and stratigraphic similarity to rocks of this age in nearby areas (Whetten and others, 1988; Yount and Gower, 1991; Haeussler and others, 1999; Schasse and Slaughter, 2005; Tabor and others, 2011; Contreras and others, 2013, 2014; Polenz and others, 2013, 2014). Four silica-replaced foraminiferal specimens from GD15 (sec. 1, T28N R1W) are not tectonically deformed, but too poorly preserved to permit definitive identification. We speculate that unit ΦEm does not range to the Miocene because a (limited) record of Miocene terrestrial rocks in the Puget Lowland (Fulmer, 1975; Yount and Gower, 1991; Haugerud, 2005) suggests a regional (?) transition to subaerial conditions, whereas rhythmic bedding in at least some exposures of unit ΦEm suggests a deeper marine basin.

Ev$_c$ **Crescent Formation basalt (early to middle Eocene)**—Aphanitic basalt in massive to columnar flows, plagioclase phenocrysts rarely visible in hand sample, greater than 0.5 in. augite crystals common in at least one flow (site G2; sec. 19, T28N R1E); rarely brecciated, except along flow contacts; contains pillows just south of Olele Point (Thoms, 1959; Yount and Gower, 1991) and at Shine Quarry (Bryan Garcia, Washington Division of Geology and Earth Resources, oral commun., 2015); south of Olele Point basalt is interbedded with marine siltstone and sandstone (Yount and Gower, 1991); medium to pale gray and dark gray where fresh; weathers gray and medium yellow-brown. In thin section, basalt groundmass texture is cryptocrystalline to micro-gabbroic. Phenocrysts are commonly elongate plagioclase, with no obvious orientation; pyroxene and olivine are typically less than 5 to 10 percent of phenocrysts; olivine is rarely altered to iddingsite.

Basalt within the map area only crops out in the Port Ludlow quadrangle between Chimacum Valley and Hood Canal. This distribution and shallow subsurface basalt occurrences documented by well records along Oak Bay generally coincide with the Port Ludlow uplift. Surface relief suggests that unit Ev$_c$ is more than 450 ft thick south of Port Ludlow; water well W18 indicates the unit is more than 400 ft thick in the subsurface west of Port Ludlow (sec. 18, T28N R1E); more than 1,300 ft of Crescent Formation is shown in the cross section because it is the oldest known rock in the map area and because the magnetic and gravity highs that help define the Port Ludlow uplift (Fig. 1) likely result from significant amounts of near-surface basalt. However, the Crescent Formation is more than 10 mi thick along the Dosewallips River 13 mi southwest of the map area (Hirsch and Babcock, 2009), and it is not clear that it maintains this thickness in the map area—for four main reasons: (1) observed flows are no more than about 60 ft thick—much thinner than along the Dosewallips section; (2) local peaks in magnetic field strength do not simply correspond to the presence of basalt at the surface—perhaps the field strength has more to do with magnetic signal orientation than basalt thickness; (3) gravity data are less densely spaced than the magnetic data, and we did not draw detailed conclusions from them; (4) the tectonic regime in the area is not well understood, and the surficial presence of basalt may be a result of thrusting of basalt over sedimentary rocks—this might help explain the presence of bedding plane shear and a clastic dike of sedimentary rock in basalt at the Shine Quarry. Stacked thin thrust sheets of unit Ev$_c$ and sedimentary rocks might produce the observed gravity high in the area without requiring significant thickness of unit Ev$_c$.

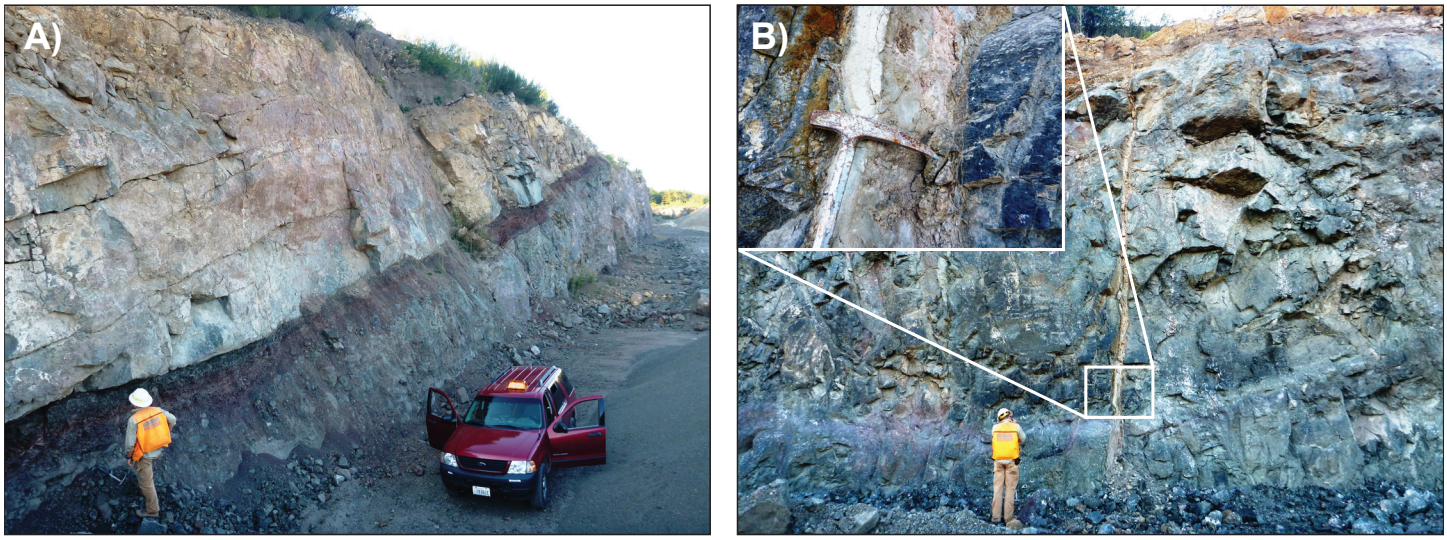

Figure 4. **A)** Basalt flows at Shine Quarry. Basalt flows at the quarry are between 12- and 40-ft-thick and massive to locally columnar. They consistently dip 16 to 24 degrees west. A distinctive 2.5-ft-thick red and dark green contact is the boundary between two basalt flows. Phyllitic luster and elongated fabric in microbreccia at this and other flow bed contacts suggest low-grade metamorphism from shearing along bedding planes. View to northeast in the fall of 2014. **B)** Clastic dike in basalt at Shine Quarry (sec. 30, T28N R1E). Dike is fine-grained, texturally immature sandstone, apparently derived from a felsic source. Geologist in lower left is 6 ft tall; the 25-ft-high quarry wall exposes a single flow. Brown, weathered basalt marks the top of the flow; the base of the 30-ft-thick flow is not exposed in the photo. View to northwest in the fall of 2014.

In the southwest part of the quadrangle, outcrops—most notably at Shine Quarry (Fig. 4) and a Pope Resources quarry site (G2 and G3; sec. 19, T28N R1E)—and lineations from lidar indicate that west dipping basalt flows cover more than a square mile. Yount and Gower (1991) cite pronounced red interflow weathered zones as evidence of subaerial deposition. At Shine Quarry, one red flow contact zone was examined for microfossils (GD32) but did not yield any (E. Nesbitt, written commun., 2015). Some red and green flow contacts (Fig. 4) contain basaltic microbreccia in which phyllitic luster and elongated fabric suggest bedding plane slip that we suspect to be tectonic; Allison (1959) and Thoms (1959) mapped several flow-bed-parallel faults at and near Olele Point. Whole-rock geochemistry analyses (G1 to G13; Appendix B) indicate basalt and are similar to prior analyses of Crescent Formation basalt (Clark, 1989; Babcock and others, 1994; Polenz and others, 2012c, 2014). Port Ludlow basalt samples plot as intra-plate on the Zr/Y vs. Ti/Y diagram of Pearce and Gale (1977) and as continental arc on the Zr/Y vs. Zr diagram of Pearce and Norry (1979). Sample G1 (sec. 36, T29N R1W) plots outside the intra-plate basalt field as a plate-margin basalt and may have been altered after emplacement.

The Eocene age of unit Evc is well established south of Olele Point from biostratigraphic analysis (see *Ages of Bedrock Units*) and a new 50.51 ±0.16 Ma $^{40}Ar/^{39}Ar$ age (Table A3). However, fossiliferous sandstone at GD19 (sec. 29, T29N R1E), which was included in the Crescent Formation because it is flanked by basalt exposures on both sides, did not yield identifiable macrofossil shell fragments or foraminifera (E. Nesbitt, written commun., 2015). Thus, we do not know if this sandstone is a sedimentary interbed within unit Evc or part of a younger sedimentary rock unit.

A clastic dike was observed in the Shine Quarry, where it is 1.5–6 in. wide, nearly vertical, and cuts >25 ft-high walls of gently west-northwest-dipping basalt flows. The dike is composed of moderately sorted, texturally immature, fine-grained pale gray sandstone with sparse rip-up clasts of darker mudstone; mineral grains and rare lithic fragments are angular to subangular. No grain alignment, strain, or fabric is apparent. Major minerals include monocrystalline quartz, plagioclase, and hornblende with less mica, some pyroxene (?), a few percent potassium feldspar, and a few subangular to subrounded volcanic lithic fragments; 18 rip-up clasts up to 0.5 in. across consist of 13 siltstones, 2 schists, 1 granite (?), and 2 pale greenish gray rocks (perhaps andesite or a metamorphic rock).

Mineralogy suggests the source for the original sediments was granitic, perhaps the Cascade Range or Coast Plutonic complex, although the dike material has not been linked to any specific unit. We infer from the amount of lithification that it was most likely injected prior to the Quaternary. The dike could be derived from the Blue Mountain unit associated mostly with the base of the Crescent Formation (Tabor and Cady, 1978a). Our inference of a granitic source for the dike at least partly matches Einarsen's (1987) conclusion that the Blue Mountain unit was partly derived from the Coast Plutonic complex. However, we note that our dike sample contains a few percent potassium feldspar, which Einarsen (1987) found to be so rare in the Blue Mountain unit that most of his samples contained none. Alternatively, the dike could be sourced from units ΦEm, ΦEmq, or several other bedrock units near the map area. Regardless of which unit the dike was sourced

from, it was likely injected from below as the relatively rigid Crescent Formation basalt was thrust over sediments that were unlithified at the time. Alternative explanations in which the dike was injected from above or laterally are unsatisfying, but have not been ruled out.

AGES OF BEDROCK UNITS

The oldest unit in the map area is early to middle Eocene Crescent Formation basalt (unit Evc). A new 50.51 ±0.16 Ma $^{40}Ar/^{39}Ar$ date at GD33 (sec. 33, T29N R1E; Table A3) confirms this early Eocene age and is consistent with prior Crescent Formation basalt ages. Yount and Gower (1991) reported "Ulatisian foraminifera" among marine siltstone interbeds between basalt flows (GD34, sample G-79-60, sec. 28, T29N R1E). Everywhere else in the map area, unit Evc is undated but characterized by similarly thick basalt flows (where recognized) and geochemical composition (Appendix B), rarity of pillows, and absence of observed sedimentary interbeds. Further discussion of Crescent Formation age is offered by Arnold (1906), Allison (1959), Brown and others (1960), Rau (1964, 1981, 2000, 2004), Cady and others (1972a,b), Wolfe and McKee (1972), Spencer (1984), Whetten and others (1988), Babcock and others (1992, 1994); Squires and others (1992), Hirsch and Babcock (2009), and Polenz and others (2012a,b,c).

The lower Oligocene-Eocene Quimper Sandstone (unit ΦEmq) rests unconformably on unit Evc along the shore of Oak Bay, where Jacobson (1927) documented 1,800 ft of sandstone and siltstone. Durham (1942, 1944) reported that in the map area the unit contains fossil mollusks, coral, echinoids, and brachiopods (GD35; sec. 29, T29N R1E, and GD36; sec. 19, T29N R1E). Jillson (1915) added that the unit also contains pelecypods, gastropods, scaphopods, and arthropods (GD37; sec. 19, T29N R1E). Jillson (1915) inferred a lower Miocene age correlative to the Blakeley Formation of Weaver (1912) and Fulmer (1954, 1975), whereas Durham (1942, 1944) indicated "Refugian" (GD35) and "Lower Oligocene" (GD36) ages. Armentrout and Berta (1977) assigned the unit to the Refugian foraminiferal stage. Prothero and Thompson (2001) assign the Refugian stage a late Eocene (36.5 Ma) to earliest Oligocene (about 33.7 Ma) age.

Undated sandstone and mudstone (unit ΦEm) are exposed in Chimacum Valley. We have no evidence to exclude pre-Eocene or post-Oligocene ages for these rocks, but note that some of the rocks are not obviously lithified (in outcrop and petrographic examination). Even if we were confident of an Oligocene to Eocene age, we would not have followed Yount and Gower (1991) in mapping these rocks as Twin River Formation or the Twin River Group of Snavely and others (1978), because correlation to these units is now discouraged (E. Nesbitt, written and oral commun., 2014). Other recent workers in nearby areas have similarly avoided mapping Twin River Formation (Haeussler and others, 1999; Schasse and Slaughter, 2005; Tabor and others, 2011; Contreras and others, 2014; Polenz and others, 2014).

AGES OF QUATERNARY UNITS AND TIMING OF GLACIAL EVENTS

We rely on age estimates from within and outside the map area to calibrate the ages of Pleistocene units. The timeline remains tentative and is summarized in Figure 2, where ages of Olympia nonglacial and older units are defined mostly by correlation to global proxies for glacial and interglacial intervals. Age analyses from the end of the Pleistocene are more abundant, and since transitions between nonglacial and glacial settings are regionally time-transgressive, these data can justify local adjustments to the interval boundaries in some instances. For example, the Vashon-age Puget ice lobe advanced into the map area after detrital wood had been buried at sites GD11 and GD12 (south of Point No Point in the Hansville quadrangle) at 18.4–17.6 ka. This is consistent with more regional data that suggest ice advanced to this latitude about 18 ka (Fig. 3), but also indicates that ice arrived in the map area well after the Vashon Stade began close to 19 ka (Figs. 2 and 3) farther north near the Canadian border. Our interpretation of events at GD11 and GD12 is not compelling, however (see *Deposits of the Possession Glaciation*), and even if it were, such local constraints can conflict with more regional data. For instance, data from the southern Puget Lowland suggest that Vashon-age ice persisted until after 16 ka, but those data appear to conflict with a post-glacially ice-free record that suggests Everson glaciomarine inundation began before 16.2 ka at Carpenter Lake ~5 mi south of the map area (Fig. 3). Additionally, field relations indicate that glaciomarine inundation of substantially ice-free areas occurred during the Everson Interstade while other parts of the map area were still covered by Vashon-age ice. Together, these data appear to imply that the time ranges for the Vashon Stade and Everson Interstade overlap and need revision in this map area. We did not revise Figure 2 because we have no definitive indication of when these transitions and overlaps occurred, but we strongly suspect that Vashon-age ice persisted longer than shown on Figure 2 and therefore show Vashon ice recession occurring later in Figure 3.

Paleomagnetically Reversed Deposits

Pre-Vashon deposits have been widely noted in and near the map area (Bretz, 1913; Birdseye, 1976a,b; Gayer, 1976, 1977; Hanson, 1976, 1977; Deeter, 1979; Carson, 1980; Grimstad and Carson, 1981; Schasse and Slaughter, 2005; Schasse and others, 2009; Polenz and others, 2006; Tabor and others, 2011; Contreras and others, 2013, 2014; Brett Cox, USGS, oral commun., 2015). Most exposures of pre-Vashon sediment in the map area remain undated, but two of six paleomagnetic samples reveal reversed polarity and a third may be transitional—suggesting that some deposits may be of early Pleistocene age (Fig. 2).

Whereas the two paleomagnetic samples collected in the Hansville quadrangle are normal polarity (sites M1, unit Qgdp, and M4, unit Qps), samples from unit Qpf in the Port Ludlow quadrangle are reversed (sites M2 and M5); sample M3 is magnetically transitional, but the lab cautioned that the signal could be an artifact of laboratory processing (Bernard Housen, Western Washington University, written commun., 2015). Brief subchrons like the Laschamp could yield reversely magnetized polarities from the Olympia nonglacial or other post-Matuyama intervals. However, among the four paleomagnetic samples from the Port Ludlow quadrangle, only one is clearly normal (M6), and that sample is also the only one upsection of an Olympia-age date (GD31). The simplest interpretation is that the reversely magnetized and transitional samples may be of Matuyama age (more than 780 ka)(Fig. 2). The laminated silt at reversed-polarity

sample M2 (columnar section 1) contained a granitic clast that we interpreted as probable dropstone and therefore suggests a pre-Olympia glacial origin. Additionally, Carson (1980) stated that "three diamictons of apparently different ages are exposed" on the east side of Chimacum Valley, supporting the interpretation that some sediment in Chimacum Valley pre-dates the Olympia nonglacial interval.

Deposits of the Possession Glaciation

Possession Drift is mapped in the Hansville quadrangle near and south of Foulweather Bluff. The main rationale for mapping these deposits as Possession Drift is provided by a 56.37 ±5.08 ka OSL date (GD28) from northern-sourced sand at beach-top level, just below glaciomarine drift at columnar section 3 (0.7 mi south of Foulweather Bluff). Although the date is on the younger end of the 60–80 ka age of Possession Drift (Fig. 2), this interpretation is the most attractive given the glacial character of the pre-Vashon deposit. Additional constraints are provided by paleomagnetically normal glaciomarine drift at Foulweather Bluff (M1; GD14; CS9) which is mapped as unit Qgdp because it is also exposed at and slightly above beach-top level, and detrital wood from upsection unit Qco is radiocarbon infinite (GD8). These relationships confirm that the glaciomarine drift and overlying cliff contain pre-Vashon deposits. We agree with Deeter (1979; CS9) that at least some of the deposits above the glaciomarine drift at Foulweather Bluff appear to be nonglacial.

We suspect that sand and silt mapped as queried Olympia nonglacial deposits (unit Qco?) along the east shore of the Kitsap Peninsula, south of Point No Point, might also be Possession-age outwash. We mapped unit Qco in agreement with Deeter (1979) because at CS19 he obtained late Olympia-age radiocarbon dates from detrital wood 8 ft above the beach (GD11, 18.4–17.6 ka, and GD12, 18.6–17.6 ka). Additionally, 1,275 ft farther south at columnar section 2, sand at about 63 ft elevation yielded luminescence dates of 71.1 and >65 ka (GD27), and wood from detrital peat at about 62 ft elevation yielded a >43,500 BP radiocarbon date (GD6). We queried the Olympia age assignment because the sand and silt particles in at least five upward-fining sequences at columnar section 2 were not clearly glacial or nonglacial, and the fine-grained end members of the fining-up sequences lack appreciable amounts of organic matter except as detrital fragments (such as at GD6, which was reworked from older deposits). Detrital organic fragments reworked from older deposits have been documented in at least some ice-proximal outwash deposits, such the Partridge Gravel in central Whidbey Island (Carlstad, 1992; Polenz and others, 2005). In addition, the late Olympia-age radiocarbon dates at CS19 appear to be stratigraphically lower than the older dates at columnar section 2.

One way to interpret these conflicting relationships is to question the validity of Deeter's (1979) dates. However, those dates represent two separate samples processed at different labs, both of which yielded consistent age estimates. Since exposure was not continuous between CS19 and columnar section 2, either a cut-and-fill section north of columnar section 2 or structural offset could account for younger dates at lower elevation. Alternatively, the paradoxical distribution of dates and the potential for proglacial deposition might favor a Possession age instead of an Olympia age (either just for columnar section 2, or more regionally if Deeter's [1979] dates are erroneously young).

These relationships could also be interpreted as indicating deposits of Vashon advance age, but only if the too-old luminescence dates at GD27 were incompletely reset—as is common in glacial deposits (Rhodes, 2011). This interpretation might explain the wide (74%) scatter at GD27. The radiocarbon-infinite date at site GD6 is also compatible with Vashon advance outwash (Qgas) because the sample is detrital and derived from older peat. Deeter's (1979) dates (GD11 and GD12), at 18.6–17.6 ka are so close to the ~17.8 ka time of Vashon ice arrival at this latitude suggested by Porter and Swanson (1998) that they are at least as compatible with the Vashon Stade (Fig. 2) as with the Olympia nonglacial association that he favored. In summary, the Olympia nonglacial unit assignment along this part of the Hansville shore is questionable. A Possession age for at least some of the section presents a reasonable alternative, but a Vashon age is perhaps more viable.

Deposits of the Olympia Nonglacial Interval

Olympia nonglacial deposits (unit Qco) are widespread in the map area and in adjacent quadrangles (Birdseye, 1976a,b; Gayer, 1976, 1977; Hanson, 1976, 1977; Deeter, 1979; Schasse and Slaughter, 2005; Contreras and others, 2014, 2013; Schasse and others, 2009; Polenz and others, 2006; Polenz and others, 2014; Brett Cox, USGS, oral commun., 2015). Although early mapping (Hanson, 1976, 1977) relied solely on stratigraphy and weathering to infer deposits of Olympia age in Chimacum Valley and isolated segments of the Hood Canal shore, our mapping benefits from new radiocarbon and optically stimulated luminescence (OSL) dates at columnar section 1 on the west side of the Chimacum Valley (GD4, 41.8–40.7 ka, and GD29, 35.58–25.78 ka, sec. 12, T28N R1W), and an OSL date at GD31 (38.59–30.95 ka) on the east side of the valley (sec. 6, T28N R1E). East of Chimacum Valley, OSL date site GD30 (53.55–39.59 ka, sec. 6, T28N R1E) supports an Olympia age for deposits at higher elevation (Table A2).

Taken together, the four new dates (GD4, and GD29–GD31) provide good evidence for Olympia age deposits along and east of Chimacum Valley. Such an age is consistent with our interpretation that the relatively basalt-rich sand mineralogy at columnar section 1 (and farther east at GD30–GD31) reflects nonglacial fluvial sediment from an Olympic Mountains source. An apparent westward-younging trend among OSL age sites (GD30, GD31, and GD29) is more likely an artifact of the large uncertainties in using OSL to date these types of deposits than post-depositional west-down tectonic offset or complex stratigraphy. We are also inclined to invoke such scatter to explain the older radiocarbon date at GD4 relative to the downsection and slightly younger OSL date at GD29.

A new radiocarbon date at GD3 (27.7–27.5 ka), south of Port Ludlow, supports identification of Olympia-age deposits at ~180 ft elevation elsewhere in the Port Ludlow quadrangle. Organic-rich sediment in well records at similar elevation farther southeast along the cross section—and an apparently widespread stratigraphic break downsection of GD3 between Tala Point and the southern map boundary—give us confidence in interpreting a thin (?) layer of Olympia-age nonglacial deposits south to the map

boundary. In the quadrangle to the south, Contreras and others (2013) interpreted thicker sections as Olympia-age deposits.

We follow Deeter (1979) in extensively mapping or inferring Olympia-age deposits in the coastal cliffs and subsurface of the Hansville quadrangle. At the northwest end of the Kitsap Peninsula, a late Olympia age is supported by a new beach-level radiocarbon date at GD2 (26.6–26.2 ka, sec. 13, T28N R1E) and the recognition of nonglacial sediment above Possession Drift to the north and east, including radiocarbon infinite wood (GD8) at Foulweather Bluff. Farther east, along the north-facing cliffs between Skunk Bay and Norwegian Point, several lines of evidence are consistent with either Olympia age or other pre-Vashon deposits: (1) a radiocarbon infinite date from nonglacial sediment, (2) an apparently upsection magnetically normal silt sample (GD7 and M4, sec. 17, T28N R2E), and (3) a lack of downsection Possession Drift. We therefore mapped nonglacial sediment as unit Qc without assigning the deposits to a specific pre-Vashon age. We did not follow Deeter's (1979) interpretation of some sediment along these cliffs as Possession Drift and Whidbey Formation (CS17, CS18) because we were unable to confirm that what he labeled Possession Drift is of pre-Vashon age. Possible Olympia-age sand and silt exposed in the cliffs south of Point No Point is discussed above in the context of Possession Drift; our mapping did not yield additional constraints from that location south to the map edge.

Deposits and Shorelines of the Fraser Glaciation

GLACIAL ADVANCE

The deposits at GD11 and GD12 are mapped as unit Qco, but the unit assignment is queried in part because these deposits could alternatively be interpreted as Vashon advance outwash (see *Deposits of the Possession Glaciation*). If the deposits are correctly mapped as unit Qco, then the radiocarbon data at the site suggest that Vashon advance outwash (unit Qgas) was deposited in the map area sometime after 18.4–17.6 ka (GD11 and GD12; CS19; Deeter, 1979). Alternatively, the deposits at GD11 and GD12 could themselves be unit Qgas, in which case GD11 and GD12 indicate that Vashon advance outwash had already reached the map area by 18.4–17.6 ka. A 17.8–17.5 ka radiocarbon date from 13.8 mi southwest of the map area dates impoundment, apparently by ice of the Puget lobe, of a lake at 1,350 ft elevation in a valley of the Olympic Mountains at the latitude of Brinnon (Polenz and others, 2012c). This impoundment likely post-dates the arrival of Vashon ice in the more northern parts of the Port Ludlow and Hansville quadrangles. If these dates and their corresponding unit assignments are correct, then the end of Olympia nonglacial conditions occurred sometime after 18.4 ka and Vashon advance outwash and ice arrived before 17.5 ka. These estimates are consistent with—and appear to narrowly constrain—the ice-advance timeline advocated by Porter and Swanson (1998, fig. 4) and Booth and others (2004, fig. 9).

GLACIAL RECESSION

Within the map area, two radiocarbon dates from marine shells (GD9 and GD10, at or near Basalt Point) suggest that ice sheet disintegration and glaciomarine inundation occurred later than the 17 ka suggested in Figure 2, which is based on an interpretation of the Seabeck and Poulsbo areas south of our map area by Polenz and others (2013). Later ice disintegration also would be more easily reconciled with southern Puget Lowland ice advance dates (Fig. 3) that are not accommodated by Figure 2.

A marine shell from near the base of glaciomarine drift (GD10; "13, 470 ±90" ^{14}C yr BP) and another from near the top of the same drift (GD9; "12,990 ±100" ^{14}C yr BP) produce dates that, if valid, suggest at least 500 radiocarbon years of glaciomarine inundation. We did not convert these dates to calendar years because the validity of shell dates is difficult to assess (Webb and others, 2007; E. Nesbitt, oral commun., 2014), and the marine reservoir correction is difficult to quantify. Both age statements exclude reservoir correction, which would make the age estimates between 400 and 760 years younger (Swanson, 1994; Anundsen and others, 1994).

The shell dates from GD9 and GD10 allow us to compare ages with those obtained by Anundsen and others (1994) from Carpenter Lake. For the start of glaciomarine inundation, Anundsen and others (1994) present a 14,610 ±340 ^{14}C yr BP date for a marine shell (one sigma; not reservoir corrected; sample T-6798). At two sigma (95% confidence), this date is at least 13,930 radiocarbon years old. GD10 was similarly sampled near the base of glaciomarine deposits, but the two sigma age range of 13,650 to 13,290 radiocarbon years does not overlap T-6798 and suggests that the glaciomarine drift is at least 280 radiocarbon years younger than suggested at Carpenter Lake.

For the end of glaciomarine inundation, Anundsen and others (1994) present a 14,070 ±190 date for a marine shell from near the top of glaciomarine deposits (sample UA-767). At two sigma (95% confidence), this date is at least 13,690 radiocarbon years old. GD9 was similarly sampled near the top of glaciomarine deposits, but the two-sigma age range of 13,190 to 12,790 radiocarbon years does not overlap UA-767 and suggests that the glaciomarine drift is at least 500 radiocarbon years younger than suggested at Carpenter Lake. Anundsen and others further present a 13,600 ±280 ^{14}C yr BP date (one sigma; sample QL4065) for gyttja that was deposited after final isolation from seawater following glaciomarine inundation. At two sigma (95% confidence), this date is at least 13,040 radiocarbon years old. The two-sigma range for GD9 (13,190 to 12,790 radiocarbon years) overlaps the Carpenter Lake date by 150 radiocarbon years, but if reservoir correction were applied to GD9, this overlap would disappear because the reservoir correction would yield a younger age estimate. Gyttja that post-dates marine inundation at Carpenter Lake similarly appears anomalously old relative to dates that constrain the advance of the Vashon ice farther south in the Puget Lowland (Fig. 3). The Carpenter Lake dates appear to systematically conflict with the dates from Basalt Point and elsewhere. We agree with R. Haugerud (oral commun., 2015) in suspecting that the Carpenter Lake age statements are systematically older than they should be, and we show Vashon ice recession occurring sometime between 15 and 16 ka in Figure 3—at least 1,000 years later than suggested by Figure 2. We offer no explanation for the Carpenter Lake discrepancy, and note that the other records could also be compromised; sources of variability among radiocarbon data can be difficult to recognize, much less exclude, as illustrated for freshwater shell dates by Webb and others (2007).

DEGLACIATION, MELTWATER CHANNELS, AND VALLEY INCISION

Field relations within or near the map area offer some insight into the timing, sequence of events, and unit deposition during late Vashon Stade deglaciation. On the flanks of Chimacum Valley, many drainages dissect the fluted valley walls and upland surfaces. Alluvial fan deposits at the base of the drainages (units Qaf and Qgoaf) document post-ice sedimentation on the floor of Chimacum Valley, fed from incision of the valley walls and upland surfaces. A few alluvial fans (unit Qgoaf, sec. 25, T29N R1W and sec. 6, T28N R1E) must be relict because they are dissected by streams that feed ongoing deposition of separate alluvial fans farther downslope. The downslope end of these relict fans appears to have been eroded and no drainage in the modern environment is large enough to achieve this erosion. We suggest instead that Vashon-age recessional meltwater eroded the distal ends of these relict alluvial fans in Chimacum Valley and West Valley (the upper drainage basin of Chimacum Creek, one mile west of the Port Ludlow quadrangle). This scenario is strengthened by the observation that meltwater deposited large deltas ~4 mi north of the map area, on both sides of the Quimper Peninsula (Fig. 1) between 130 ft and less than 95 ft elevation (Dethier and others, 1995; Schasse and Slaughter, 2005; Polenz and others, 2014). A continuous set of relict channels and stream terraces extend south from those deltas into Chimacum and West valleys. Marine shells in the western delta on the Quimper Peninsula (Dethier and others, 1995; Schasse and Slaughter, 2005) indicate that the deltas there formed during the marine incursion of the Everson Interstade. It follows that the relict fans of unit Qgoaf are most likely similar in age, or slightly older.

When compared to the limited size of the drainage basins of Chimacum and West Valleys, the large stream channels and deltas north of the map area imply large discharge volumes that could only have been generated by meltwater (see *Glacial Lakes and Shorelines*). The valley floor in both valleys includes deposits of relatively loose ice contact deposits (unit Qgic), and Rigg (1958) noted that varied thickness of valley floor peat implies an irregular valley floor morphology beneath the peat. Both the irregular valley floor morphology and mid-valley deposits of unit Qgic suggest residual ice in parts of Chimacum Valley at the time of marine delta formation north of the map area. In contrast, the formation of the alluvial fans of unit Qgoaf suggests ice free areas along parts of the valley flanks. The deposition of glaciomarine drift farther east in the map area—at elevations that rival or exceed the 130 ft glaciomarine elevation of the deltas farther north on the Quimper Peninsula—requires that large parts of the map area were ice free for at least part of the glaciomarine inundation.

We infer that the post-Everson inundation date (16.7–15.9 ka) of Carpenter Lake (Anundsen and others, 1994) approximates the time of ice wasting in the map area with two caveats: (1) The Lake Carpenter record at less than 30 ft elevation is much lower than the glaciomarine deltas on the Quimper Peninsula, and we do not know how much time passed, nor how much ice melted, between the formation of the deltas and the emergence of Carpenter Lake from marine inundation; (2) preservation of the elevated channels and relict Quimper Peninsula deltas implies that the voluminous meltwater that constructed the deltas ceased before sea level fell to the ~30 ft elevation at which Carpenter Lake emerged from the sea; otherwise the meltwater would have cut deeper channels and constructed lower-elevation deltas. This may indicate that the map area had become substantially ice free before Carpenter Lake emerged from marine conditions, although some ice patches locally persisted for millennia (Porter and Carson, 1971).

After glacial lakes drained, portions of the Puget Lowland may have experienced valley incision that was followed by marine inundation and valley-floor aggradation (Schasse and others, 2009). Aggradation continued until postglacial isostatic rebound raised the crust in the Puget Lowland and caused relative sea level to drop below modern sea level (Dragovich and others, 1994; Mosher and Hewitt, 2004), which in turn caused some valleys to incise below modern sea level. This deeper incision is recorded in drainages where loose fill in the lower reaches of postglacial valleys extends below sea level (Polenz and others, 2013; Schasse and others, 2004). We did not find that drainages within the map area were similarly affected—with the possible exception of two unnamed drainages on the Kitsap Peninsula (secs. 20, 21, 28, 29, T28N R2E, and sec. 16, T28N R2E), where alluvial plains in the lower valley reaches are graded to modern sea level and valley morphology is consistent with possible infilling of deeper post-glacial valleys. Most drainages in the map area are either tightly incised upvalley of the top of modern alluvial fans or alluvial fans that developed and substantially reached their present size during deglaciation (units Qaf and Qgoaf), or the drainages are narrowly incised along their lower reaches into glaciorecessional deposits (units Qgod, Qgdm$_e$). The latter observation suggests (and the former observation permits) that most upslope valley incision occurred during deglaciation when base level was locally elevated by ice dammed lakes or elevated marine waters of the Everson glaciomarine inundation. Unlike Schasse and others (2009) at southern Whidbey Island, we did not see evidence for substantial valley incision prior to glaciomarine inundation. Instead, the geomorphology in our map area suggests that valley incision and glaciomarine or lacustrine inundation were coeval—either because ice-dammed lakes prevailed in the map area during valley incision on Whidbey Island, or because meltwater-driven erosion and sedimentation in the map area commenced later than on Whidbey Island.

GLACIOMARINE CONDITIONS AND THE EVERSON INTERSTADE

The presence of a voluminous meltwater source in Chimacum Valley (and perhaps West Valley) sometime close to maximum glaciomarine inundation during the Everson Interstade suggests that at least some of the map area remained ice-covered during this time. However, the preceding discussion highlights that at least some drainages in the map area were substantially incised by meltwater at the end of the Vashon Stade (Carson, 1980). The implication for sedimentary units in the map area is that at least some alluvial fans and valley fill date mostly or entirely to the time of ice melting—as previously suggested by Hanson's (1976) mapping of glaciorecessional units (Vrd and Vro) in parts of the Port Ludlow quadrangle. This inference is also consistent with our field observations of valleys that lack active channels, such as at significant sites S4 (south of Port Ludlow; sec. 21, T28N R1E)

and S3 (west side of Chimacum Valley; sec. 36, T29N R1W). Site S4 is up-valley of, and perhaps graded to a glaciorecessional delta (unit Qgod; sec. 16, T28N R1E). Consequently, we suggest that much or all of units Qoa and Qgoaf and much or most of units Qa and Qaf were deposited during ice melting. Although post-glacial geomorphic processes are much less dynamic than periglacial processes (Ballantyne, 2002), headward erosion, valley incision, and associated mass wasting and alluvial deposition (units Qa, Qoa, Qaf, and Qgoaf) clearly continue in some areas such as near GD1 and upslope thereof (sec. 32, T29N R1E).

POST-GLACIAL CONDITIONS

Dates on late-Vashon ice disintegration and on post-glacial conditions constrain the end of the Vashon Puget lobe ice incursion. About 17 mi south of the map area, Polenz and others (2013) obtained a 17.130 ±1.08 ka IRSL age estimate for partial Puget lobe ice disintegration. Radiocarbon data from Carpenter Lake 4.9 mi south of the Hansville quadrangle, presented by Anundsen and others (1994) and converted to calendar years by Porter and Swanson (1998), appear more tightly constrained and suggest ice-free conditions sometime between 16.6 and 16.2 ka (sample QL-4067). A separate sample from the same site suggests the end of glaciomarine inundation at 31 ft elevation sometime between 16.7 and 15.9 ka (sample QL-4065). This younger date—and multiple dates upsection at Carpenter Lake—are attractive because they rely on non-marine samples that do not require marine reservoir correction. However, the dates at Carpenter Lake and sample GD15 of Polenz and others (2013) are so old that they appear to pre-date advance of the Vashon ice in the southern Puget Lowland between 17.8 and 15.3 ka (Walsh and others, 2003; Polenz and others, 2010, 2011, 2012a,b,c).

The above discussion suggests that post-Vashon ice-free conditions occurred sometime between about 16.6 and 15.3 ka. USGS Fact Sheet 2010-3059 places the Holocene–Pleistocene boundary at 11,700 ±99 yr and we therefore distinguish between Holocene units (af, ml, Qb, Qm) and units that range from Pleistocene to Holocene age (Qp, Qls, Qmw, Qa, Qoa, Qaf). We limit units Qb and Qm to the late Holocene because sea level was much lower before about 6,000 years ago (Dragovich and others, 1994; Mosher and Hewitt, 2004; Schasse and others, 2004), and these deposits could only have formed when sea level was near its present level.

Glacial Lakes and Shorelines

Ice-dammed lakes filled large parts of the Puget Lowland during deglaciation (Bretz, 1910, 1913; Thorson, 1980). Southwest of the map area, shorelines and deltas above Hood Canal document two prominent lake levels (Bretz, 1910, 1913; Thorson, 1980, 1981, 1989; Waitt and Thorson, 1983; Booth and others, 2004; Polenz and others, 2012a,b,c). Haugerud (2009) recognized at least five lake levels on the Kitsap Peninsula, the lowest of which is similar to the maximum elevation of the Everson Interstade marine inundation.

EVERSON INTERSTADE GLACIOMARINE SHORELINES AT ~140 FT ELEVATION

We systematically examined lidar-based images in search of landforms that suggest relict lake or marine shores. We document relict shorelines mostly below 140 ft and interpret these features as a record of glaciomarine inundation. Polenz and others (2014) documented an Everson marine shore at up to 135 ft at the south end of Discovery Bay (6 mi west of the map area), Schasse and Slaughter (2005) and Dethier and others (1995) documented delta-front slope breaks at 130 ft on the Quimper Peninsula 1.5 to 4 mi northwest of the map area, Schasse and Slaughter (2005) mapped glaciomarine drift at elevations up to 135 ft northwest of the map area, and Polenz and others (2006) inferred shorelines at 125–130 ft near Double Bluff in the Whidbey Island part of the Hansville quadrangle. On the Kitsap Peninsula part of the Hansville quadrangle, our estimate for maximum marine inundation elevation therefore exceeds the 100 ft estimate of Haugerud (2009). Our inference that shorelines below 140 ft are glaciomarine implies that the Vashon Stade and the Everson Interstade were partly coeval in the map area because meltwater discharge formed marine deltas at similar elevations, and this meltwater was derived from either an ice-dammed lake or from ice at least partly within the map area. Haugerud (2009) mentions Lake Bretz-fed meltwater channels at multiple elevations in eastern Jefferson County. Chimacum and West Valleys may be among those locations, and if so, then the Quimper Peninsula glaciomarine deltas (Fig. 1) don't necessarily require that melting of ice in the map area contributed appreciably to their development. However, multiple lines of evidence cause us to interpret the record of north-flowing meltwater across the map area as at least partly englacial, subglacial, or supraglacial. The valley floors of Chimacum and West Valleys have an irregular morphology and contain fragile and loose ice-contact deposits (unit Qgic) that would likely have been obliterated by entirely subaerial discharge; ice could have sheltered these deposits. There is considerable relief in possible meltwater channels that appear to feed Chimacum Valley near the southwest end of the map area (secs. 25 and 36, T28N R2W; and secs. 19, 30 [and perhaps 31 and 32], T28N R1W); subaerial discharge might have carved these channels, but parts of the channel morphology are subdued, the depth of erosion into surrounding landforms is modest, and channel margins are not everywhere sharply defined. This morphology may be easier to develop subglacially than subaerially. Finally, if the meltwater discharge through Chimacum Valley was fed by Lake Bretz, ice within the map area was needed to dam that lake. If the meltwater was not lake fed, ice within the map area was needed to produce and (or) deliver such voluminous meltwater. Either way, ice of the Vashon Stade persisted through the Everson Interstade maximum glaciomarine inundation within the map area.

LAKE BRETZ GLACIOLACUSTRINE SHORELINES AT ~350 FT ELEVATION

Shorelines above 140 ft are less abundant, but readily apparent in several areas. The most elevated 'shorelines' are mapped at about 350 ft elevation in the southwest corner of the Port Ludlow quadrangle from slope breaks identified as shorelines farther south by Contreras and others (2013). Within the Port Ludlow quadrangle

(secs. 25 and 36, T28N R1W), these slope breaks are more suggestive of outwash channel margins. This morphology, their elevation, and other observations suggest association with Lake Bretz. An approximately 200 ft drop in elevation separates the 350 ft shorelines at the southern map edge (secs. 25 and 26, T28N R1E) from the floor of Chimacum Valley at about 140 ft (near sec. 18, T28N R1E). Surface morphology reveals north-sloping channels (secs. 19 and 30, [and perhaps 31 and 32], T28N R1E) that connect the 350 ft-level shorelines at the southern map boundary to the much lower Chimacum Valley floor. Along most of the 200 ft elevation drop, the surface is basalt bedrock and channel morphology is somewhat subdued. Although the north-down slope strongly favors north-directed flow, we were unable to conclusively determine paleoflow direction from bedload exposures, channel forms, or channel gradients. The north-down slope could have resulted from post-drainage tectonic tilting or glacial rebound. Additionally, if the discharge was subglacial, the water could have flowed uphill given the correct hydraulic conditions. Despite these concerns, we favor north-directed discharge because Lake Bretz drained to the north, and these channels appear to have fed meltwater to Chimacum Valley.

Finally, the presence of Lake Bretz along the southern margin of the Port Ludlow quadrangle is further supported by shorelines and associated delta deposits (unit Qgos) between 280 and 240 ft in the map area and similar features down to about 220 ft within 0.5 mi south of the map area (Contreras and others, 2013). If north-directed discharge drained from Lake Bretz to Chimacum Valley, the lowest channel surfaces are at about 210 ft—just below the lowest shore features identified by Contreras and others (2013) south of the map area.

Although we only observed and mapped shorelines below 140 ft in the Hansville quadrangle, Haugerud (2009) interpreted other elevated surfaces as Lake Bretz outwash surfaces. Our mapping of apparent glaciolacustrine deposits (unit Qgos) between 140 ft and about 280 ft elevation supports the interpretation that Lake Bretz extended into the Hansville part of the map area.

STRUCTURAL INTERPRETATION OF THE MAP AREA

We discriminate between northwest-striking structures that are regionally pervasive, and in some cases tectonically active, and structures at various other orientations in Eocene-Oligocene bedrock. Northwest-striking structures are shown on Figure 1 and include the active (post-glacial) southern Whidbey Island fault zone (SWIF)(Johnson and others, 1996; Sherrod and others, 2005, 2008; Blakely and others, 2011; Mace and Keranen, 2012), the Pleistocene (to Holocene?) Dabob Bay fault zone (Blakely and others, 2009; Polenz and others, 2013; Contreras and others, 2014), and the regional Olympic–Wallowa lineament (Raisz, 1945; Blakely and others, 2011). Within the map area, we find that earthquake focal mechanisms have diverse solutions and that all events with solutions are more than 12 km (7.5 mi) deep; small upper-crustal events imply shallow faulting as well (Polenz and others, 2014, fig. 3). We also find localized areas of deformation in Pleistocene sediments, other inconclusive suggestions of post-glacial deformation, and evidence of rotating structural bedrock blocks. Linkage of at least some of these features to regional north-south contraction, northwest-striking faults associated with the Southern Whidbey Island fault, or uplift of the Olympic Mountains appears likely—but complex, and not yet adequately supported.

Scattered observations of deformed Pleistocene sediment (see *Deformation of Quaternary Units*) are noted in the context of specific structures below. In each case, they fall short of providing conclusive evidence for Pleistocene to Holocene tectonic activity because the deformation could be ascribed to other mechanisms and definitive association with a specific fault was lacking. Therefore, we generally did not use these data to draw specific structures across the map area. However, taken together and in the context of all the structures, the deformed Pleistocene sediments provide considerable support for the interpretation that some active faults cross the map area.

Northwest-striking Faults

Northwest-striking faults in the map area are interpreted mostly from seismic profiles and aeromagnetic anomalies. They include the Portage Canal fault, unnamed faults at Pilot Point, and unnamed faults beneath Hood Canal. These structures are subparallel to the SWIF. Southeast of the map area, Sherrod and others (2005a,b, 2008) suggested that the SWIF is at least 12 km (7.5 mi) wide. If the SWIF is similarly wide at the latitude of the map area, it overlaps the Portage Canal fault and suggests that northwest-striking faults in the map may be related to the SWIF.

PORTAGE CANAL FAULT

A northwest-striking fault at Portage Canal (Fig. 1), north of the Port Ludlow quadrangle (MacLeod and others, 1977), was shown as a northeast-up structure and named by Gower (1978, 1980) and Gower and others (1985). Whetten and others (1988) similarly show the fault as northeast-up high angle fault. For reasons we are not aware of, Johnson and others (2000) show the fault as Quaternary structure. Unlike Yount and Gower (1991) and Yount and others (1993), Dragovich and others (2002) show it continuing to south of Foulweather Bluff. We locate the fault along three seismic profiles: seismic section 73C has a basin-bounding southwest-down structure around common depth point (CDP) 2650; seismic section PG71-020 has a basin-bounding south-down structure around CDP 1100; and seismic section 101 has a basin-bounding south-down structure around CDP 1200. Based on these three consistent offsets we agree with the southern continuation shown by Dragovich and others (2002), but shift it 0.7 mi farther east and infer a slight southward bend within the map area.

Our seismic interpretation suggests that the fault may intersect a south-facing beach cliff between GD2 and Deeter's (1979) columnar section site CS7 (sec. 13, T28N R1E). At this location, steeply dipping faults with varied orientations and senses of displacement disrupt late Olympia- and Vashon-age sediment. However, the faulting at this beach cliff could alternatively be: (1) a northwest continuation of the "unnamed faults at Pilot Point", (2) a northward continuation of a west-down fault inferred beneath Hood Canal (Cross Section A; Faults Beneath Hood Canal), or (3) the result of glaciotectonic deformation. Additionally, the observed fault orientations between GD2 and CS7 do not match the overall orientation of these other structures. We therefore

chose not to show the faults between GD2 and CS7 as connected to any other structures.

UNNAMED FAULTS AT PILOT POINT

Mace and Keranen (2012) used seismic reflection data and upper plate seismicity to infer a northwest-trending flower structure near the Kingston arch. We show the northernmost of their three fault strands offshore north of Pilot Point (secs. 22, 27, and 35, T28N R1E); their other fault strands are south of our map area. This cluster of northwest-striking faults appears to be a northwest continuation of faults inferred from geophysical lineaments farther southeast and attributed to the SWIF (Sherrod and others, 2008). Mace and Keranen (2012) also suggest that these faults continue northwest onto or across the Kitsap Peninsula. This faulting may be expressed by localized disturbances that we observed in Pleistocene sediment generally along strike to the northwest of the mapped fault segments. However, we chose not to map the faults of Mace and Keranen (2012) on shore because the disturbances we observed were not conclusively tectonic. If the faults do continue across the Kitsap Peninsula, they may connect to the Portage Canal fault at or near Foulweather Bluff.

The distribution of age control data along the cliffs near Pilot Point may support the inference of an onshore fault strand that disturbs Olympia nonglacial deposits. At CS19, Deeter (1979) obtained late Olympia-age radiocarbon dates from detrital wood 8 ft above the beach (GD11, GD12; Table A1). If these dates and our own, older radiocarbon and luminescence dates (GD 6 and GD27; Tables A1 and A2) from about 50 ft above the beach at columnar section 2 (1,275 ft south of Deeter's dates) are all valid, either more than 40 ft of south-up structural offset, or a lateral stratigraphic discontinuity within the Olympia nonglacial interval is implied between the two sites. Neither were observed, and nonstructural explanations were explored above in *Ages of Quaternary Units* and *Timing of Ice Wasting*. South-up structural offset is not apparent in glaciomarine shorelines 500 to 2,000 ft farther west.

FAULTS BENEATH HOOD CANAL

We tentatively inferred northwest-striking faults beneath and slightly west of Hood Canal based on offsets in seismic line 74 (around CDP 1300), and seismic line PG71-042 (around CDP 100). We use aeromagnetic and gravity surveys to refine the fault orientations. These faults are similar in orientation to focal mechanism solutions for some earthquakes below 12 km (7.5 mi) depth within and south of the map area (Polenz and others, 2014, fig. B1) and are parallel to the dominant orientation of drainages and other topographic lineaments (Polenz and others, 2014, fig. 1) along and west of the Port Ludlow quadrangle. We speculate that the northwest-striking faults suggested by Mace and Keranen (2012) within and south of the Hansville quadrangle, and those suggested by Sherrod and others (2005a,b; 2008) as part of the SWIF southeast of the map area, may continue farther northwest than shown in our map. A previously mapped syncline within and west of the Port Ludlow quadrangle (Gower and others, 1985; *North-striking Fault along Chimacum Valley*) may be part of a related, fault-bounded basin between Crescent Formation basalt outcrops in the Port Ludlow quadrangle.

We infer that some northwest-striking faults beneath Hood Canal are offset by northeast-striking faults based on prior mapping of a northeast-striking fault that follows magnetic anomalies across Hood Head north of the Lofall fault (Brocher and others, 2001; Contreras and others, 2014) and offset of seismic packages in seismic line 100 (around CDP 600). We add a second northeast-striking fault strand 0.4 mi farther northwest, just west of Hood Head, based on offsets of seismic packages in seismic line 100 (around CDP 800) and seismic line 74 (around CDP 2200), and our observation of brecciated and sheared Pleistocene sediment at significant site S2 (sec. 35, T28N R1E). Additionally, most parts of the inferred faults align with aeromagnetic anomalies (courtesy Richard Blakely, USGS, written commun., 2012, 2013; older renditions of mostly the same data are available in Blakely and others, 1999). These anomalies systematically favor northeast and northwest-striking features and are brought into sharp focus by higher resolution marine survey data north of Hood Head that we acquired in collaboration with Geometrics, Inc. We caution, however, that the combination of northeast- and northwest-trending magnetic anomalies could alternatively be interpreted as expressions of dipping chevron folds.

For the faults north of Hood Head just described, we do not know if the northwest-striking faults offset the northeast-striking ones or vice versa. We chose to show the northeast-striking faults offsetting the northwest-striking faults because this is compatible with our continuation of the northeast-striking fault of Brocher and others (2001) and Contreras and others (2014). We do not know, however, if the disruption of sediment at site S2 is tectonic, nor if it includes deposits of Vashon age.

Not shown on Figure 1 or the Map Sheet is the north-striking Hood Canal fault (Daneš and others, 1965; Gower and others, 1985; Yount and Gower, 1991). Like Contreras and others (2014) and Polenz and others (2012, 2013), we omit this fault because we have little sense of its location or character in the map area. Unless it bends or steps to follow Hood Canal northeast from where Daneš and others (1965) originally inferred it several miles southwest of the map area, it cannot help explain the character and distribution of known deposits in the Port Ludlow quadrangle or the Port Ludlow uplift as inferred by Pratt and others (1997). An east-down stratigraphic discontinuity across this part of Hood Canal is consistent with the bedrock surface relief and stratigraphy.

Eocene Crescent Formation basalt (unit Ev_c) is exposed along the eastern Port Ludlow quadrangle shoreline to the west of Hood Canal. East of Hood Canal, even the deepest wells in the map area did not intersect basalt. Sedimentary bedrock was reached below 1,105 ft in well HC4 (east side of the Kitsap Peninsula; Fig. 1), and the Mobil Kingston no. 1 well (~4.6 miles south of the Hansville quadrangle; Fig. 1) reached siltstone at 1,206 ft and intersected basalt at 7,200 ft. The nearly 7,000 ft drop of the basalt from G9 southeast to the Mobil Kingston no. 1 well is an 8.4° average slope. If this slope is not depositional, then the offset is structural, and the implications of such an offset are difficult to interpret. For example, we have no information on basalt flow orientation at G9 or the Mobil Kingston no. 1 well and faults separate basalt flows elsewhere in the Port Ludlow quadrangle. The depth to basalt beneath the Hansville quadrangle itself is unresolved and may be affected by a northwest-striking

flower structure (Mace and Keranen, 2012), the faults at Pilot Point, and (or) the Kingston arch.

The deepening of bedrock across Hood Canal is consistent with a fault-bound eastern edge of the poorly understood Port Ludlow uplift. Seismic sections suggest a fault-bound synclinal basin beneath Hood Canal (Cross Section A) that may have formed during southeast-down slip along the eastern edge of the Port Ludlow uplift. Interpretation of seismic section 100 indicates that west-down offset on the north-northwest-striking fault farther east beneath Hood Canal may have also helped to form the synclinal basin, but our inability to correlate individual seismic packages across the fault makes this interpretation tentative; we cannot exclude east-down offset across this fault, and the eastern limit of the Port Ludlow uplift remains poorly constrained.

Faults of Other Orientations

Faults of other orientations include faults exposed in bedrock that typically coincide with (and where queried are at least partly inferred from) scarps that truncate flows in basalt (unit Evc). They commonly have no consistent orientation, but north- and northeast-striking faults are strongly expressed in surface morphology and magnetic anomalies. South of the map area, Brocher and others (2001) and Contreras and others (2013) inferred the east-striking Lofall fault. It remains unclear in what manner and to what extent these faults relate to ongoing regional north-south contraction (Pratt and others, 1997; Brocher and others, 2001; Johnson and others, 2004; ten Brink and others, 2002; Tabor and others, 2011) and (or) uplift and rotation of the Olympic Mountains (Babcock and others, 1994; Brandon and others, 1998; Tabor and others, 2011; Wells and McCaffrey, 2014). Tabor and others (2011) reported strong evidence that one of these faults has generated post-glacial surface rupture and Contreras and others (2013) suggested that tilting of late Pleistocene sediment at the southern margin of the Port Ludlow uplift (Fig. 1) is associated with activity on the Lofall fault. East-striking faults offshore to the north and northwest have been identified based on seismic profiles, gravity, and magnetic data (McLeod and others, 1977; Johnson and others, 2000) and include some that were interpreted as active (Johnson and others, 2000; Blakely and others, 2011).

We interpret some sheared basalt-flow contacts at Shine Quarry as the likely result of flexural slip, and Allison (1959) and Thoms (1959) show faults parallel to flow contacts along the shore near Olele Point. We do not show these flow contact faults on the map, but do not doubt their widespread presence.

LOFALL FAULT

The west-northwest-striking Lofall fault is inferred at the southern map boundary based on prior mapping by Brocher and others (2001) and Contreras and others (2013). Contreras and others (2013) used seismicity, mostly more than 10 km (6.25 mi) deep (see also Polenz and others, 2014, fig. 3), an absence of surficial bedrock south of the fault, north-up geomagnetic and gravity gradients, and south-dipping Pleistocene sediment to map the Lofall fault. We show the fault continuing into the Port Ludlow quadrangle, consistent with Contreras and others (2013), but unlike Brocher and others (2001), who suggested that the fault continues to the western margin of the Port Ludlow uplift. We query and terminate the fault shortly after it enters the Port Ludlow quadrangle because the north-up gravity and magnetic field strength boundaries either lose definition, shift, or bend to a more southern location outside our map area. Additionally, there is little crustal seismicity beneath this part of the map area (Polenz and others, 2014, fig. 3), and there was insufficient evidence to map the fault across the Center quadrangle to the west (Polenz and others, 2014).

FAULTS BETWEEN CRESCENT FORMATION AND SEDIMENTARY ROCKS

We agree with Yount and Gower (1991) that the contact between Crescent Formation basalt and Quimper Sandstone along the shore of Oak Bay implies a hiatus and is therefore unconformable. Crescent Formation basalt flows are exposed at the south end of Oak Bay where they dip north more steeply than the overlying Quimper Sandstone. Unless basalt flows shallow in the subsurface farther north, they appear to be truncated by the contact, possibly suggesting an angular unconformity.

We observed basalt north and south of sandstone at GD19 (sec. 29, T29N R1E) and included this sandstone exposure with unit Evc, although it could also correlate with the Quimper Sandstone. The sandstone is stratigraphically within 15 ft of the contact between unit Evc and unit ΦEmq, but we were unable to establish whether the contact between the sandstone and basalt on either side is conformable or faulted. The sandstone outcrop is also lithologically compatible with the Quimper Sandstone, and several faults cut basalt and sandstone nearby—including faults with orientations similar to the contact. Several water wells up to 4,500 ft northeast of GD19 also record alternating layers of basalt and either "shale" (some drillers have occasionally identified basalt as "shale") or sandstone. It remains unclear if these alternating layers of basalt and sandstone are bounded by faults, and whether they are associated with Crescent Formation, the Blue Mountain unit (interbedded Crescent Formation basalt and sedimentary rocks of the Blue Mountain unit has been documented farther west along the northern margin of the Olympic Peninsula—Tabor and Cady, 1978a; Einarsen, 1987; Babcock and others, 1992, 1994; Schasse and Polenz, 2002; Schasse and others, 2004; Polenz and others, 2004), or younger sedimentary rock units like Aldwell Formation or Quimper Sandstone.

Undated sandstone and mudstone (unit ΦEm) is exposed near the north and south ends of a 3-mile stretch of Chimacum Valley. We suspect, but cannot confirm, that these exposures of unit ΦEm are confined to a fault-bound trough between unit Evc to the north and south. East of Chimacum Valley, no bedrock is exposed in a 2.5 to 3 mi-wide west-trending corridor between Mats Mats Bay and Port Ludlow, consistent with the postulated fault-bound trough. The corridor approximately coincides with a faint gravity low, and magnetic anomalies can be interpreted as aligning with the northern and southern margins of the corridor. We partly illustrate the inferred trough by showing a southeast-side-up fault on the map and cross section. The Chimacum Valley floor slopes north to the north of sec. 1, T28N R1W, but otherwise slopes south. These different slope directions might be evidence for post-Vashon folding. We prefer not to infer such post-glacial deformation because post-ice valley fill from tributaries could account for the opposing slopes of the valley floor.

UNNAMED FAULT SOUTH OF BEAVER VALLEY

We infer a northeast-striking structural discontinuity in bedrock 0.7 mi south of the town of Beaver Valley (west of Port Ludlow), based on at least three lines of evidence: (1) bedrock surface relief between surficial exposures southeast of the structure and the depth to bedrock in water wells northwest of it, (2) magnetic anomaly gradients that roughly coincide with a linear topographic depression, and (3) the observation that the orientation of the inferred fault is similar to the orientation of a fault in the Shine Quarry (2.2 mi to the south), and to the orientation of additional inferred bedrock faults (0.8, 2, and 2.8 mi to the south). More than 300 ft of basalt surface relief is inferred across the structure between water well W18 (sec. 18, T28N R1E) which intersected basalt at 128 feet below mean sea level (msl) and the nearest basalt outcrop (0.5 mi to the south), at 200 ft above msl. Basalt bedrock crops out again 2.5 miles to the north, where exposures coincide with another topographic and magnetic gradient anomaly. Together, these features suggest a broad, approximately east–west-trending basin. Gower and others (1985), and Yount and Gower (1991) appear to have attributed this depression to a southeast-plunging syncline, which they truncate with a north-striking fault 1.7 mi to the northwest. We find evidence that the basin extends east of their truncating fault but find no evidence for a southeast-plunging fold. We propose that a fault bounds the south side of this basin and that the north side may be similarly faulted, but evidence there is less clear and we choose to not show a structure.

NORTH-STRIKING FAULT ALONG CHIMACUM VALLEY

Near the western map boundary, Gower and others (1985), Yount and Gower (1991), and Dragovich and others (2002) show a southeast-plunging syncline truncated by a north-striking fault in Chimacum Valley. We speculate that the fault was inferred based on east-side-up offset suggested by mapping of basalt east of the fault and Twin River Formation west of the fault (Yount and Gower, 1991). The syncline may have been inferred based on south–southeast-dipping beds in sedimentary rocks; perhaps the presence of a north-trending magnetic low along this part of Chimacum Valley also contributed. We find no field evidence to support offset of bedrock units by a north-striking structure in Chimacum Valley. Instead, our mapping documents similar exposures of sedimentary rock and basalt along the floor of Chimacum Valley on both sides of the putative fault. Additionally, new luminescence dates from Quaternary sediment on both sides of Chimacum Valley have similar ages. We find evidence that a basin exists east of the north-striking fault first inferred by Gower and others (1985), but find no evidence for a southeast-plunging fold in that basin.

We interpret aeromagnetic data to suggest that a north-striking fault, if present, would be west of the map boundary and approximately 0.5 mi west of the fault mapped by Gower and others (1985), Yount and Gower (1991), and Dragovich and others (2002). In that location, a fault could be invoked to explain a southward-widening gap in bedrock exposures to the west—the gap is 1 mi wide on the north end of the postulated fault, and 3.5 mi wide on the south end (this study; Polenz and others, 2014). It might also coincide with the transition from ample pre-Vashon-age sediment along Chimacum Valley to only exposures of Vashon advance outwash to the west (this study; Polenz and others, 2014). We do not advocate such a fault, however, because the arguments for its existence are not compelling, and the structural reality is likely more complex than a single north-striking structure. If structures do exist here, magnetic and topographic lineaments suggest northwest- and northeast-striking faults or chevron folds, subparallel to and west of Chimacum Valley.

UNNAMED FAULTS IN BASALT SOUTHWEST OF PORT LUDLOW

Approximately four square miles of basalt that crop out immediately southwest of Port Ludlow are dissected by northeast-, northwest-, north-, and west-striking faults. These faults are apparent where they offset basalt flows in lidar-based images. Faults mapped as certain were observed in outcrop; queried faults coincide with zones of fractured and altered basalt in outcrops and (or) are inferred from lidar and other morphologic observations. We measured 13 fractured zones in basalt along 0.2 mi of SR19 roadcut exposure (sec. 19, T28N R1E); in at least two locations, these correspond to a southwest continuation of scarps that offset basalt flows. We also observed a set of northeast-striking faults in the Shine Quarry, 230 ft northwest of geochemistry site G7 (sec. 29, T28N R1E). These closely spaced faults are represented on the map by a single, steeply southeast-dipping slickenside symbol, although some fault surfaces share the same strike but dip steeply northwest. These faults parallel and were located between 40 and 100 ft southeast of a minor linear topographic depression visible in lidar-based images. Numerous parallel lineaments and scarps nearby suggest that the observed minor fault surfaces are part of a broader fault zone. Therefore, the map shows additional queried faults where lidar reveals disruption of basalt flows. The validity of this interpretation is reinforced by additional slickensided surfaces on strike with one of the morphologically inferred faults 0.6 mi northeast of site G7 (at the north end of sec. 29, T28N R1E).

Immediately east of site G7, a north-striking east-down scarp marks the east end of the Shine Quarry excavation (as of fall 2014). This scarp coincides with a steeply dipping fault exposed in the quarry (Fig. 5) that truncates west-dipping basalt flows to the west (Fig. 4). The observed fault parallels or approximates numerous other scarps and lineaments farther east, north, and west in the basalt bedrock. We interpret some of these as basalt flow contacts, but have concluded that others truncate flows. We therefore show some of the most distinctive scarps as queried faults 0.3 mi east and 0.4 mi west of the Shine Quarry fault.

Approximately west-trending scarps and lineaments comprise some of the most distinctive morphologic features within the ~4 square mi of exposed basalt. Many of these features disrupt or truncate the morphologic expression of basalt flow contacts, and we therefore show some of the most prominent scarps and lineaments as queried faults on the map even where we lack field observations of faulting. At significant site S5 (boundary of secs. 17 and 20, T28N R1E), this interpretation is validated by exposure of a slickensided basalt surface on strike with one of the morphologically inferred faults. Although more queried

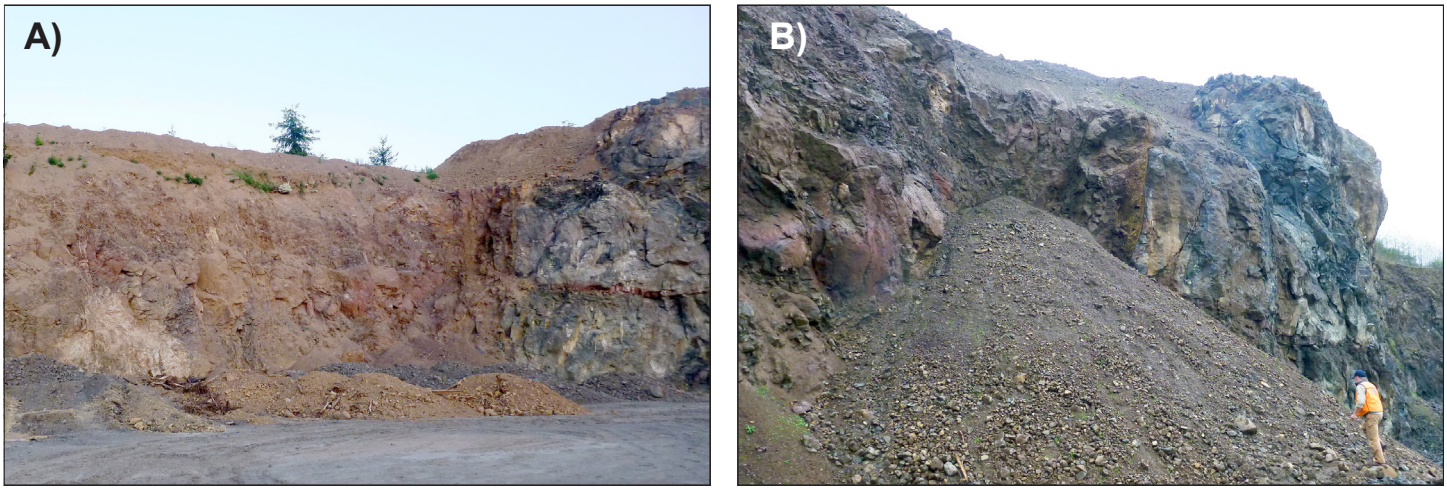

Figure 5. **A)** Fault at east end of Shine Quarry excavation. Quarry wall follows north-striking fault and is marked by orange-brown, brecciated, and altered basalt. Near the right side of photo A, the near-vertical fault is marked by an abrupt change from red brown fault breccia (left side) to three dark gray and gently west-dipping basalt flows (right side). The three flows are similar in thickness, and the contact between the lower two is defined by a zone of red-colored rock. Similar red (and green) contacts elsewhere in the quarry (Fig. 4a) contain basalt-fragment-rich sheared rocks. View to southeast in the fall of 2014. **B)** Close-up of steeply east-dipping and north-striking fault in photo A. Fault is clearly visible between lilac and gray, brecciated and altered basalt on the left, and comparatively undisturbed dark-gray basalt on the right. A 1.5-ft-wide zone of dark yellowish-brown fault gouge is on the left side of the fault. It is unclear if the fault is contained entirely in the 1.5-ft-thick gouge, or (more likely) includes the entire >10-ft-wide zone of brecciated and altered basalt. Quaternary deposits above the basalt were removed or never present; thus, it is unclear if the fault cuts these younger deposits. View to south in the fall of 2014.

faults could be placed on the map using these criteria, we chose to illustrate only the most distinct features.

The eastern margin of the basalt exposure south of Port Ludlow is bounded by an inferred and queried, north–northeast-striking fault. This fault follows a distinct and linear topographic depression that separates the basalt on the west from glacial sediment on the east. Nearly 500 ft of relief in the basalt surface is inferred between the sediment-covered upland where water well W21 intersects basalt at 156 feet below msl, and 0.2 mi west of the topographic depression where unit Evc rises to 320 ft above msl. Based on this nearly 500 ft of relief, and the strong morphologic expression of the boundary, we infer a queried fault.

FAULTING IN BASALT NORTHWEST OF MATS MATS BAY

We infer a series of subparallel northeast-striking faults in unit Evc ~1 mile northwest of Mats Mats Bay. These faults are oriented sub-parallel to faults exposed along the shore at Oak Bay. The continuation of these faults beyond Oak Bay was inferred from linear topographic anomalies in lidar that separate Evc outcrops and offset features we interpret as basalt flows. The apparent truncation of flows implies that the faults we show are separate from north-dipping faults that previous workers (Allison, 1959; Thoms 1959) mapped sub-parallel to flow contacts along the shore in this area. None of the faults we show in this area appear to offset Quaternary stratigraphy, though collapse and mass-wasting features too small to show at map scale are aligned along the strike of these faults. The faults we show have a consistent trend, similar to a pervasive northeast-trending topographic fabric that coincides with other mapped faults in the Port Ludlow quadrangle.

Other Structures

PORT LUDLOW UPLIFT

Bedrock exposures west of Hood Canal in the Port Ludlow quadrangle contrast with the absence of bedrock throughout the Hansville quadrangle. A 1,204 ft-deep hydrocarbon exploration well (HC4) southwest of Hansville (Fig. 1) drilled through 1,105 ft of sediment before penetrating possible sedimentary bedrock. Hydrocarbon well Mobil Kingston no. 1, ~4.5 miles south of the southeastern quadrangle corner (Fig. 1), penetrated 1,206 ft of sediment before intersecting sedimentary bedrock and intersected volcanic bedrock 7,200 ft below the surface. These data indicate that sediment thickness generally increases eastward (Jones, 1996; Eungard, 2014). Well records and patchy bedrock exposures in the Port Ludlow quadrangle document varied sediment thickness.

Although most bedrock in the map area is folded, jointed, or tilted, available data do not support identification of specific folds at map scale. A change in the apparent dip of bedding at significant site S1 (south of Oak Bay, sec. 29, T29N R1E) suggests a gentle, open, east- to northeast trending syncline, but the fold could not be adequately characterized. On the west side of the map area, anomalies in the magnetic and gravity field suggest shallow basalt bedrock that roughly coincides with the Port Ludlow uplift (Fig. 1). In the Center quadrangle to the west, Polenz and others (2014) used these data to schematically show unit Evc within 300 ft of the surface near the east end of their cross section A. To better align the southwestern margin of the Port Ludlow uplift with magnetic and gravity anomalies, we show part of the southern edge of the Port Ludlow uplift as following the Lofall fault (Fig. 1).

Contact relations between units Evc and ΦEmq along the shore of Oak Bay suggest that the Port Ludlow uplift could at least partly date to Eocene time. South of Oak Bay, Eocene volcanic flows dip 45° north at Mats Mats Quarry and Olele Point

(Allison, 1959), and 45° northeast 0.7 mi west of Olele Point. Bedding in the overlying unit ΦEmq dips between 3–22° northeast (Jillson, 1915; Allison, 1959) to the west of Olele Point and northward to the map boundary. This same contact is 235 feet below the surface at water well W71 (sec 19, T29N R1E), 1.8 miles to the north and indicates a gentle 1–2° slope. This gradual northward slope suggests that the contact is not conformable with the moderately dipping basalt, but is subparallel to the more gently dipping sandstone.

Overall, these data suggest a north-dipping angular unconformity between units Evc and ΦEmq at Oak Bay. The gently dipping Quimper Sandstone beds may have been deposited on, or onlapped against, an erosional basalt surface before being slightly tilted northeast. This in turn suggests that the Port Ludlow uplift may have initially tilted the basalt flow beds to the north sometime after 50.51 Ma, but prior to the late Eocene–early Oligocene deposition of unit ΦEmq, although we have no information on depositional basalt flow dips. Tilting of both units occurred sometime thereafter. However, we do not know the orientation of unit Evc directly beneath unit ΦEmq, and have been unable to exclude a faulted contact at the south end of Oak Bay.

EVIDENCE FOR PLEISTOCENE TO RECENT DEFORMATION

Seismicity

Mace and Keranen (2012) observed that much of the crustal seismicity beneath the Puget Lowland is not explained by mapped faults, a pattern that holds true in this map area. Mace and Keranen (2012) also infer that a set of northwest-striking faults form a flower structure southeast of Hansville, about 4.3 mi south of the Southern Whidbey Island fault zone. Seismicity appears clustered along such an alignment, especially beneath Hood Canal (Polenz and others, 2014) within 3 mi of the southern map edge, and farther southeast beneath the Kitsap Peninsula, outside of the map area. The seismicity thereby supports a possible northwest continuation of the structures proposed by Mace and Keranen (2012) across much of the map area (see *Unnamed Faults at Pilot Point*). The nearly west-striking Lofall fault appears to mark the southern fringe of the cluster of seismicity. Many lineaments not aligned with bedding orientations, nor explained by fluting or slope aspect, are also oriented northwest (or northeast) and may be an expression of the northwest-striking, regional structural fabric of the SWIF and Olympic Wallowa Lineament, and conjugate (?) northeast-striking structures.

Deformation of Quaternary Units

Several locations throughout the map area expose deformed Quaternary deposits. Along the shore of Hood Canal (360 ft northwest of CS5, sec. 18, T28N R2E), apparently conjugate sets of shears (oriented 027°/53° and 228°/72°) cut till from beach level to cliff top, where they appear to die out in near-surface deposits. Due to space constraints on the map, only the first set of shears is shown. Farther southeast along the same cliff, we observed widespread and generally chaotic folds in silt at the base of the section; a fold axial plane (010°/72°) may be representative. The silt intrudes otherwise undisturbed, planar-bedded sand above it. Along the shore above Skunk Bay (280 ft southwest of CS15, sec. 18, T28N R2E), boat-level observations of laminated silt or interbedded sand and silt ~50 ft above the beach suggest generally south dips and a possible fold; beds appear to dip 15° on the east, and 5° on the west. There was no evidence that landsliding influenced these dips. It is unclear to us whether this apparent fold is among the "diapir folds" noted by Deeter (1979, p. 121), who also documented clastic dikes at the base of the cliff a few hundred feet farther northwest along the shore of Skunk Bay. In a shore bluff at site M4 (sec. 17, T28N R2E), gently tilted (1–9°) silt beds contain steep west-dipping joints and moderately to steeply southeast-dipping shears. The cause of the disturbances at this site (tectonic versus mass-wasting) were equivocal.

These three locations add to evidence for tectonic (?) deformation of Pleistocene deposits west of Hansville at sites GD2 and CS7 (sec. 13, T28N R1E), where multiple faults of different orientations cut Olympia- and Vashon-age deposits. At least one vertical shear cuts from beach level across all mid-cliff units and appears to offset the contact between Vashon till and a cover of Everson Glaciomarine Drift; we were unable to resolve if the shear also penetrates to the surface of the drift. This offset is not visible at map scale. We deem these sparsely scattered observations, most of which could be individually explained by non-tectonic mechanisms such as landsliding or ice shove, as strongly suggestive of Pleistocene or Holocene deformation. However, the evidence is insufficient to infer a systematic pattern of folding or faulting, or ascribe the deformation to any particular structure.

Paleogeographic Considerations

Deposits in most of the map area are either of northern or mixed northern and local provenance. Exceptions to this are outcrops of Olympia-age volcaniclastic-rich deposits along both sides of Chimacum Valley. These distinctive deposits were sourced from the Olympic Mountains and indicate that a river flowed across this area during the Olympia nonglacial interval. Based on lithology, likely candidate watersheds include the Dosewallips and (or) Duckabush Rivers. The deposits were noted at elevations as high as 340 ft at columnar section 1 and may also include sand at 400 ft elevation at GD30. These elevations may be influenced by Pleistocene to recent uplift, as suggested for the Port Ludlow uplift by Contreras and others (2014). An Olympic Mountains-sourced river also implies that no pre-Vashon equivalent of Hood Canal flanked the Olympic Mountains. South of the Port Ludlow quadrangle, Contreras and others (2013, 2014) have advocated for extensive Olympia-age lake or flood plain settings well above sea level, and Bretz (1913) and Polenz and others (2012c) noted that the Duckabush River deposited a delta at least 90 ft above msl prior to the arrival of Vashon-age ice. These subaerial fluvial deposits are roughly coeval with the Chimacum Valley deposits, creating a trap for Olympic Mountains-sourced sediment before it reached Chimacum Valley; however, age-control data from the site are difficult to interpret. Thus, the Dosewallips River may be the best candidate drainage. In addition, Contreras and others (2013) obtained an Olympia-age radiocarbon date from marine shells just above modern sea level less than a mile south of the Port Ludlow quadrangle. If that date is accurate, the elevation of the sample requires significant post-depositional uplift along the south margin of the Port Ludlow quadrangle because sea level during the Olympia nonglacial interval should have been well

below modern sea level (Siddall and others, 2008). Together, these data appear to require that at least one large drainage, most likely the Dosewallips River, did not enter a marine or lacustrine basin in the Puget Lowland before draining north across the Port Ludlow quadrangle during the Olympia nonglacial interval.

Near the end of the Vashon Stade, north-flowing subaerial meltwater clearly sculpted Chimacum Valley from the northwest corner of the map area to relict glaciomarine deltas on the Quimper Peninsula (Fig. 1). At the northwestern map corner, and at the southern end of the valley (south edge of sec. 18, T28N R1E), the floor of Chimacum Valley is at 140 ft elevation. Between those points, the valley floor gently rises to an apex of 173 ft (sec. 1, T28N R1W). Although the overall valley morphology suggests that meltwater likely flowed along the entire length of the valley, evidence of channels, bars, or terraces is subdued and limited to within a mile of the northern map edge. To the south the valley floor consists of alluvial fan deposits (unit Qaf), marshland and peat (unit Qp), and scattered hillocks of bedrock (units ΦEm and Ev_C) and ice-contact deposits (unit Qgic). Beneath the cover of post-glacial sediment (units Qaf and Qp), the valley floor appears to have considerable relief, and the meltwater that formed well-preserved and clearly exposed fluvial channels, bars, and terraces farther north seems to have been at least partly in contact with residual ice (see above). This makes it difficult to interpret the morphology and gradient of the whole valley floor at the end of meltwater discharge, but we note that the most elevated portion of the Chimacum Valley floor coincides with the confluence of the largest tributary drainages within the map area. We infer from this that the gentle apex at 173 ft elevation is most likely a simple expression of post-ice valley-floor aggradation and marshland deposition rather than an expression of tectonics or differential isostatic rebound.

ACKNOWLEDGMENTS

This geologic map was funded in part by the USGS National Cooperative Geologic Mapping Program under award no. G14AC00212. We thank Jeff Tepper and Ken Clark (University of Puget Sound) and Rowland Tabor (USGS) for assistance with geochemical sample selection and interpretation; Shannon Mahan (USGS) for analysis of luminescence samples; Dan Miggins (Oregon State University) for $^{40}Ar/^{39}Ar$ analysis of igneous rock samples; Elizabeth Nesbitt (Burke Museum, University of Washington) for analysis and assistance with collection of biostratigraphic samples for fossils and their ages; Bernard Housen (Western Washington University) for paleomagnetic analyses; the Jefferson County Assessor's Office for GIS data; the Washington State Department of Transportation for access to geotechnical records and Eric Dingeldein for his assistance with those records; Joe Rocchio, Joe Arnett, and Rex Crawford (all WADNR Natural Heritage Program) for assistance with plant sample identification; Richard Blakely (USGS) for aeromagnetic field-strength maps; Ralph Haugerud (USGS) for comments on the advance and recession of the Vashon-age Puget lobe ice sheet, and permission to adapt his unpublished figure on that subject; Brett Cox (USGS) for fruitful exchange of ideas about adjacent map areas; Kevin Hurley, Gretchen Schmauder, and Naiema Jackson (Geometrics, Inc.), for collaborative acquisition of new marine magnetic survey data; Andy Lamb (USGS) for magnetic, gravity, seismic line, and other data; Bill Lingley (Leslie Geological Services) for assistance with interpretation of seismic survey data; and Bob Carson (Whitman College) and Kathryn Hanson (AMEC) for sharing their field notes and knowledge of the area. We thank Washington Division of Geology and Earth Resources staff Rian Skov, Bryan Garcia, Coire McCabe, and Shawn Lombardini for help with boat-based field work. We thank countless landowners for sharing local knowledge and permitting us to map on their land.

REFERENCES CITED

Allison, R. C., 1959, The geology and Eocene megafaunal paleontology of the Quimper Peninsula area, Washington: University of Washington Master of Science thesis, 121 p., 1 plate.

Anundsen, Karl; Abella, S. E. B.; Leopold, E. B.; Stuiver, M.; Turner, S., 1994, Late-glacial and early Holocene sea-level fluctuations in the central Puget Lowland, Washington, inferred from lake sediments: Quaternary Research, v. 42, no. 2, p. 149-161.

Armentrout, J. M.; Berta, Annalisa, 1977, Eocene–Oligocene foraminiferal sequence from the northeast Olympic Peninsula, Washington: Journal of Foraminiferal Research, v. 7, no. 3, p. 216-233.

Armstrong, J. E.; Crandell, D. R.; Easterbrook, D. J.; Noble, J. B., 1965, Late Pleistocene stratigraphy and chronology in southwestern British Columbia and northwestern Washington: Geological Society of America Bulletin, v. 76, no. 3, p. 321-330.

Arnold, Ralph, 1906, Geological reconnaissance of the coast of the Olympic Peninsula, Washington: Geological Society of America Bulletin, v. 17, p. 451-468.

Babcock, R. S.; Burmester, R. F.; Engebretson, D. C.; Warnock, A. C.; Clark, K. P., 1992, A rifted margin origin for the Crescent basalts and related rocks in the northern Coast Range volcanic province, Washington and British Columbia: Journal of Geophysical Research, v. 97, no. B5, p. 6799-6821.

Babcock, R. S.; Suczek, C. A.; Engebretson, D. C., 1994, The Crescent "terrane", Olympic Peninsula and southern Vancouver Island. *In* Lasmanis, Raymond; Cheney, E. S., convenors, Regional geology of Washington State: Washington Division of Geology and Earth Resources Bulletin 80, p. 141-157. [http://www.dnr.wa.gov/publications/ger_b80_regional_geol_wa_2.pdf]

Ballantyne, C. K., 2002, Paraglacial geomorphology: Quaternary Science Reviews 21, p. 1935-2017.

Bigelow, P. K., 1987, The petrology, stratigraphy and basin history of the Montesano Formation, southwestern Washington and southern Olympic Peninsula: Western Washington University Master of Science thesis, 263 p.

Birdseye, R. U., 1976a, Geologic map of east-central Jefferson County, Washington: Washington Division of Geology and Earth Resources Open File Report 76-26, 1 sheet, scale 1:24,000. [http://www.dnr.wa.gov/publications/ger_ofr76-26_geologic_map_jefferson_co_24k.pdf]

Birdseye, R. U., 1976b, Glacial and environmental geology of east-central Jefferson County, Washington: North Carolina State University Master of Science thesis, 96 p.

Blakely, R.J.; Wells, R.E.; Weaver, C.S., 1999, Puget Sound aeromagnetic maps and data: U.S. Geological Survey Open-File Report 99–514. [http://pubs.usgs.gov/of/1999/of99-514/]

Blakely, R. J.; Wells, R. E.; Weaver, C. S.; Johnson, S. Y., 2002, Location, structure, and seismicity of the Seattle fault zone, Washington—Evidence from aeromagnetic anomalies, geologic mapping, and seismic-reflection data: Geological Society of America Bulletin, v. 114, no. 2, p. 169-177.

Blakely, R. J.; Sherrod, B. L.; Hughes, J. F.; Anderson, M. L.; Wells, R. E.; Weaver, C. S., 2009, Saddle Mountain fault deformation zone, Olympic Peninsula, Washington—Western boundary of the Seattle uplift: Geosphere, v. 5, no. 2, p. 105-125.

Blakely, R. J.; Sherrod, B. L.; Weaver, C. S.; Wells, R. E.; Rohay, A. C.; Barnett, E. A.; Knepprath, N. E., 2011, Connecting the Yakima fold and thrust belt to active faults in the Puget Lowland, Washington: Journal of Geophysical Research, v. 116, B07105, 33 p.

Booth, D. B., 1994, Glaciofluvial infilling and scour of the Puget Lowland, Washington, during ice-sheet glaciation: Geology, v. 22, no. 8, p. 695-698.

Booth, D. B.; Troost, K. G.; Clague, J. J.; Waitt, R. B., 2004, The Cordilleran ice sheet. *In* Gillespie, A. R.; Porter, S. C.; Atwater, B. F., editors, The Quaternary period in the United States: Elsevier, p. 17-43.

Bowman, J. D.; Czajkowski, J. L., 2013, Washington State seismogenic features database [GIS data]: Washington Division of Geology and Earth Resources Digital Data Series DS-1, version 3.0. [http://www.dnr.wa.gov/publications/ger_portal_seismogenic_features.zip]

Brandon, M. T.; Roden-Tice, M. K.; Garver, J. I., 1998, Late Cenozoic exhumation of the Cascadia accretionary wedge in the Olympic Mountains, northwest Washington State: Geological Society of America Bulletin, v. 110, no. 8, p. 985-1009, Data Repository item 9865. [http://minerva.union.edu/garverj/garver/pubs/Brandon_etal_1998.pdf]

Bretz, J H., 1910, Glacial lakes of Puget Sound—Preliminary paper: Journal of Geology, v. 18, no. 5, p. 448-458.

Bretz, J H., 1913, Glaciation of the Puget Sound region: Washington Geological Survey Bulletin 8, 244 p., 3 plates. [http://www.dnr.wa.gov/publications/ger_b8_glaciation_pugetsound.pdf]

Brocher, T. M.; Parsons, T. E.; Creager, K. C.; Crosson, R. S.; Symons, N. P.; Spence, G. D.; Zelt, B. C.; Hammer, P. T. C.; Hyndman, R. D., 1999, Wide-angle seismic recordings from the 1998 Seismic Hazards Investigation of Puget Sound (SHIPS), western Washington and British Columbia: U.S. Geological Survey Open-File Report 99-314, 110 p. [http://pubs.usgs.gov/of/1999/0314/]

Brocher, T. M.; Parsons, T. E.; Blakely, R. J.; Christensen, N. I.; Fisher, M. A.; Wells, R. E.; SHIPS Working Group, 2001, Upper crustal structure in Puget Lowland, Washington—Results from the 1998 seismic hazards investigations in Puget Sound: Journal of Geophysical Research, v. 106, no. B7, p. 13,541-13,564.

Brocher, T. M.; Blakely, R. J.; Wells, R. E.; Sherrod, B. L.; Ramachandran, Kumar, 2005, The transition between N–S and NE–SW directed crustal shortening in the central and northern Puget Lowland—New thoughts on the southern Whidbey Island fault [abstract]: Eos (American Geophysical Union Transactions), v. 86, no. 52, p. F1459.

Brown, R. D., Jr.; Gower, H. D.; Snavely, P. D., Jr., 1960, Geology of the Port Angeles–Lake Crescent area, Clallam County, Washington: U.S. Geological Survey Oil and Gas Investigations Map OM-203, 1 sheet, scale 1:62,500. [http://ngmdb.usgs.gov/Prodesc/proddesc_5357.htm]

Cady, W. M.; Sorensen, M. L.; MacLeod, N. S., 1972a, Geologic map of the Brothers quadrangle, Jefferson, Mason and Kitsap Counties, Washington: U.S. Geological Survey Geologic Quadrangle Map GQ-969, 1 sheet, scale 1:62,500. [http://pubs.usgs.gov/gq/0969/report.pdf]

Cady, W. M.; Tabor, R. W.; MacLeod, N. S.; Sorensen, M. L., 1972b, Geologic map of the Tyler Peak quadrangle, Clallam and Jefferson Counties, Washington: U.S. Geological Survey Geologic Quadrangle Map GQ-970, 1 sheet, scale 1:62,500. [http://pubs.usgs.gov/gq/0970/report.pdf]

Carlstad, C. A., 1992, Late Pleistocene deglaciation history at Point Partridge, central Whidbey Island, Washington: Western Washington University Master of Science thesis, 1 v.

Carson, R. J., 1980, Quaternary, environmental, and economic geology of the eastern Olympic Peninsula, Washington: [Unpublished], 275 p.

Clark, K. P., 1989, The stratigraphy and geochemistry of the Crescent Formation basalts and the bedrock geology of associated igneous rocks near Bremerton, Washington: Western Washington University Master of Science thesis, 171 p., 1 plate.

Contreras, T. A.; Spangler, Eleanor; Fusso, L. A.; Reioux, D. A.; Legorreta Paulín, Gabriel; Pringle, P. T.; Carson, R. J.; Lindstrum, E. F.; Clark, K. P.; Tepper, J. H.; Pileggi, Domenico; Mahan, S. A., 2012a, Geologic map of the Eldon 7.5-minute quadrangle, Jefferson, Kitsap, and Mason Counties, Washington: Washington Division of Geology and Earth Resources Map Series 2012-03, 1 sheet, scale 1:24,000, 60 p. text. [http://www.dnr.wa.gov/publications/ger_ms2012-03_geol_map_eldon_24k.zip]

Contreras, T. A.; Weeks, S. A.; Perry, B. B., 2012b, Analytical data from the Holly 7.5-minute quadrangle, Jefferson, Kitsap, and Mason Counties, Washington—Supplement to Open File Report 2011-5: Washington Division of Geology and Earth Resources Open File Report 2011-6, 16 p. [http://www.dnr.wa.gov/publications/ger_ofr2011-6_holly_supplement.pdf]

Contreras, T. A.; Weeks, S. A.; Stanton, K. M. D.; Stanton, B. W.; Perry, B. B.; Walsh, T. J.; Carson, R. J.; Clark, K. P.; Mahan, S. A., 2012c, Geologic map of the Holly 7.5-minute quadrangle, Jefferson, Kitsap, and Mason Counties, Washington: Washington Division of Geology and Earth Resources Open File Report 2011-5, 1 sheet, scale 1:24,000, with 13 p. text. [http://www.dnr.wa.gov/publications/ger_ofr2011-5_geol_map_holly_24k.zip]

Contreras, T. A.; Stone, K. A; Legorreta Paulín, Gabriel, 2013, Geologic map of the Lofall 7.5-minute quadrangle, Jefferson and Kitsap Counties, Washington: Washington Division of Geology and Earth Resources Map Series 2013-03, 1 sheet, scale 1:24,000, with 19 p. text. [http://www.dnr.wa.gov/publications/ger_ms2013-03_geol_map_lofall_24k.zip]

Contreras, T. A.; Patton, A. I.; Legoretta Paulín, Gabriel; Cakir, Recep; Carson, R. J., 2014, Geologic map of the Quilcene 7.5-minute quadrangle, Jefferson County, Washington: Washington Division of Geology and Earth Resources Map Series 2014-03, 1 sheet, scale 1:24,000, with 28 p. text. [http://www.dnr.wa.gov/publications/ger_ms2014-03_geol_map_quilcene_24k.zip]

Dadisman, S. V.; Johnson, S. Y.; Childs, J. R., 1997, Marine, high-resolution, multichannel, seismic-reflection data collected during Cruise G3-95-PS, northwestern Washington: U.S. Geological Survey Open-File Report 97-735, 3 CD-ROM disks. [http://pubs.er.usgs.gov/pubs/ofr/ofr97735]

Daneš, Z. F.; Bonno, M.; Brau, J. E.; Gilham, W. D.; Hoffman, T. F.; Johansen, D.; Jones, M. H.; Malfait, Bruce; Masten, J.; Teague, G. O., 1965, Geophysical investigation of the southern Puget Sound area, Washington: Journal of Geophysical Research, v. 70, no. 22, p. 5573-5580.

Deeter, J. D., 1979, Quaternary geology and stratigraphy of Kitsap County, Washington: Western Washington University Master of Science thesis, 175 p., 1 plate, scale 1:42,000. [https://fortress.wa.gov/dnr/geologydata/library/thesis/Deeter_1979_thesis.pdf]

Dethier, D. P.; Pessl, Fred, Jr.; Keuler, R. F.; Balzarini, M. A.; Pevear, D. R., 1995, Late Wisconsinan glaciomarine deposition and isostatic rebound, northern Puget Lowland, Washington: Geological Society of America Bulletin, v. 107, no. 11, p. 1288-1303.

Dickinson, W. R., 2006, Geotectonic evolution of the Great Basin: Geosphere, v. 2, no. 7, p. 353-368.

Domack, E. W., 1982, Facies of late Pleistocene glacial marine sediments on Whidbey Island, Washington: Rice University Doctor of Philosophy thesis, 312 p., 11 plates.

Domack, E. W., 1983, Facies of late Pleistocene glacial-marine sediments on Whidbey Island, Washington—An isostatic glacial-marine sequence. *In* Molnia, B. F., editor, Glacial-marine sedimentation: Plenum Press, p. 535-570.

Domack, E. W., 1984, Rhythmically bedded glaciomarine sediments on Whidbey Island, Washington: Journal of Sedimentary Petrology, v. 54, no. 2, p. 589-602.

Dragovich, J. D.; Pringle, P. T.; Walsh, T. J., 1994, Extent and geometry of the mid-Holocene Osceola mudflow in the Puget Lowland—Implications for Holocene sedimentation and paleogeography: Washington Geology, v. 22, no. 3, p. 3-26. [http://www.dnr.wa.gov/publications/ger_washington_geology_1994_v22_no3.pdf]

Dragovich, J. D.; Logan, R. L.; Schasse, H. W.; Walsh, T. J.; Lingley, W. S., Jr.; Norman, D. K.; Gerstel, W. J.; Lapen, T. J.; Schuster, J. E.; Meyers, K. D., 2002, Geologic map of Washington—Northwest quadrant: Washington Division of Geology and Earth Resources Geologic Map GM-50, 3 sheets, scale 1:250,000, with 72 p. text. [http://www.dnr.wa.gov/publications/ger_gm50_geol_map_nw_wa_250k.pdf]

Dragovich, J. D.; Petro, G. T.; Thorsen, G. W.; Larson, S. L.; Foster, G. R.; Norman, D. K., 2005, Geologic map of the Oak Harbor, Crescent Harbor, and part of the Smith Island 7.5-minute quadrangles, Island County, Washington: Washington Division of Geology and Earth Resources Geologic Map GM-59, 2 sheets, scale 1:24,000. [http://www.dnr.wa.gov/Publications/ger_gm59_geol_map_oakharbor_crescentharbor_24k.zip]

Duncan, R. A., 1982, A captured island chain in the coast range of Oregon and Washington: Journal of Geophysical Research, v. 87, no. B13, p. 10,827-10,837.

Durham, J. W., 1942, Eocene and Oligocene coral faunas of Washington: Journal of Paleontology, v. 16, no. 1, p. 84-104.

Durham, J. W., 1944, Megafaunal zones of the Oligocene of northwestern Washington: University of California Department of Geological Sciences Bulletin, v. 27, no. 5, p. 101-212.

Easterbrook, D. J., 1968, Pleistocene stratigraphy of Island County: Washington Department of Water Resources Water-Supply Bulletin 25, part 1, 34 p., 1 plate (in 4 parts). [http://www.ecy.wa.gov/programs/eap/wsb/wsb_All.html]

Einarsen, J. M., 1987, The petrography and tectonic significance of the Blue Mountain unit, Olympic Peninsula, Washington: Western Washington University Master of Science thesis, 175 p.

Engebretson, D. C.; Cox, A. V.; Gordon, R. G., 1985, Relative motions between oceanic and continental plates in the Pacific Basin: Geological Society of America Special Paper 206, 59 p.

Eronen, Matti; Kankainen, Tuovi; Tsukada, Matsuo, 1987, Late Holocene sea-level record in a core from the Puget Lowland, Washington: Quaternary Research, v. 27, no. 2, p. 147-159.

Eungard, D. W., 2014, Models of bedrock elevation and unconsolidated sediment thickness in the Puget Lowland, Washington: Washington Division of Geology and Earth Resources Open File Report 2014-04, 20 p, 2 plates, scale 1:475,000. [http://www.dnr.wa.gov/publications/ger_ofr2014-04_puget_lowland_depth_to_bedrock.zip]

Fulmer, C. V., 1954, Stratigraphy and paleontology of the type Blakeley Formation of Washington [abstract]: Geological Society of America Bulletin, v. 65, no. 12, part 2, p. 1340-1341.

Fulmer, C. V., 1975, Stratigraphy and paleontology of the type Blakeley and Blakely Harbor Formations. *In* Weaver, D. W.; Hornaday, G. R.; Tipton, Ann, editors, Paleogene symposium and selected technical papers—Conference on future energy horizons of the Pacific coast: American Association of Petroleum Geologists Pacific Section, 50th Annual Meeting, p. 210-271.

Garling, M. E.; Molenaar, Dee, 1965, Water resources and geology of the Kitsap Peninsula and certain adjacent islands: Washington Division of Water Resources Water-Supply Bulletin 18, 309 p., 5 plates.

Gayer, M. J., 1976, Geologic map of northeastern Jefferson County, Washington: Washington Division of Geology and Earth Resources Open File Report 76-21, 1 sheet, scale 1:24,000. [http://www.dnr.wa.gov/publications/ger_ofr76-21_geol_map_jefferson_co_24k.pdf]

Gayer, M. J., 1977, Quaternary and environmental geology of northeastern Jefferson County, Washington: North Carolina State University Master of Science thesis, 140 p.

Gerstel, W. J.; Small, John; Schlenger, Paul, 2012a, Kitsap Regional Shoreline Restoration Feasibility and Prioritization Study Demonstration Project—Restoration Feasibility and Prioritization Analysis of Sediment Sources in Kitsap County: Kitsap County Community Development, Contract KC-390-11, 37 p. [http://www.kitsapgov.com/dcd/KCRSRP/kcrsrp.htm#Kitsap_County_Sediment_Source_Analysis_And_Restoration_Prioritization_Study]

Gerstel, W. J.; Small, John; Schlenger, Paul, 2012b, Kitsap Regional Shoreline Restoration Feasibility and Prioritization Study Demonstration Project—Restoration Feasibility and Prioritization Analysis of Sediment Sources in Kitsap County Appendix C: Kitsap County Community Development, Contract KC-390-11, 15 maps. [http://www.kitsapgov.com/dcd/KCRSRP/AppendixC_DeeterCrossSections.pdf]

Glassley, W. E., 1974, Geochemistry and tectonics of the Crescent volcanic rocks, Olympic Peninsula, Washington: Geological Society of America Bulletin, v. 85, no. 5, p. 785-794.

Glassley, W. E., 1976, New analyses of Eocene basalt from the Olympic Peninsula, Washington; Discussion: Geological Society of America Bulletin, v. 87, no. 8, p. 1200-1201.

Gower, H. D., 1978, Tectonic map of the Puget Sound region, Washington, showing locations of faults, principal folds and large scale Quaternary deformation: U.S. Geological Survey Open-File Report 78-426, 1 sheet, scale 1:250,000, with 17 p. text. [http://pubs.er.usgs.gov/publication/ofr78426]

Gower, H. D., 1980, Bedrock geologic and Quaternary tectonic map of the Port Townsend area, Washington: U.S. Geological Survey Open-File Report 80-1174, 1 sheet, scale 1:100,000, with 19 p. text. [http://pubs.er.usgs.gov/usgspubs/ofr/ofr801174]

Gower, H. D.; Yount, J. C.; Crosson, R. S., 1985, Seismotectonic map of the Puget Sound region, Washington: U.S. Geological Survey Miscellaneous Investigations Series Map I-1613, 1 sheet, scale 1:250,000, with 15 p. text. [http://pubs.usgs.gov/imap/1613/plate-1.pdf]

Grimstad, Peder; Carson, R. J., 1981, Geology and ground-water resources of eastern Jefferson County, Washington: Washington Department of Ecology Water-Supply Bulletin 54, 125 p., 3 plates. [http://www.ecy.wa.gov/programs/eap/wsb/wsb_All.html]

Haeussler, P. J.; Yount, J. C.; Wells, R. E., 1999, Preliminary geologic map of the Uncas 7.5-minute quadrangle, Clallam and Jefferson Counties, Washington: U.S. Geological Survey Open-File Report 99-421, 1 sheet, scale 1:24,000. [http://pubs.er.usgs.gov/usgspubs/ofr/ofr99421]

Hanson, K. L., 1976, Geologic map of the Uncas–Port Ludlow area, Jefferson County, Washington: Washington Division of Geology and Earth Resources Open File Report 76-20, 1 sheet, scale 1:24,000. [http://www.dnr.wa.gov/publications/ger_ofr76-20_geol_map_uncas_port_ludlow_24k.pdf]

Hanson, K. L., 1977, The Quaternary and environmental geology of the Uncas–Port Ludlow area, Jefferson County, Washington: University of Oregon Master of Science thesis, 82 p., 5 plates.

Harding, S. T.; Barnhard, T. P.; Urban, T. C., 1988, Preliminary data from the Puget Sound multichannel seismic-reflection survey: U.S. Geological Survey Open-File Report 88-698, 7 p., 17 plates. [http://pubs.er.usgs.gov/publication/ofr88698]

Haugerud, R. A., 2005, Preliminary geologic map of Bainbridge Island, Washington: U.S. Geological Survey Open-File Report 2005-1387, version 1.0, 1 sheet, scale 1:24,000. [http://pubs.usgs.gov/of/2005/1387]

Haugerud, R. A., 2009, Preliminary geomorphic map of the Kitsap Peninsula, Washington: U.S. Geological Survey, Open-File Report 2009-1033, 2 sheets, scale 1:36,000. [http://pubs.usgs.gov/of/2009/1033/]

Hirsch, D. M.; Babcock, R. S., 2009, Spatially heterogeneous burial and high-P/T metamorphism in the Crescent Formation, Olympic Peninsula, Washington: American Mineralogist, v. 94, no. 8-9, p. 1103-1110.

Jacobson, D. A., 1927, Geology of the Quimper Peninsula: University of Washington Bachelor of Science thesis, 59 p., 1 plate.

Jillson, W. R., 1915, A preliminary report on the stratigraphy and the paleontology of the Quimper Peninsula of the State of Washington: University of Washington Master of Science thesis, 65 p., 1 plate.

Johnson, S. Y., 1993, Analysis of Cenozoic subsidence at three sites in vicinity of the Seattle basin, Washington: U.S. Geological Survey Open-File Report 93-332, 17 p.

Johnson, S. Y.; Potter, C. J.; Armentrout, J. M.; Miller, J. J.; Finn, C. A.; Weaver, C. S., 1996, The southern Whidbey Island fault—An active structure in the Puget Lowland, Washington: Geological Society of America Bulletin, v. 108, no. 3, p. 334-354, 1 plate.

Johnson, S. Y.; Blakely, R. J.; Stephenson, W. J.; Dadisman, S. V.; Fisher, M. A., 2004, Active shortening of the Cascadia forearc and implications for seismic hazards of the Puget Lowland: Tectonics, v. 23, TC1011, 27 p. [doi:10.1029/2003TC001507]

Johnson, S. Y.; Mosher, D. C.; Dadisman, S. V.; Childs, J. R.; Rhea, S. B., 2000, Tertiary and Quaternary structures of the eastern Juan de Fuca Strait—Interpreted map. *In* Mosher, D. C.; Johnson, S. Y., editors; Neotectonics of the eastern Juan de Fuca Strait—A digital geological and geophysical atlas: Geological Survey of Canada Open File Report 3931, 1 CD-ROM disk. [doi:10.4095/212099]

Jones, M. A., 1996, Thickness of unconsolidated deposits in the Puget Sound lowland, Washington and British Columbia: U.S. Geological Survey Water-Resources Investigations Report 94-4133, 1 sheet. [http://pubs.er.usgs.gov/usgspubs/wri/wri944133]

Kelsey, H. M.; Sherrod, B. L.; Johnson, S. Y.; Dadisman, S. V., 2004, Land-level changes from a late Holocene earthquake in the northern Puget Lowland, Washington: Geology, v. 32, no. 6, p. 469-472. [http://earthweb.ess.washington.edu/~bsherrod/brian/SWIFZ Kelsey Geology 2004.pdf]

Kuiper, K. F.; Deino, A.; Hilgen, F.J.; Krijgsman, W.; Renne, P. R.; Wijbrans, J. R., 2008, Syncrhonizing rock clocks of earth history: Science, v. 320, n. 5875, p. 500-504. [doi:10.1126/science.1154339]

Laprade, W. T., 2003, Subglacially reworked till in the Puget Lowland [abstract]: Geological Society of America Abstracts with Programs, v. 35, no. 6, p. 216.

Le Bas, M. J.; Le Maitre, R.W.; Streckeisen, A.; Zanettin, B., 1986, A chemical classification of volcanic rocks based on the total alkali silica diagram: Journal of Petrology, v. 27, p. 745-750.

Liberty, L. M.; Pape, K. M., 2006, Seismic characterization of the Seattle and Southern Whidbey Island fault zones in the Snoqualmie River valley, Washington—Final technical report: U.S. Geological Survey Earthquake Hazards Program, External Research Support, Funded Research Final Technical Reports, 17 p. [http://earthquake.usgs.gov/research/external/reports/06HQGR0111.pdf]

Mace, C. G.; Keranen, K. M., 2012, Oblique fault systems crossing the Seattle basin—Geophysical evidence for additional shallow fault systems in the central Puget Lowland: Journal of Geophysical Research, v. 117, B03105, 19 p.

Macleod, N.S.; Tiffin, D.L.; Snavely, P.D., Currie, R.G., 1977, Geologic interpretation of magnetic and gravity anomalies in the Strait of Juan de Fuca, U.S.-Canada: Canadian Journal of Earth Sciences, v. 14, no. 2, p. 223-238.

McCaffrey, Robert; Qamar, A. I.; King, R. W.; Wells, Ray; Khazaradze, Giorgi; Williams, C. A.; Stevens, C. W.; Vollick, J. J.; Zwick, P. C., 2007, Fault locking, block rotation and crustal deformation in the Pacific Northwest: Geophysical Journal International, v. 169, no. 3, p. 1315-1340.

Morrison, R. B., 1991, Introduction. *In* Morrison, R. B., editor, Quaternary nonglacial geology—Conterminous U.S.: Geological Society of America DNAG Geology of North America, v. K-2, p. 1-12.

Mosher, D. C.; Hewitt, A. T., 2004, Late Quaternary deglaciation and sea-level history of eastern Juan de Fuca Strait, Cascadia: Quaternary International, v. 121, no. 1, p. 23-39.

Mullen, E. D., 1983, $MnO/TiO_2/P_2O_5$—A minor element discriminant for basaltic rocks of oceanic environments and its implications for petrogenesis: Earth and Planetary Science Letters, v. 62, p. 53-62.

Pearce, J. A.; Gale, G. H. 1977, Identification of ore-deposition environment from trace-element geochemistry of associated igneous host rocks, Geological Society, London, Special Publications v. 7, no. 1, p. 14-24. [doi:10.1144/gsl.sp.1977.007.01.03]

Pearce, J.A.; Norry, M.J., 1979, Petrogenetic implications of Ti, Zr, Y, and Nb. Variations in volcanic rocks: Contributions to Mineralogy and Petrology, v. 69, p. 33-37.

Pettijohn, F. J., 1957, Sedimentary rocks: Harper and Brothers, 718 p.

Polenz, Michael; Wegmann, K. W.; Schasse, H. W., 2004, Geologic map of the Elwha and Angeles Point 7.5-minute quadrangles, Clallam County, Washington: Washington Division of Geology and Earth Resources Open File Report 2004-14, 1 sheet, scale 1:24,000 [http://www.dnr.wa.gov/publications/ger_ofr2004-14_geol_map_elwha_angelespoint_24k.pdf]

Polenz, Michael; Slaughter, S. L.; Thorsen, G. W., 2005, Geologic map of the Coupeville and part of the Port Townsend North 7.5-minute quadrangles, Island County, Washington: Washington Division of Geology and Earth Resources Geologic Map GM-58, 1 sheet, scale 1:24,000. [http://www.dnr.wa.gov/Publications/ger_gm58_geol_map_coupeville_24k.pdf]

Polenz, Michael; Schasse, H. W.; Petersen, B. B., 2006, Geologic map of the Freeland and northern part of the Hansville 7.5-minute quadrangles, Island County, Washington: Washington Division of Geology and Earth Resources Geologic Map GM-64, 1 sheet, scale 1:24,000. [http://www.dnr.wa.gov/Publications/ger_gm64_geol_map_freeland_hansville_24k.pdf]

Polenz, Michael; Alldritt, Katelin; Heheman, N. J.; Logan, R. L., 2009a, Geologic map of the Burley 7.5-minute quadrangle, Kitsap and Pierce Counties, Washington: Washington Division of Geology and Earth Resources Open File Report 2009-8, 1 sheet, scale 1:24,000. [http://www.dnr.wa.gov/publications/ger_ofr2009-8_geol_map_burley_24k.pdf]

Polenz, Michael; Alldritt, Katelin; Heheman, N. J.; Sarikhan, I. Y.; Logan, R. L., 2009b, Geologic map of the Belfair 7.5-minute quadrangle, Mason, Kitsap, and Pierce Counties, Washington: Washington Division of Geology and Earth Resources Open File Report 2009-7, 1 sheet, scale 1:24,000. [http://www.dnr.wa.gov/publications/ger_ofr2009-7_geol_map_belfair_24k.pdf]

Polenz, Michael; Contreras, T. A.; Czajkowski, J. L.; Legorreta Paulín, Gabriel; Miller, B. A.; Martin, M. E.; Walsh, T. J.; Logan, R. L.; Carson, R. J.; Johnson, C. N.; Skov, R. H.; Mahan, S. A.; Cohan, C. R., 2010, Supplement to geologic maps of the Lilliwaup, Skokomish Valley, and Union 7.5-minute quadrangles, Mason County, Washington—Geologic setting and development around the Great Bend of Hood Canal: Washington Division of Geology and Earth Resources Open File Report 2010-5, 27 p. [http://www.dnr.wa.gov/publications/ger_ofr2010-5_lilliwaup_skokomish_valley_union_suppl_24k.pdf]

Polenz, Michael; Czajkowski, J. L.; Legorreta Paulín, Gabriel; Contreras, T. A.; Miller, B. A.; Martin, M. E.; Walsh, T. J.; Logan, R. L.; Carson, R. J.; Johnson, C. N.; Skov, R. H.; Mahan, S. A.; Cohan, C. R., 2011, Geologic map of the Skokomish Valley and Union 7.5-minute quadrangles, Mason County, Washington: Washington Division of Geology and Earth Resources Open File Report 2010-3 revised, 21 p., 1 plate, scale 1:24,000. [http://www.dnr.wa.gov/publications/ger_ofr2010-3_geol_map_skokomish_valley_union_24k.zip]

Polenz, Michael; Miller, B. A.; Davies, Nigel; Perry, B. B.; Clark, K. P.; Walsh, T. J.; Carson, R. J.; Hughes, J. F., 2012a, Geologic map of the Hoodsport 7.5-minute quadrangle, Mason County, Washington: Washington Division of Geology and Earth Resources Open File Report 2011-3, 1 sheet, scale 1:24,000, with 16 p. text. [http://www.dnr.wa.gov/publications/ger_ofr2011-3_geol_map_hoodsport_24k.zip]

Polenz, Michael; Miller, B. A.; Davies, Nigel; Perry, B. B.; Hughes, J. F.; Clark, K. P.; Walsh, T. J.; Tepper, J. H.; Carson, R. J., 2012b, Analytical data from the Hoodsport 7.5-minute quadrangle, Mason County, Washington—Supplement to Open File Report 2011-3: Washington Division of Geology and Earth Resources Open File Report 2011-4, 42 p. [http://www.dnr.wa.gov/publications/ger_ofr2011-4_hoodsport_supplement.pdf]

Polenz, Michael; Spangler, Eleanor; Fusso, L. A.; Reioux, D. A.; Cole, R. A.; Walsh, T. J.; Cakir, Recep; Clark, K. P.; Tepper, J. H.; Carson, R. J.; Pileggi, Domenico; Mahan, S. A., 2012c, Geologic map of the Brinnon 7.5-minute quadrangle, Jefferson and Kitsap Counties, Washington: Washington Division of Geology and Earth Resources Map Series 2012-02, 1 sheet, scale 1:24,000, with 47 p. text. [http://www.dnr.wa.gov/publications/ger_ms2012-02_geol_map_brinnon_24k.zip]

Polenz, Michael; Petro, G. T.; Contreras, T. A.; Stone, K. A.; Legorreta Paulín, Gabriel; Cakir, Recep, 2013, Geologic map of the Seabeck and Poulsbo 7.5-minute quadrangles, Kitsap and Jefferson Counties, Washington: Washington Division of Geology and Earth Resources Map Series 2013-02, 1 sheet, scale 1:24,000, with 39 p. text. [http://www.dnr.wa.gov/publications/ger_ms2013-02_geol_map_seabeck-poulsbo_24k.zip]

Polenz, Michael; Gordon, H. O.; Hubert, I. J.; Contreras, T. A.; Patton, A. I.; Paulín, Gabriel Legorreta; Cakir, Recep, 2014, Geologic map of the Center 7.5-minute quadrangle, Jefferson County, Washington: Washington Division of Geology and Earth Resources Map Series 2014-02, 1 sheet, scale 1:24,000, with 35 p. text. [http://www.dnr.wa.gov/Publications/ger_ms2014-02_geol_map_center_24k.zip]

Porter, S. C.; Carson, R. J., 1971, Problems of interpreting radiocarbon dates from dead-ice terrain, with an example from the Puget Lowland of Washington: Quaternary Research, v. 1, no. 3, p. 410-414.

Porter, S. C.; Swanson, T. W., 1998, Radiocarbon age constraints on rates of advance and retreat of the Puget lobe of the Cordilleran ice sheet during the last glaciation: Quaternary Research, v. 50, no. 3, p. 205-213.

Pratt, T. L.; Johnson, S. Y.; Potter, C. J.; Stephenson, W. J.; Finn, C. A., 1997, Seismic reflection images beneath Puget Sound, western Washington State—The Puget Lowland thrust sheet hypothesis: Journal of Geophysical Research, v. 102, no. B12, p. 27,469-27,489.

Prescott, J. R.; Hutton, J. T., 1994, Cosmic ray contribution to dose rates for luminescence and ESR dating—Large depths and long-term time variations: Radiation Measurements, v. 23, no. 2-3, p. 497-500.

Prothero, D. D.; Thompson, Matthew, 2001, Magnetic Stratigraphy of the Type Refugian Stage (Late Eocene–Early Oligocene), Western Santa Ynez Range, Santa Barbara County, California. *In* Prothero, D.R., editor, Magnetic Stratigraphy of the Pacific Coast Cenozoic: Pacific Section SEPM Book 91.

Raisz, E. J., 1945, The Olympic–Wallowa lineament: American Journal of Science, v. 243A [Daly volume], p. 479-485. [http://earth.geology.yale.edu/~ajs/1945A/479.pdf]

Rau, W. W., 1964, Foraminifera from the northern Olympic Peninsula, Washington: U.S. Geological Survey Professional Paper 374-G, 33 p., 7 plates. [http://pubs.er.usgs.gov/usgspubs/pp/pp374G]

Rau, W. W., 1981, Pacific Northwest Tertiary benthic foraminiferal biostratigraphic framework—An overview. *In* Armentrout, J. M., editor, Pacific Northwest Cenozoic biostratigraphy: Geological Society of America Special Paper 184, p. 67-84.

Rau, W. W., 2000, Appendix 4—Foraminifera from the Carlsborg 7.5-minute quadrangle, Washington. *In* Schasse, H. W.; Wegmann, K. W., Geologic map of the Carlsborg 7.5-minute quadrangle, Clallam County, Washington: Washington Division of Geology and Earth Resources Open File Report 2000-7, p. 24-26. [http://www.dnr.wa.gov/publications/ger_ofr2000-7_geol_map_carlsborg_24k.zip]

Rau, W. W., 2004, Pacific Northwest Tertiary foraminiferal collections of the U.S. Geological Survey and the State of Washington: Washington Division of Geology and Earth Resources Digital Report 4, 1 Excel file. [http://www.dnr.wa.gov/publications/ger_dr4_pacific_nw_foram_collections.zip]

Rauch, W. E., 1985, Sedimentary petrology, depositional environment, and tectonic implications of the upper Eocene Quimper Sandstone and Marrowstone Shale, northeastern Olympic Peninsula, Washington: Western Washington University Master of Science thesis, 102 p.

Roberts, T. H., 1991, Gravity investigation of crustal structure in the eastern Olympic Peninsula-Puget Lowland area, Washington: Western Washington University Master of Science thesis, 65 p.

Rhodes, E. J., 2011, Optically stimulated luminescence dating of sediments over the past 200,000 years: Annual Review of Earth and Planetary Sciences, v. 39, p. 461-488.

Rigg, G. B., 1958, Peat Resources of Washington: Division of Mines and Geology, p. 66-67. [http://www.dnr.wa.gov/publications/ger_b44_peat_reasources_wa_1.pdf]

Schasse, H. W.; Kalk, M. L.; Petersen, B. B.; Polenz, Michael, 2009, Geologic map of the Langley and western part of the Tulalip 7.5-minute quadrangles, Island County, Washington: Washington Division of Geology and Earth Resources Geologic Map GM-69, 1 sheet, scale 1:24,000. [http://www.dnr.wa.gov/publications/ger_gm69_geol_map_langley_24k.pdf]

Schasse, H. W.; Polenz, Michael, 2002, Geologic map of the Morse Creek 7.5-minute quadrangle, Clallam County, Washington: Washington Division of Geology and Earth Resources Open File Report 2002-8, 2 sheets, scale 1:24,000, with 26 p. text [http://www.dnr.wa.gov/publications/ger_ofr2002-8_geol_map_morsecreek_24k.zip]

Schasse, H. W.; Slaughter, S. L., 2005, Geologic map of the Port Townsend South and part of the Port Townsend North 7.5-minute quadrangles, Jefferson County, Washington: Washington Division of Geology and Earth Resources Geologic Map 57, 1 sheet, scale 1:24,000 [http://www.dnr.wa.gov/publications/ger_gm57_geol_map_porttownsends_24k.pdf]

Schasse, H. W.; Wegmann, K. W., 2000, Geologic map of the Carlsborg 7.5-minute quadrangle, Clallam County, Washington: Washington Division of Geology and Earth Resources Open File Report 2000-7, 2 sheets, scale 1:24,000, with 33 p. text [http://www.dnr.wa.gov/publications/ger_ofr2000-7_geol_map_carlsborg_24k.zip]

Schasse, H. W.; Wegmann, K. W.; Polenz, Michael, 2004, Geologic map of the Port Angeles and Ediz Hook 7.5-minute Quadrangles, Clallam County, Washington: Washington Division of Geology and Earth Resources Open File Report 2004-13, 1 sheet, scale 1:24,000 [http://www.dnr.wa.gov/publications/ger_ofr2004-13_geol_map_portangeles_edizhook_24k.pdf]

Schweitzer-Hopkins, C. E., 1996, Fossil decapod crustaceans of the late Oligocene to early Miocene Pysht Formation and late Eocene Quimper Sandstone, Olympic Peninsula, Washington: Kent State University Master of Science thesis, 206 p.

Sherrod, B. L., 2005, Prehistoric earthquakes in the Puget Lowland, Washington [abstract]: Eos (American Geophysical Union Transactions), v. 86, no. 52, p. F1458-1459.

Sherrod, B. L.; Blakely, R. J.; Weaver, Craig; Kelsey, Harvey; Barnett, Elizabeth; Wells, Ray, 2005, Holocene fault scarps and shallow magnetic anomalies along the southern Whidbey Island fault zone near Woodinville, Washington: U.S. Geological Survey Open-File Report 2005-1136, 35 p. [http://pubs.usgs.gov/of/2005/1136/]

Sherrod, B. L.; Blakely, R. J.; Weaver, C. S.; Kelsey, H. M.; Barnett, Elizabeth; Liberty, Lee; Meagher, K. L.; Pape, Kristin, 2008, Finding concealed active faults—Extending the southern Whidbey Island fault across the Puget Lowland, Washington: Journal of Geophysical Research, v. 113, B05313. [doi:10.1029/2007JB005060, 2008]

Siddall, M.; Rohling, E. J.; Thompson, W. G.; Waelbroeck, C., 2008, Marine isotope stage 3 sea level fluctuations: Data synthesis and new outlook, Reviews of Geophysics, v. 46, RG4003. [doi:10.1029/2007RG000226.]

Simonds, F. W.; Longpre, C. I.; Justin, G. B., 2004, Ground-water system in the Chimacum Creek basin and surface water/ground water interaction in Chimacum and Tarboo Creeks and the Big and Little Quilcene Rivers, eastern Jefferson County, Washington: U.S. Geological Survey Scientific Investigations Report 2004-5058, 1 sheet, scale 1:31,680, 49 p. text. [http://pubs.water.usgs.gov/sir2004-5058]

Singhroy, V. H.; Kenny, F. M.; Barnett, P. J., 1992a, Imagery for Quaternary Geological Mapping in Glaciated Terrains: Canadian Journal of remote Sensing, v. 18, n. 2, p. 112-117.

Singhroy, V. H.; Kenny, F. M.; Barnett, P. J., 1992b, Quaternary Mapping in Glaciated and Vegetated Areas Using SAR and Multispectral Images: Proceeding I, XVII International Society of Photogrammetry and Remote Sensing congress, Washington, D.C., v. XXIX, part B7. [http://www.isprs.org/proceedings/XXIX/congress/part7/874_XXIX-part7.pdf]

Snavely, P. D., Jr., 1983, Day 1—Peripheral rocks—Tertiary geology of the northwestern part of the Olympic Peninsula, Washington. *In* Muller, J. E.; Snavely, P. D., Jr.; Tabor, R. W., The Tertiary Olympic terrane, southwest Vancouver Island and northwest Washington: Geological Association of Canada Victoria Section Field Trip 12, p. 6-31.

Snavely, P. D., Jr.; Niem, A. R.; Pearl, J. E., 1978, Twin River Group (upper Eocene to lower Miocene); Defined to include the Hoko River, Makah, and Pysht Formations, Clallam County, Washington. *In* Sohl, N. F.; Wright, W. B., Changes in stratigraphic nomenclature by the U.S. Geological Survey, 1977: U.S. Geological Survey Bulletin 1457-A, p. 111-120. [http://ngmdb.usgs.gov/Geolex/resources/docs/USGS_B-1457-A_t.pdf]

Spencer, P. K., 1983, Depositional environment of some Eocene strata near Quilcene, Washington, based on trace-, macro-, and micro-fossils and lithologic associations. *In* Larue, D. K.; Steel, R. J., editors, Cenozoic marine sedimentation: Pacific margin, U.S.A.: Society of Economic Paleontologists and Mineralogists Pacific Section, p. 233-239.

Spencer, P. K., 1984, Lower Tertiary biostratigraphy and paleoecology of the Quilcene–Discovery Bay area, northeast Olympic Peninsula, Washington: University of Washington Doctor of Philosophy thesis, 173 p., 2 plates.

Squires, R. L.; Goedert, J. L.; Kaler, K. L., 1992, Paleontology and stratigraphy of Eocene rocks at Pulali Point, Jefferson County, eastern Olympic Peninsula, Washington: Washington Division of Geology and Earth Resources Report of Investigations 31, 27 p. [http://www.dnr.wa.gov/publications/ger_ri31_eocene_rock_jefferson_county.pdf]

Stock, J. and Molnar, P., 1988, Uncertainties and implications of the late Cretaceous and Tertiary position of the North America relative to the Farallon, Kula, and Pacific plates, Tectonics, v. 7, no. 6, p. 1339-1384.

Swanson, T. W., 1994, Determination of ^{36}Cl production rates from the deglaciation history of Whidbey Island, Washington: University of Washington Doctor of Philosophy thesis, 121 p.

Tabor, R. W.; Cady, W. M., 1978a, Geologic map of the Olympic Peninsula, Washington: U.S. Geological Survey Miscellaneous Investigations Series Map I-994, 2 sheets, scale 1:125,000. [http://pubs.er.usgs.gov/publication/i994]

Tabor, R. W.; Cady, W. M., 1978b, The structure of the Olympic Mountains, Washington—Analysis of a subduction zone: U.S. Geological Survey Professional Paper 1033, 38 p. [http://pubs.er.usgs.gov/publication/pp1033]

Tabor, R. W.; Haessler, P. J.; Haugerud, R. A.; Wells, R. E., 2011, Lidar-revised geologic map of the Uncas 7.5-minute quadrangle, Clallam and Jefferson Counties, Washington: U.S. Geological Survey Scientific Investigations Map: 3160, 1 sheet, scale 1:24,000 with 13 p. text. [http://pubs.usgs.gov/sim/3160/]

ten Brink, U. S.; Molzer, P. C.; Fisher, M. A.; Blakely, R. J.; Bucknam, R. C.; Parsons, T. E.; Crosson, R. S.; Creager, K. C., 2002, Subsurface geometry and evolution of the Seattle fault zone and the Seattle basin, Washington: Seismological Society of America Bulletin, v. 92, no. 5, p. 1737-1753.

Thoms, R. E., 1959, The geology and Eocene biostratigraphy of the southern Quimper Peninsula area, Washington: University of Washington Master of Science thesis, 102 p., 7 plates.

Thorson, R. M., 1980, Ice-sheet glaciation of the Puget Lowland, Washington, during the Vashon Stade (late Pleistocene): Quaternary Research, v. 13, no. 3, p. 303-321.

Thorson, R. M., 1981, Isostatic effects of the last glaciation in the Puget Lowland, Washington: U.S. Geological Survey Open-File Report 81-370, 100 p., 1 plate. [http://pubs.er.usgs.gov/publication/ofr81370]

Thorson, R. M., 1989, Glacio-isostatic response of the Puget Sound area, Washington: Geological Society of America Bulletin, v. 101, no. 9, p. 1163-1174.

Troost, K. G.; Booth, D. B., 2008, Geology of Seattle and the Seattle area, Washington. *In* Baum, R. L.; Godt, J. W.; Highland, L. M., editors, Landslides and engineering geology of the Seattle, Washington, area: Geological Society of America Reviews in Engineering Geology XX, p. 1-35. [http://www.wou.edu/las/physci/taylor/g473/seismic_hazards/troost_booth_2008_geo_seattle.pdf]

U.S. Coast & Geodetic Survey, 1870 "T-sheet" coastal survey (register no. 1126). [http://riverhistory.ess.washington.edu/tsheets/framedex.htm]

U.S. Department of Agriculture, Natural Resource Conservation Service, 2009, Web Soil Survey, status 12/06/2013 [GIS data]. [accessed July, 2014, at http://websoilsurvey.nrcs.usda.gov/]

U.S. Geological Survey Geologic Names Committee, 2010, Divisions of geologic time—Major chronostratigraphic and geochronologic units: U.S. Geological Survey Fact Sheet 2010-3059, 2 p. [http://pubs.usgs.gov/fs/2010/3059/]

U.S. Geological Survey Pacific Coastal & Marine Science Center, 2015, National Archive of Marine Seismic Surveys [geophysical data]: United States Geological Survey Pacific Coastal & Marine Science Center. [accessed April 27th, 2015, at https://walrus.wr.usgs.gov/NAMSS]

Van Wagoner, T. M.; Crosson, R. S.; Creager, K. C.; Medema, G. F.; Preston, L. A.; Symons, N. P.; Brocher, T. M., 2002, Crustal structure and relocated earthquakes in the Puget Lowland, Washington, from high-resolution seismic tomography: Journal of Geophysical Research, v. 107, no. B12, 2381, p. ESE 22-1–22-23. [doi:10.1029/20012JB000710]

Waitt, R. B., Jr.; Thorson, R. M., 1983, The Cordilleran ice sheet in Washington, Idaho, and Montana. *In* Porter, S. C., editor, The late Pleistocene; Volume 1 of Wright, H. E., Jr., editor, Late-Quaternary environments of the United States: University of Minnesota Press, p. 53-70.

Walsh, T. J.; Logan, R. L.; Polenz, Michael; Schasse, H. W., 2003, Geologic map of the Nisqually 7.5-minute quadrangle, Thurston and Pierce Counties, Washington: Washington Division of Geology and Earth Resources Open File Report 2003-10, 1 sheet, scale 1:24,000. [http://www.dnr.wa.gov/publications/ger_ofr2003-10_geol_map_nisqually_24k.pdf]

Weaver, C. E., 1912, A preliminary report on the Tertiary paleontology of western Washington: Washington Geological Survey Bulletin 15, 80 p. [http://www.dnr.wa.gov/publications/ger_b15_prelim_rep_teriary_paleo_western_wa.pdf]

Weaver, C. E., 1937, Tertiary stratigraphy of western Washington and northwestern Oregon: University of Washington Publications in Geology, v. 4, 266 p.

Webb, G. E.; Price, G. J.; Nothdurft, L. D.; Deer, Linda; Rintoul, Llew, 2007, Cryptic meteoric diagenesis in freshwater bivalves: Implications for radiocarbon dating: Geology, v. 7, no. 9, p. 803-806. [doi: 10.1130/G23823A.1]

Wells, R. E.; Weaver, C. S.; Blakely, R. J., 1998, Fore-arc migration in Cascadia and its neotectonic significance: Geology, v. 26, no. 8, p. 759-762.

Wells, R. E.; McCaffrey, R., 2013, Steady Rotation of the Cascade arc: Geology, v. 41, no. 9, p. 1027-1030.

Whetten, J. T.; Carroll, P. I.; Gower, H. D.; Brown, E. H.; Pessl, Fred, Jr., 1988, Bedrock geologic map of the Port Townsend 30- by 60-minute quadrangle, Puget Sound region, Washington: U.S. Geological Survey Miscellaneous Investigations Series Map I-1198-G, 1 sheet, scale 1:100,000. [http://pubs.er.usgs.gov/publication/i1198G]

Wolfe, E. W.; McKee, E. H., 1972, Sedimentary and igneous rocks of the Grays River quadrangle, Washington: U.S. Geological Survey Bulletin 1335, 70 p. [http://pubs.er.usgs.gov/usgspubs/b/b1335]

Yount, J. C.; Gower, H. D., 1991, Bedrock geologic map of the Seattle 30′ by 60′ quadrangle, Washington: U.S. Geological Survey Open-File Report 91-147, 37 p., 4 plates. [http://pubs.er.usgs.gov/publication/ofr91147]

Yount, J. C.; Minard, J. P.; Dembroff, G. R., 1993, Geologic map of surficial deposits in the Seattle 30- by 60-minute quadrangle, Washington: U.S. Geological Survey Open-File Report 93-233, 2 sheets, scale 1:100,000. [http://ngmdb.usgs.gov/Prodesc/proddesc_12654.htm]

Appendix A. New Radiocarbon, Luminescence, and $^{40}Ar/^{39}Ar$ Age Estimates

Table A1. Radiocarbon ages from the map area. ^{14}C yr BP age estimates (including AMS) are in radiocarbon years before 1950 and uncertainty estimates are reported at 1σ (68% confidence). Ages in ka are calendar years before 1950 divided by 1,000 and have 2σ uncertainty. An age range is preferred because uncertainties are unequally distributed as a result of the calibration curves used to convert between radiocarbon and calendar years. Ages and uncertainties in quotation marks are those reported by the original publication; levels of uncertainty and the calibration method used (if any) are unknown. Uncertainty statements reflect random and lab errors; errors from unrecognized sample characteristics or flawed methodological assumptions (for example, ^{14}C sample contamination from younger carbon flux) are not known. Radiocarbon 'greater than' age statements (for example, >43,500 BP) include a 2σ variance against background radiation. Ages (including AMS) are adjusted for measured $^{13}C/^{12}C$ ratio (a 'conventional' age) if a $^{13}C/^{12}C$ ratio is shown; samples without a ratio did not report if the ages were 'measured' or 'conventional'.

Geologic units are the interpretation of this study and may differ from the original publication for compiled data. For samples GD8 (derived from unit Qco, but sampled from a landslide) and approximately located samples GD9 and GD10, these differ from map units. Elevations were estimated using Puget Sound Lidar Consortium lidar data projected to State Plane South, NAD 83 HARN, US Survey feet, supplemented by visual elevation estimates on bluffs. Lidar level 0 is theoretically 3.52 to 3.67 ft below base map level 0 [http://www.ngs.noaa.gov/cgi-bin/VERTCON/vert_con.prl]. Lidar elevation statements were not adjusted to account for systematic projection differences relative to the base map. Latitude and longitude coordinates are in WGS84. – – – indicates no data.

^{14}C sample ID (geologic unit)		Reference	Material	Method	$^{13}C/^{12}C$ (o/oo)	Age estimate
GD1 (Qa)		this study	delicate plant material	^{14}C (AMS)	-28.0	160 ±30 ^{14}C yr BP (0.285–0.240, 0.230–0.060, or 0.040–post 0 ka)
Lab ID[a]	Beta 398213	Delicate, flattened, tubular marsh(?) plant fragments (likely graminoid—[Oral communication, Joe Rocchio, Joe Arnett, and Rex Crawford, Washington Department of Natural Resources) from a 2–3 in.-thick seam in massive, soft, gray, clayey silt. Date suggests aggradation due to transient damming by a downvalley landslide. Because it would be too small to show at map scale, it was included with unit Qmw).				
TRS	sec. 32, T29N R1E					
Lat/long. (degrees)	47.960013 -122.706627					
Elev. (ft)	~165					
GD2 (Qco)		this study	wood	^{14}C (AMS)	-27.6	22,200 ±80 ^{14}C yr BP (26.585–26.190 ka)
Lab ID[a]	Beta 398209	Wood fragments from peat at beach level, below a 50-ft-high cliff of clean sand overlain by till. Date suggests that a late Olympia nonglacial (MIS 3) organic deposit is covered by late Olympia age sandy channel sediment and distal Vashon (MIS 2) advance outwash.				
TRS	sec. 13, T28N R1E					
Lat/long. (degrees)	47.924654 -122.612558					
Elev. (ft)	~11					
GD3 (Qco)		this study	plant material	^{14}C (AMS)	-27.2	23,470 ±90 ^{14}C yr BP (27.745–27.530 ka)
Lab ID[a]	Beta 398215	Plant material from peat amid thinly interbedded floodplain deposits (sand, silt, clay) at about 180 ft elevation, overlain by stiff clay and silt.				
TRS	sec. 21, T28N R1W					
Lat/long. (degrees)	47.910947 -122.682710					
Elev. (ft)	~180					
GD4 (Qco)		this study	organic sediment	^{14}C (AMS)	-28.2	36,670 ±320 ^{14}C yr BP (41.805–40.680 ka)
Lab ID[a]	Beta 398211	Organic sediment from 4-in.-thick, gray, organic-rich clay that caps a channel cut-and fill section amid 30 ft of fluvial section that overall fines upward from cobble gravel to pea-gravel and sand.				
TRS	sec. 12, T28N R1W					
Lat/long. (degrees)	47.938468 -122.743407					
Elev. (ft)	~335					
GD5 (Qgas)		this study	organic material	^{14}C (AMS)	-26.0	43,130 ±650 ^{14}C yr BP (47.680–45.210 ka)
Lab ID[a]	Beta 398216	Abraded, small, detrital organic fragment about 15 ft below cliff top in dense, horizontally bedded, gray, medium to coarse sand downsection from, but part of the same unit as, 4–5-ft-thick pebble gravel. The character of the sample and the pre-Vashon date suggest reworking of organic fragments into locally abundant and thick Vashon advance outwash (MIS 2). Alternatively, and less likely based on elevation and character of the deposit, could be an Olympia nonglacial deposit (MIS 3).				
TRS	sec. 25, T29N R1W					
Lat/long. (degrees)	47.981438 -122.738931					
Elev. (ft)	~280					

^{14}C sample ID (geologic unit)		Reference	Material	Method	^{13}C/^{12}C (o/oo)	Age estimate
GD6 (Qc$_o$)		this study	wood	^{14}C (AMS)	-28.0	> 43,500 ^{14}C yr BP
Lab ID[a]	Beta 398214	Wood from a detrital peat fragment, in 10-ft-thick fining-upward section of coarse sand to clay, with some detrital coal. Sampled near base of over 40 ft repeated fining-up sections above 40 ft debris to beach. Late olympia-age dates at nearby—upsection?—sites GD11 and GD12 suggest that the sample is significantly older than its host sediment.				
TRS	sec. 22, T28N R2E					
Lat/long. (degrees)	47.90349 -122.528347					
Elev. (ft)	~62					
GD7 (Qc)		this study	delicate organic matter	^{14}C (AMS)	-28.5	> 43,500 ^{14}C yr BP
Lab ID[a]	Beta 398212	Flattened fragments of plant or algal organic matter from a one inch thick gyttja exposed at beach top. Sampled just east and seemingly downsection of a 40-ft-thick, rhythmically bedded section of laminated silt and sand. Part of the exposure dips west-down (apparent), and sample may be landslide-affected but can be taken to represent conditions within some part of the lower bluff, where Deeter (1979) also mapped nonglacial pre-Vashon sediment.				
TRS	sec. 17, T28N R2E					
Lat/long. (degrees)	47.919991 -122.564159					
Elev. (ft)	~10					
GD8 (Qc from Qls block)		this study	wood	^{14}C	-24.2	> 43,500 ^{14}C yr BP
Lab ID[a]	Beta 398210	Detrital wood stick, about 1.25 in. in diameter, embedded in wavy, laminated silt that appears to be part of a landslide block above a marine shell-bearing diamicton that we, like Bretz (1913) and Deeter (1979), mapped as pre-Vashon glaciomarine drift. Cliff-top above landslide exposes at least 40 ft of till.				
TRS	sec. 12, T28N R1E					
Lat/long. (degrees)	47.939145 -122.616724					
Elev. (ft)	~12					
Compiled dates:						
GD9 GD10 (Qgdm$_e$)		Swanson (1994, p. 14, 36, 37, and 49)	marine shells	"^{14}C"	– – – – – –	GD9 – AA-10077 "12,990 ±100" ^{14}C yr BP[b] GD10 – QL-4665 "13,470 ±90" ^{14}C yr BP[b]
Lab ID[a]	GD9 – AA-10077 GD10 – QL-4665	Dates reported by Swanson (1994) from aragonite fraction of articulated shells sampled at upper (GD9/QL-4665) and lower (GD10/AA-10077) ends of glaciomarine drift "at Basalt Point". Sample location ambiguous in Swanson (1994)—he (p. 14, 36, and 37) refers to Basalt Point (sec. 33, T29N R1E) but in table 1 (p. 14) provides latitude and longitude coordinates that place the samples at ~480 ft elevation 2.1 mi west-northwest of Basalt Point; in fig. 10 (p. 49) he graphically locates the same samples at the east end of Foulweather Bluff (sec. 7, T28N R2E). He clarified (written commun., 2015) that the samples "are from the quarry location", at or within 0.5 mi of Basalt Point. Reported dates exclude reservoir correction. Swanson argued that upwelling of deep ocean water would have been less during the late glaciation than modern upwelling at Orcas Island; he therefore advocated a 400 yr reservoir correction (vs. 725 yrs for modern samples from Orcas Island)—such that his corrected age statements are 12,590 ±100 and 13,070 ±90 ^{14}C yr BP.				
TRS	~sec. 33, T29N R1E[b]					
Lat/long. (degrees)	47.95783 -122.676870[b]					
Elev. (ft)	?[b]					
GD11 GD12 (Qc$_o$)		Deeter (1979, p. 65 to 68 and 77)	wood – – –	"^{14}C"	– – – – – –	GD11 – I-10374 "15,350 ±210" ^{14}C yr BP (Cal BP 18,400–17,560; see notes) GD12 – UW-448 "15,450 ±250" ^{14}C yr BP (Cal BP 18,590–17,590; see notes)
Lab ID[a]	GD11 – I-10374 GD12 – UW-448	Compiled from Deeter (1979); Calibrated 2-sigma ages were inferred from 1-sigma calibrated ages calculated by Yount and others (1993) from the original data. Yount and others (1993) cited calibration procedures of Stuiver and others (1991). Dates represent separate samples from the same site and appear to be from downsection of GD6 and GD27; if so, Deeter's dates are unexpectedly young relative to GD6 and GD27, although GD6 on wood from detrital peat appears to be reworked from an older deposit.				
TRS	sec. 22, T28N R2E[c]					
Lat/long. (degrees)	47.906970 -122.527953[c]					
Elev. (ft)	"2.5 m [8.2 ft] above the beach"					

[a] Letters identify radiocarbon labs: AA, NSF-Arizona AMS Facility; Beta, Beta Analytic; I, Teledyne Isotopes; QL, Quaternary Isotope Laboratory; UW, University of Washington.

[b] Swanson reported sample coordinates 47°58′ and 122°43′. He did not describe the location in TRS format or provide sample elevations. He did not explicitly state that the reported dates are in radicarbon years but appears to imply that in his text.

[c] Deeter reported sample coordinates as 47°54′09″ and 122°31′36″, which appear to place the sample 270 ft offshore and 1,630 ft south of the sample site shown in this report (map plate). We show the sample location based on our interpretation of Deeter's text and diagrams, and the field conditions we observed.

Table A2. Infrared and optically stimulated luminescence age-control results from the map area. All dates are new. Optically stimulated luminescence (OSL) analyses (on quartz) and infrared stimulated luminescence (IRSL) analyses (on fine-grained feldspar) performed by Shannon Mahan and staff, USGS. Sites are shown on the Map Sheet. Uncertainty estimates span one standard deviation (1σ = 68% confidence interval) and are the values reported by the lab. Uncertainty statements reflect random and lab errors; errors from unrecognized sample characteristics or flawed methodological assumptions (for example, incomplete pre-depositional re-setting of luminescence samples) are not known. – – – indicates no data

Luminescence sample ID (geologic unit)		Water content (%)[a]	K (%)[b]	U (ppm)[b]	Th (ppm)[b]	Cosmic dose additions (Gy/ka)[c]	Equivalent dose (Gy)	Total dose rate (Gy/ka)	N[d]	Scatter (%)[e]	Method	Age (ka)[f]
GD27 (Qc_o)		22 (33)	1.52 ±0.07	1.81 ±0.38	5.14 ±0.38	0.03 ±0.01	>130	1.98 ±0.11	10 (15)	74	OSL	>65 ka
							199 ±12.9[g]	2.81 ±0.15[g]	– – –	– – –	IRSL	71.07 ±6.04 ka[g]
Lab ID	X669a	Sand from 10 ft section of planar-bedded to cross-laminated sand that fines up to clay; sampled 1–2 ft upsection from age site GD6, near the base of a 50-ft-thick package of at least five fining-up sections that range from sand to clay. Bedding is planar to gently cross-bedded. The sections lack appreciable organic matter, except as detritus (such as at GD6). Thin section petrography reveals moderately well-sorted sand with 95% of the grains angular or subangular. Contains 45% quartz, 15% biotite, 10% lithics, 10% white mica, 7% hornblende, 5% potassium feldspar, 2% plagioclase, 1% chlorite, 1% calcite, and 4% high relief accessory minerals. Provenance unresolved. Sand to clay fining-up sections and sedimentary structures suggest a low-energy lacustrine to flood plain paleo-environment.									
TRS	sec. 22, T28N R2E											
Lat/long. (degrees)	47.903490 -122.528347											
Elev. (ft)	~63											
Material	sand											
GD28 (Qgd_p)		5 (31)	1.31 ±0.08	1.23 ±0.21	3.10 ±0.35	0.10 ±0.01	92.4 ±7.48	1.64 ±0.10	9 (15)	32	OSL	56.36 ±5.08 ka
Lab ID	X204C	8 ft pale yellowish brown, near-horizontal planar bedded sand and pebble gravel with interbeds of silt and pea gravel; locally brecciated with injections of sand and gravel. Thin section petrography reveals moderately sorted sand with 80% angular or subangular grains. Contains 60% lithics (polycrystalline quartz, basalt, ultramafics, granite, schist, and gneiss), 25% quartz, 4% potassium feldspar, 2% plagioclase, 2% chlorite, 2% hornblende, and 5% accessory minerals (titanite, chloritoid, opaques). High content of polycrystalline quartz and high-grade metamorphic and granitic clasts suggest a northern provenance and glacial paleo-environment. The sand is overlain by a 4-ft-thick shallow marine shell-bearing diamicton (biostratigraphy site GD13) that we suspect is glaciomarine drift.									
TRS	sec. 22, T28N R1E											
Lat/long. (degrees)	47.929753 -122.613224											
Elev. (ft)	~10											
Material	sand											
GD29 (Qc_o)		9 (28)	1.10 ±0.03	0.97 ±0.12	2.19 ±0.33	0.03 ±0.01	23.6 ±1.18	1.30 ±0.09	14 (20)	31	OSL	30.68 ±2.45 ka
Lab ID	M114g	8 ft section of compact planar-bedded and well-sorted sand, provenance and paleo-environment unknown; unconformably overlies paleomagnetically reversed silt (sample M1) and uncomformably overlain by fluvial sand and peat (GD4; 41.81–40.68 ka). Sand contains 45% lithics (basalt, polycrystalline quartz, phyllite, and schist), 30% quartz, 7% potassium feldspar, 3% plagioclase, 3% biotite, and 12% accessory minerals (chlorite, hornblende, olivine, pyroxene, pumpellyite). Provenance unresolved, but high content of basalt, phyllite, and schist suggests a large Olympic Mountains source that drains both peripheral and core rocks, such as the Dosewallips or Duckabush Rivers. Exposure suggests a lacustrine or large channel setting.									
TRS	sec. 12, T28N R1W											
Lat/long. (degrees)	47.938231 -122.743190											
Elev. (ft)	~299											
Material	sand											
GD30 (Qc_o)		9 (33)	1.17 ±0.03	0.84 ±0.12	2.46 ±0.23	0.10 ±0.01	64.4 ±2.57	1.39 ±0.13	27 (30)	58	OSL	46.57 ±3.49 ka
Lab ID	M116	10 ft dense, gray to light and dark brown; locally iron-stained orange, gently cross-bedded, fine- to medium-grained sand with lenses of silt and short trains of rounded pebbles. The silt lenses are occasionally deformed, but the deformation is localized and non-pervasive—suggestive of syn-depositional soft-sediment deformation. Thin section petrography reveals that the sand is moderately to well-sorted, and 95% of the sand grains are subangular or angular. Sand contains 55% lithics (basalt, polycrystalline quartz, and phyllite), 30% quartz, 5% potassium feldspar, 2% plagioclase, 2% biotite, and 6% accessory minerals (chloritoid, pumpellyite, clinopyroxene). Provenance and paleoenvironmental setting are unresolved, but the high content of basalt and phyllite suggests a large Olympic Mountains source that drains both peripheral and core rocks, such as the Dosewallips or Duckabush Rivers. The sand is unconformably(?) overlain by 5 ft of interbedded silt and sand, which also contains localized folding and is further overlain by 5 ft of light brown sand. All exposed layers are compact. Exposure in a tightly incised drainage suggests that these deposits predate the surficial till on the surrounding upland surface. A pre-Vashon till is exposed 0.5 mi farther down-valley (north) and appears to be downsection of the sand; however, exposure is discontinuous, and the upper end of the till reaches nearly the same elevation as the sampled sand.									
TRS	sec. 6, T28N R1E											
Lat/long. (degrees)	47.943397 -122.715776											
Elev. (ft)	~400											
Material	sand											

Luminescence sample ID (geologic unit)	Water content (%)[a]	K (%)[b]	U (ppm)[b]	Th (ppm)[b]	Cosmic dose additions (Gy/ka)[c]	Equivalent dose (Gy)	Total dose rate (Gy/ka)	N[d]	Scatter (%)[e]	Method	Age (ka)[f]
GD31 (Qc_O)	14 (24)	0.70 ±0.04	0.75 ±0.11	2.09 ±0.33	0.03 ±0.01	0.94 ±0.10	32.7 ±1.47	4 (12)	103	OSL	34.77 ±1.91

Lab ID	X622a	Medium- to coarse-grained sand lens in 10 ft of dense, dark brown, oxidized, poorly sorted, coarse-sand to pebble and cobble gravel; matrix is moderately weathered but clasts are less weathered. Thin section petrography reveals 60% angular or subangular grains, poor sorting, and iron oxide alteration. San contains 90% lithics (basalt and polycrystalline quartz), 5% quartz, and 5% accessory minerals (olivine, plagioclase, and clinopyroxene). Provenance and paleo-environment unknown, but high content of basaltic lithics suggests a large Olympic Mountains source that drains both peripheral and core rocks, such as the Dosewallips or Duckabush Rivers. A greater thickness of gravel is suggested by 10 ft of similar gravel exposed in a small stream channel about 30 ft above the sample site. The higher gravel exposure is overlain by 4 ft of compact, paleomagnetically normal silt (M6).
TRS	sec. 12, T28N R1E	
Lat/long. (degrees)	47.94356 -122.732012	
Elev. (ft)	~288	
Material	sand	

[a] Field moisture, with number in parentheses indicating the complete sample saturation %. Ages calculated using approximately 55% of saturation values.

[b] Analyses obtained using high-resolution gamma spectrometry (HPGe detector).

[c] Cosmic doses (in Grays per 1,000 yr) and attenuation with depth were calculated using the methods of Prescott and Hutton (1994). See text for details.

[d] Number of replicated equivalent dose (De) estimates used to calculate the equivalent dose. Number in parentheses indicate total number of measurements included in calculating the represented equivalent dose and age using the minimum age model (MAM).

[e] Defined as 'over-dispersion' of the De values. Obtained by taking the average over the std deviation. Values >35% are considered to be poorly bleached sediments.

[f] Dose rate and age for 250–180 micron quartz. Exponential + linear fit used on single aliquot regeneration equivalent doses; errors to one sigma; ages and errors rounded.

[g] Dose rate and IRSL age for feldspar from 4–11 micron polymineral silt. Exponential fit used for multiple aliquot additive dose. Errors to one sigma. Fade tests indicate ~1 g/decade correction.

Table A3. $^{40}Ar/^{39}Ar$ age summary for sample GD33/X166D. Analysis by Daniel Miggins and staff, Argon Geochronology Lab, College of Oceanic and Atmospheric Sciences, Oregon State University, Corvallis, Oregon. Sample site is shown on the Map Sheet. Uncertainty values span two standard deviations (2σ = 95% confidence interval). Uncertainty statements reflect random and lab errors; errors from unrecognized sample characteristics or flawed methodological assumptions (for example, unrecognized post-depositional re-setting of $^{40}Ar/^{39}Ar$ ratios) are not known. – – – indicates no data

$^{40}Ar/^{39}Ar$ sample ID (geologic unit)			Basalt (geochemistry site G4) from center of a massive flow in western high wall of inactive Mats Mats Quarry, where several exposed flows are each tens of feet thick and dip 45° north. Sample represents one of the uppermost flows in the quarry, and analysis produced the northeastern-most date so far obtained for Crescent Formation basalt. Initial analysis indicated an age (weighted plateau) of 51.39 ±0.22 Ma and an argon recoil pattern. The inverse isochron suggested a real age of 50.54 ±0.40 Ma, and the initial $^{40}Ar/^{36}Ar$ value indicated excess argon. The age was therefore recalculated using an initial $^{40}Ar/^{36}Ar$ intercept of 574.1 ±117.3, which yielded the reported analytical parameters below, including the revised age of 50.51 ±0.16 Ma.				
GD33/X166D (Evc)							
TRS	sec. 33, T29N R1E						
Lat/long (degrees)	47.961045 -122.683877						
Elev. (ft)	~60						
Result type	**$^{40}Ar^{(r)}/^{39}Ar^{(k)}$**	**±2σ**	**$^{39}Ar^{(k)}$ (%.n)**	**K/Ca ±2σ**	**Age(Ma) ±2σ**		**MSWD**
Age Plateau	16.73274	±0.03990	58.46	0.0434 ±0.0002	50.51	±0.16	2.10
		±0.24%	15			±0.32%	1%
						Full external error	±1.14
						Analytical error	±0.12
Total Fusion	16.08522	±0.02544	34	0.0381 ±0.0001	48.58	±0.13	
		±0.16%	– – –			±0.27%	
						Full external error	±1.10
						Analytical error	±0.08

(k) potassium

(r) radiogenic

(%.n) normalized percentage

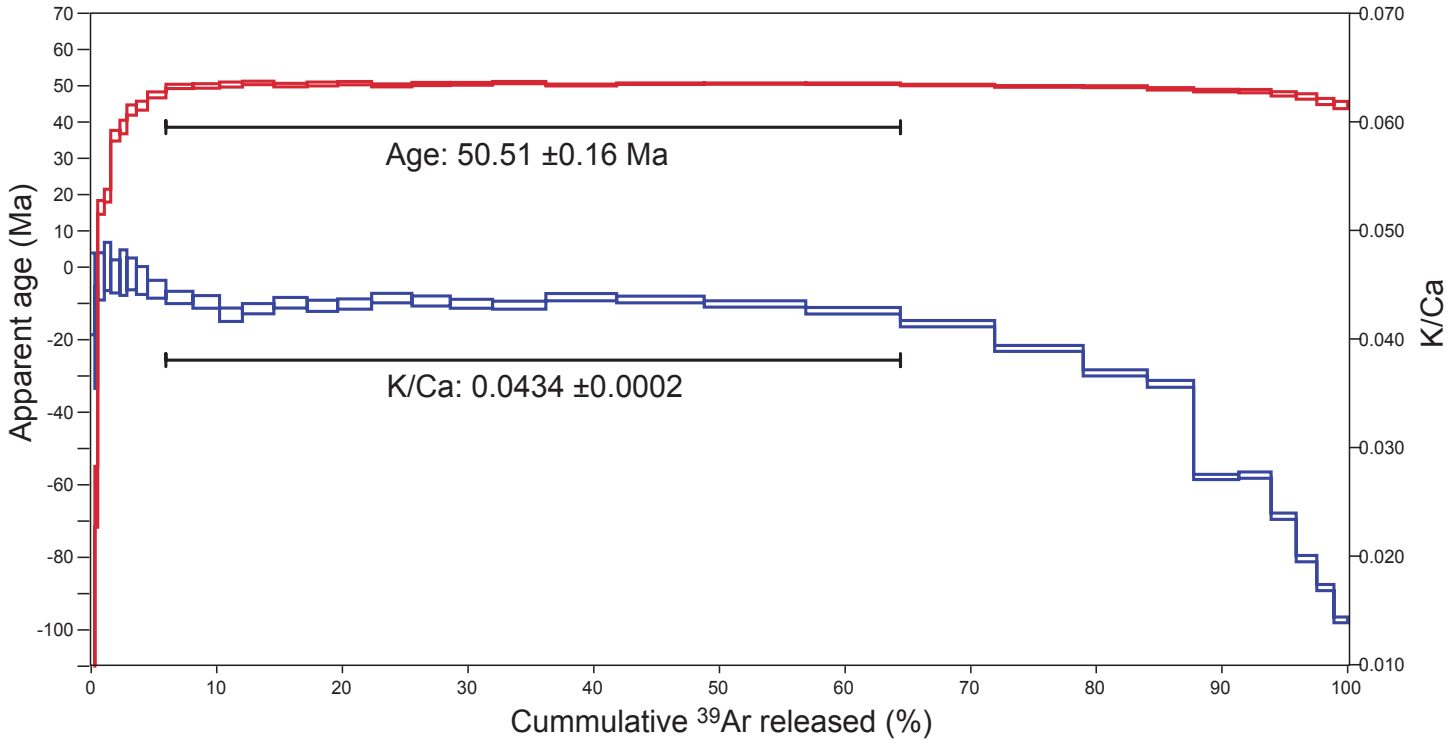

Figure A1. $^{40}Ar/^{39}Ar$ step-heating age and K/Ca spectra for sample GD33/X166D. See Table A3 for summary of age data and step-heating results.

Table A4. $^{40}Ar/^{39}Ar$ step-heating results for sample GD33/X166D. Light gray shading indicate steps used for weighted age plateau.

Heating step	Power (%)	$^{36}Ar^{(a)}$ [fA]	$^{37}Ar^{(ca)}$ [fA]	$^{38}Ar^{(cl)}$ [fA]	$^{39}Ar^{(k)}$ [fA]	$^{40}Ar^{(r)}$ [fA]	$^{40}Ar^{(r)}$	$^{39}Ar^{(k)}$	K/Ca	Age (Ma)
15D07797	1.9	0.2467266	9.8742	0.0024501	1.01688	-41.2963	-41.15	0.29	0.0443 ±0.0038	-128.79 ±11.23
15D07798	2	0.1226938	7.9623	0.0429145	0.74578	-15.1494	-27.40	0.22	0.0403 ±0.0047	-63.28 ±8.38
15D07800	2.2	0.0938476	16.9893	0.0000000	1.81298	9.8031	15.39	0.52	0.0459 ±0.0022	16.48 ±1.89
15D07801	2.4	0.0788700	16.3372	0.0109348	1.77817	11.5242	20.29	0.51	0.0468 ±0.0022	19.73 ±1.78
15D07802	2.6	0.0610213	24.0097	0.0000000	2.56230	30.6429	46.66	0.74	0.0459 ±0.0015	36.24 ±1.45
15D07804	2.8	0.0376294	17.7831	0.0000000	1.91233	24.4223	53.06	0.55	0.0462 ±0.0021	38.68 ±1.87
15D07805	3	0.0347943	24.4591	0.0000000	2.62309	37.5597	65.28	0.76	0.0461 ±0.0015	43.31 ±1.41
15D07806	3.3	0.0315474	28.7804	0.0000000	3.04608	44.8482	71.23	0.88	0.0455 ±0.0013	44.52 ±1.24
15D07808	3.6	0.0347723	48.8603	0.0382195	5.07888	79.8464	79.99	1.47	0.0447 ±0.0008	47.49 ±0.83
15D07809	4	0.0292937	72.8732	0.0111845	7.44923	122.9602	87.96	2.15	0.0440 ±0.0006	49.83 ±0.58
15D07811	4.3	0.0243295	72.0900	0.0120750	7.29998	120.8259	89.63	2.11	0.0435 ±0.0006	49.97 ±0.6
15D07812	4.6	0.0267068	63.6326	0.0000000	6.26869	104.5593	87.21	1.81	0.0424 ±0.0006	50.35 ±0.69
15D07813	4.9	0.0223005	87.1974	0.0000000	8.70232	146.4503	91.96	2.52	0.0429 ±0.0005	50.79 ±0.48
15D07815	5.2	0.0200420	90.0376	0.0000000	9.10154	151.3254	92.93	2.63	0.0435 ±0.0005	50.19 ±0.47
15D07816	5.5	0.0151626	83.6536	0.0315177	8.40097	140.5446	94.16	2.43	0.0432 ±0.0005	50.5 ±0.52
15D07817	5.8	0.0150798	93.3103	0.0000000	9.40557	158.0661	94.80	2.72	0.0433 ±0.0005	50.73 ±0.46
15D07819	6.1	0.0164539	108.3492	0.0420752	11.05855	183.6715	95.10	3.20	0.0439 ±0.0004	50.14 ±0.41
15D07820	6.5	0.0147244	103.9420	0.0480441	10.54561	176.3644	95.42	3.05	0.0436 ±0.0005	50.48 ±0.44
15D07821	7	0.0170912	115.1971	0.0285586	11.61899	194.5239	95.19	3.36	0.0434 ±0.0004	50.54 ±0.38
15D07823	7.6	0.0147037	146.2221	0.0214693	14.70380	247.8233	96.70	4.25	0.0432 ±0.0004	50.87 ±0.31
15D07824	8.4	0.0190635	190.0515	0.0000000	19.43689	323.3756	96.72	5.62	0.0440 ±0.0003	50.22 ±0.24
15D07825	9.4	0.0215894	237.0289	0.0000000	24.12602	404.3521	97.02	6.98	0.0438 ±0.0003	50.59 ±0.20
15D07827	10.5	0.0218637	277.4778	0.0000000	27.97477	469.0280	97.39	8.09	0.0434 ±0.0003	50.61 ±0.19
15D07828	11.7	0.0208516	262.0653	0.0000000	26.03897	436.2124	97.32	7.53	0.0427 ±0.0003	50.57 ±0.20
15D07829	13.1	0.0222738	268.1671	0.0000000	25.90364	431.0323	97.11	7.49	0.0415 ±0.0003	50.23 ±0.20
15D07831	14.7	0.0243621	267.2685	0.0328353	24.40925	402.9112	96.64	7.06	0.0393 ±0.0003	49.83 ±0.21
15D07832	15.7	0.0204292	204.2885	0.0000000	17.59132	289.8122	96.10	5.09	0.0370 ±0.0003	49.74 ±0.27
15D07833	16.5	0.0167896	152.6635	0.0000000	12.78598	208.2226	95.57	3.70	0.0360 ±0.0003	49.18 ±0.34
15D07835	18.3	0.0254447	193.9550	0.0193339	12.38616	199.6474	93.18	3.58	0.0275 ±0.0002	48.68 ±0.35
15D07836	19.3	0.0191935	138.3605	0.0384732	8.89116	142.8565	92.83	2.57	0.0276 ±0.0003	48.53 ±0.48
15D07837	20.4	0.0188911	125.7257	0.0000000	6.97513	110.2801	91.04	2.02	0.0239 ±0.0003	47.76 ±0.59
15D07839	21.6	0.0225410	121.7368	0.0587675	5.64966	88.0046	87.18	1.63	0.0200 ±0.0003	47.06 ±0.74
15D07840	22.8	0.0213468	116.4656	0.0268129	4.68500	70.7680	85.23	1.35	0.0173 ±0.0003	45.66 ±0.84
15D07842	23.7	0.0200574	113.9400	0.0741788	3.79584	56.1546	82.98	1.10	0.0143 ±0.0003	44.73 ±1.00

Material – Groundmass
J – 0.00169278 ±0.00000186

Standard – FCT-NM (7B36-14)
Standard age – 28.201 ±0.023 Ma
Standard reference – Kuiper and others (2008)

Irradiation – 14-OSU-07
Analyst – Dan Miggins
Mass discrimination law – Linear

(a) atmosphere
(ca) calcium
(cl) chlorine
(k) potassium
(r) radiogenic
[fA] femtoamp

Appendix B. Geochemical Data

The chemical attributes of Port Ludlow basalt samples (Tables B1 and B2) are classified as basalt on the basis of total alkalis vs. silica (TAS)(Le Bas and others, 1986). On a TAS diagram, all samples resemble other Crescent Formation samples from nearby quadrangles (Contreras and others, 2012a; Polenz and others 2004, 2012b,c, 2013, 2014; Schasse and Logan, 1998; Schasse and others, 2004; Schasse and Polenz, 2002; Schasse and Wegmann, 2000). On tectonic discrimination diagrams, the Port Ludlow samples resemble basalt flow samples from the Black Hills, east of Hood Canal (Clarke, 1989), but contrast with some basalt samples from west of Hood Canal (Contreras and others, 2012a; Polenz and others, 2013, 2004, 2012b,c; Schasse and Logan, 1998; Schasse and others, 2004; Schasse and Polenz, 2002; Schasse and Wegmann, 2000) that plot as mix of oceanic arc source and continental arc source (Zr vs. Zr/Y) and as transitional between plate margin basalts and intraplate basalt (Ti/Y vs. Zr/Y). On a diagram of Zr vs. Zr/Y, all Port Ludlow samples plot as continental arc source; on a plot of Ti/Y vs. Zr/Y all samples except G1 plot as intra-plate basalt. Elevated P_2O_5 and Ba in sample G1 suggest post depositional alteration.

Table B1. Major oxide geochemical analyses for nine new and four compiled (Clark, 1989) whole-rock basalt samples from the Crescent Formation in the Port Ludlow quadrangle. New analyses performed by ALS Global, Vancouver, Canada. Oxides determined by x-ray fluorescence (XRF). Lab states analytical uncertainties are 5%. Constituents normalized to 100% on an anhydrous basis. LOI represents loss on ignition; total iron reported as $Fe_2O_3^T$. Light gray shading indicates samples compiled from Clark (1989); G10, Clark MM1; G11, Clark MM2; G12, Clark PL2; G13, Clark OP1; – – – indicates no data.

Analytical Method—XRF (major oxides)														
Site		G1	G2	G3	G4	G5	G6	G7	G8	G9	G10	G11	G12	G13
SiO_2	%	51.08	48.21	50.91	47.86	47.87	48.55	48.07	48.30	48.61	49.10	49.45	48.91	49.49
TiO_2	%	2.45	3.21	2.73	1.93	1.75	1.67	1.87	1.95	2.33	1.88	1.88	1.98	1.95
Al_2O_3	%	12.68	12.61	13.51	14.31	15.01	15.66	14.81	15.03	13.49	15.27	14.56	14.69	14.99
$Fe_2O_3^T$	%	18.56	18.39	16.21	13.11	12.77	12.06	12.81	12.8	15.53	13.2	12.37	13.70	13.07
MgO	%	2.14	5.47	3.89	7.29	7.66	7.78	7.58	7.02	6.23	6.60	6.96	6.79	6.65
MnO	%	0.39	0.37	0.24	0.17	0.21	0.19	0.21	0.18	0.20	0.16	0.20	0.19	0.23
CaO	%	7.18	7.49	8.10	12.57	11.93	10.00	11.72	11.29	8.61	12.35	12.35	12.26	11.95
Na_2O	%	3.52	3.75	3.43	2.30	2.32	3.66	2.56	2.69	4.30	2.29	2.37	2.32	2.45
K_2O	%	0.64	0.14	0.51	0.19	0.23	0.18	0.12	0.42	0.38	0.15	0.23	0.19	0.21
P_2O_5	%	1.32	0.36	0.41	0.19	0.17	0.17	0.18	0.19	0.25	0.19	0.18	0.20	0.20
LOI	%	0.86	4.55	1.49	2.17	2.63	3.80	3.55	2.42	2.89	– – –	– – –	– – –	– – –
Orig total	%	100.05	100.05	99.90	99.61	99.96	100.10	100.00	99.93	99.86	99.66	99.50	98.65	101.18

Table B2. Trace-element geochemical analyses for nine new and four compiled (Clark, 1989) whole-rock basalt samples from the Crescent Formation in the Port Ludlow quadrangle. New analyses performed by ALSGlobal, Vancouver, Canada. Trace elements determined by inductively coupled plasma mass spectrometry (ICP-MS). Lab states analytical uncertainties are 10%. Light gray shading indicates samples compiled from Clark (1989); G10, Clark MM1; G11, Clark MM2; G12, Clark PL2; G13, Clark OP1; – – – indicates no data.

Analytical Method—ICP-MS (trace elements)														
Site		G1	G2	G3	G4	G5	G6	G7	G8	G9	G10	G11	G12	G13
Ba	ppm	152.5	42.6	105.0	52.3	44.6	45.1	51.7	109.0	68.3	80.0	38.0	62.0	67.0
Cr	ppm	10	10	<10	340	260	260	280	240	50	160	216	232	166
Cs	ppm	0.11	<0.01	0.03	0.03	0.02	0.06	<0.01	<0.01	0.05	– – –	– – –	– – –	– – –
Ga	ppm	30.5	24.5	24	18.9	18.7	18.2	19.6	19.8	20.2	20.0	17.0	20.0	23.0
Hf	ppm	16.2	5.8	7	3.2	3	2.6	3	3.4	3.6	– – –	– – –	– – –	– – –
Nb	ppm	33.6	17.6	23.7	11.4	9.7	9.6	10.8	12.2	13.9	13.0	12.0	13.0	12.0
Rb	ppm	9.1	0.3	5	1.2	2.4	1.4	0.5	3.3	3.7	2.0	3.0	1.0	3.0
Sn	ppm	4	2	2	1	1	1	1	1	2	– – –	– – –	– – –	– – –
Sr	ppm	217.0	154.0	212.0	225.0	197.5	165.5	210.0	253.0	177.0	211.0	206.0	193.0	203.0
Ta	ppm	1.9	1.0	1.3	0.6	0.5	0.6	0.6	0.7	0.8	– – –	– – –	– – –	– – –
Th	ppm	2.51	1.19	1.93	0.82	0.79	0.95	1.51	1.15	1.16	– – –	– – –	– – –	– – –
U	ppm	0.88	0.34	0.57	0.29	0.23	0.19	0.22	0.28	0.31	– – –	– – –	– – –	– – –
V	ppm	25	497	272	360	332	312	339	334	425	320	327	333	347
W	ppm	<1	1	2	<1	<1	<1	<1	<1	<1	– – –	– – –	– – –	– – –
Y	ppm	111.5	50.8	55.6	25.6	24.6	23.1	25.5	26.4	32.3	27.0	26.0	27.0	29.0
Zr	ppm	690	232	289	126	112	100	108	118	134	123	216	122	126
La	ppm	33.3	15.5	21.4	10.2	8.6	9.6	11.1	11.3	12.4	– – –	– – –	– – –	– – –
Ce	ppm	85.7	40.3	52.7	25.1	21.2	22.3	26.4	27.0	30.0	– – –	– – –	– – –	– – –
Pr	ppm	12.80	5.74	7.26	3.60	3.06	3.16	3.69	3.80	4.32	– – –	– – –	– – –	– – –
Nd	ppm	64.8	27.4	32.5	15.9	13.8	14.7	16.9	17.3	19.9	– – –	– – –	– – –	– – –
Sm	ppm	17.60	7.41	8.31	4.20	3.93	3.76	4.66	4.61	5.44	– – –	– – –	– – –	– – –
Eu	ppm	5.84	2.60	2.69	1.46	1.37	1.35	1.49	1.51	1.86	– – –	– – –	– – –	– – –
Gd	ppm	20.4	9.04	10.00	4.70	4.48	4.32	5.08	5.02	5.80	– – –	– – –	– – –	– – –
Tb	ppm	3.32	1.52	1.66	0.81	0.75	0.72	0.81	0.76	1.03	– – –	– – –	– – –	– – –
Dy	ppm	21.00	9.31	9.91	4.88	4.63	4.22	4.85	5.08	5.95	– – –	– – –	– – –	– – –
Ho	ppm	4.24	1.96	2.15	0.99	0.98	0.86	1.02	0.98	1.25	– – –	– – –	– – –	– – –
Er	ppm	12.80	5.50	5.92	2.85	2.61	2.48	2.61	2.91	3.55	– – –	– – –	– – –	– – –
Tm	ppm	1.74	0.77	0.88	0.40	0.37	0.36	0.36	0.39	0.51	– – –	– – –	– – –	– – –
Yb	ppm	11.55	5.03	5.55	2.25	2.45	2.29	2.54	2.44	3.30	– – –	– – –	– – –	– – –
Lu	ppm	1.69	0.77	0.79	0.34	0.35	0.33	0.36	0.35	0.44	– – –	– – –	– – –	– – –